CR 86072

Aerospace Research Center

DESIGN OF A THREE-AXIS ATTITUDE CONTROL SYSTEM FOR A SPACECRAFT ACTED UPON BY RANDOM PERTURBATIONS

Contract No. NAS 12-48

FINAL REPORT

Contributors:

B. Friedland
F.E. Thau
P.E. Sarachik

Submitted to:

NATIONAL AERONAUTICS AND SPACE ADMINISTRATION
ELECTRONICS RESEARCH CENTER
CAMBRIDGE, MASSACHUSETTS - 02139

April 1968

AEROSPACE RESEARCH CENTER
GENERAL PRECISION SYSTEMS INC.
KEARFOTT GROUP
LITTLE FALLS, NEW JERSEY

DESIGN OF A THREE-AXIS ATTITUDE CONTROL SYSTEM FOR A SPACECRAFT ACTED UPON BY RANDOM PERTURBATIONS

By B. Friedland, F.E. Thau and P.E. Sarachik

Prepared under Contract No. NAS 12-48 by

GENERAL PRECISION SYSTEMS INC.
Little Falls, New Jersey

Electronics Research Center
NATIONAL AERONAUTICS AND SPACE ADMINISTRATION

DESIGN OF A THREE-AXIS ATTITUDE CONTROL SYSTEM FOR A SPACECRAFT ACTED UPON BY RANDOM PERTURBATIONS

By B. Friedland, F. E. Thau and P. E. Sarachik

General Precision Systems Inc.
Little Falls, New Jersey

SUMMARY

The design of spacecraft attitude control systems to counteract the effects of random excitations such as induced by micrometeoroid bombardment is an important problem in achieving the high pointing accuracy required for projected advanced missions, including a laser beam communication system. The general problem of optimizing the design for a nonlinear system with an arbitrary statistical performance criterion has not been completely solved. In this investigation, the process to be controlled (a hypothetical laser communication vehicle) was linearized about a nominal motion and the design performance criterion was the steady-state expected value of a quadratic form in the vehicle state-variables. Use of this performance permits use of known results to develop a design algorithm for the three-axis attitude control system. This design algorithm is employed to determine the structure and parameter values of the controller for the vehicle and the statistical performance is simulated with the aid of a digital computer simulation program.

The results obtained indicate that it is possible to achieve a 1σ pointing accuracy of approximately 0.2 $\overset{\frown}{\text{sec}}$ in the assumed micrometeoroid environment existing in the vicinity of Mars. This pointing accuracy can be maintained only for about 20 minutes (as measured in "half-life").

This investigation takes into account only the effect of micrometeoroid disturbances. Further investigation of other (random and deterministic) disturbances is recommended. Also recommended is further study of the general problem of optimum stochastic control.

CONTENTS

1. INTRODUCTION

The design of control systems for attitude control of space vehicles acted upon by random perturbations has become an important practical problem in the past few years as a consequence of the need to maintain the attitude error appreciably below a level of a second of arc. Missions which require such accuracy include the fine-pointing of astronomical telescopes and the pointing of a narrow laser beam for the purpose of high data rate communication from a space vehicle.

In the conventional design approach it is generally assumed either that disturbances are absent and the control system is to be designed to return to equilibrium when the system is perturbed momentarily, or that the disturbances are simple deterministic time functions whose effect is to be overcome by the feedback action of the control system. This approach yields satisfactory system performance in most practical situations, because the requirements on performance are usually well within the capabilities of the equipment. In the fine-pointing problem, however, the performance requirements are so severe that all equipment must be used optimally; consequently it becomes important to take into account the statistical properties of the disturbance sources and the sensor errors in the control system design.

In 1966, the Aerospace Research Center of General Precision Systems Inc. initiated an investigation of the stability of attitude control systems acted upon by random perturbations. It was found [1] that micrometeoroid bombardment is a significant source of impulsive disturbance torque which can rapidly cause large attitude errors if permitted to build up. In particular, the micrometeoroid bombardment on a vehicle of the size of Mariner IV at an altitude of about 1000 km from the earth's surface, would be sufficient to cause a pure inertia to deviate from an equilibrium position by 2 degrees in not more than about 2 hours with a probability of 1/2. Since the tolerance required for precise pointing is several orders of magnitude less than 2 degrees, it is evident that the random torques due to micrometeoroids should be accounted for in the system design.

The first phase of our study (July 1966 to July 1967) of the stability of attitude control systems acted upon by random perturbations was concerned with the general theory and analytical techniques which are applicable to this problem. A tutorial exposition of the applicable results of the theory of Markov processes was given, and the concepts of "confinement probability", "half-life" and "mean confinement time" were defined and studied by analytical and numerical techniques for a few simple control systems. Our conclusions were that practical analytical techniques for studying stochastic stability were less than entirely adequate, and moreover, that the statistical properties of the random disturbance sources which may be present in a physical situation were not as well understood as would be needed for meaningful statistical control system design.

These conclusions, we believe, remain valid; practical exigencies, however, will make it necessary to design control systems for precise attitude control in the absence of a perfected analytical theory and without a good knowledge of the statistical properties of the random disturbance and noise sources which may be present. Accordingly, the phase of the investigation reported herein represents an endeavor to apply the available theory to a fairly realistic attitude control problem, that of controlling the attitude of a laser communication spacecraft.

Modulation of a laser beam appears as an attractive possibility of obtaining an energy density at the receiver high enough to maintain a data transmission rate of 10^5 to 10^6 bits/second, which would be required, for example, for transmission of television pictures in real-time. With the limited power available in space, the attainment of the required energy density at the earth necessitates the use of an extremely narrow beam, such as can be achieved only by use of a laser. The narrow beam width required, however, creates a very severe pointing problem, since very small angular errors can cause the beam to disappear from view of the receiving telescope. An indication of the pointing accuracy required can be inferred from the angle subtented by the earth's diameter at distances of the planets Mars and Jupiter, which are currently regarded as destinations for potential interplanetary excursions:

Planet	Phase	Subtended Angle
Mars	Conjunction	24 sec
	Opposition	6 sec
Jupiter	Conjunction	4 sec
	Opposition	3 sec

Since the laser beam will probably be designed to illuminate only a fraction of the earth's disk, the required pointing accuracy can be expected to be a fraction of a second of arc.

In all likelihood, the required pointing accuracy will be obtained by use of two control systems: a vehicle attitude control system to orient the vehicle and mechanical axis of the transmitting radiator, and an optical vernier control system by which the optical axis of the beam can be adjusted to accomplish the precise final adjustment.

The schematic diagram of a possible control system is given in Fig. 1.1, which shows the vehicle attitude control system in heavy-weight lines and the vernier control system in lighter weight lines. The total angular misalignment φ of the optical axis with respect to the desired orientation is the sum of the mechanical misalignment angle θ and the angle η between the mechanical axis and the optical axis. Since the angle η can be adjusted by the vernier loop, the ultimate pointing accuracy is governed by performance capability of that loop. It is observed, however, that the mechanical axis misalignment is the source of excitation to the optical loop. Consequently, it is desirable to keep the mechanical misalignment as small as possible, in some appropriately defined sense.

In the present study, attention has been confined to an investigation of the design of the attitude control system. A thorough investigation would necessarily entail examination of all sources of disturbance and errors which may be present, with particular attention being given to those sources which experience would indicate to be major contributions to attitude errors. For current state-of-the-art equipment, the major error sources include such factors as sensor bias, null drift and misalignment, mechanical misalignments,

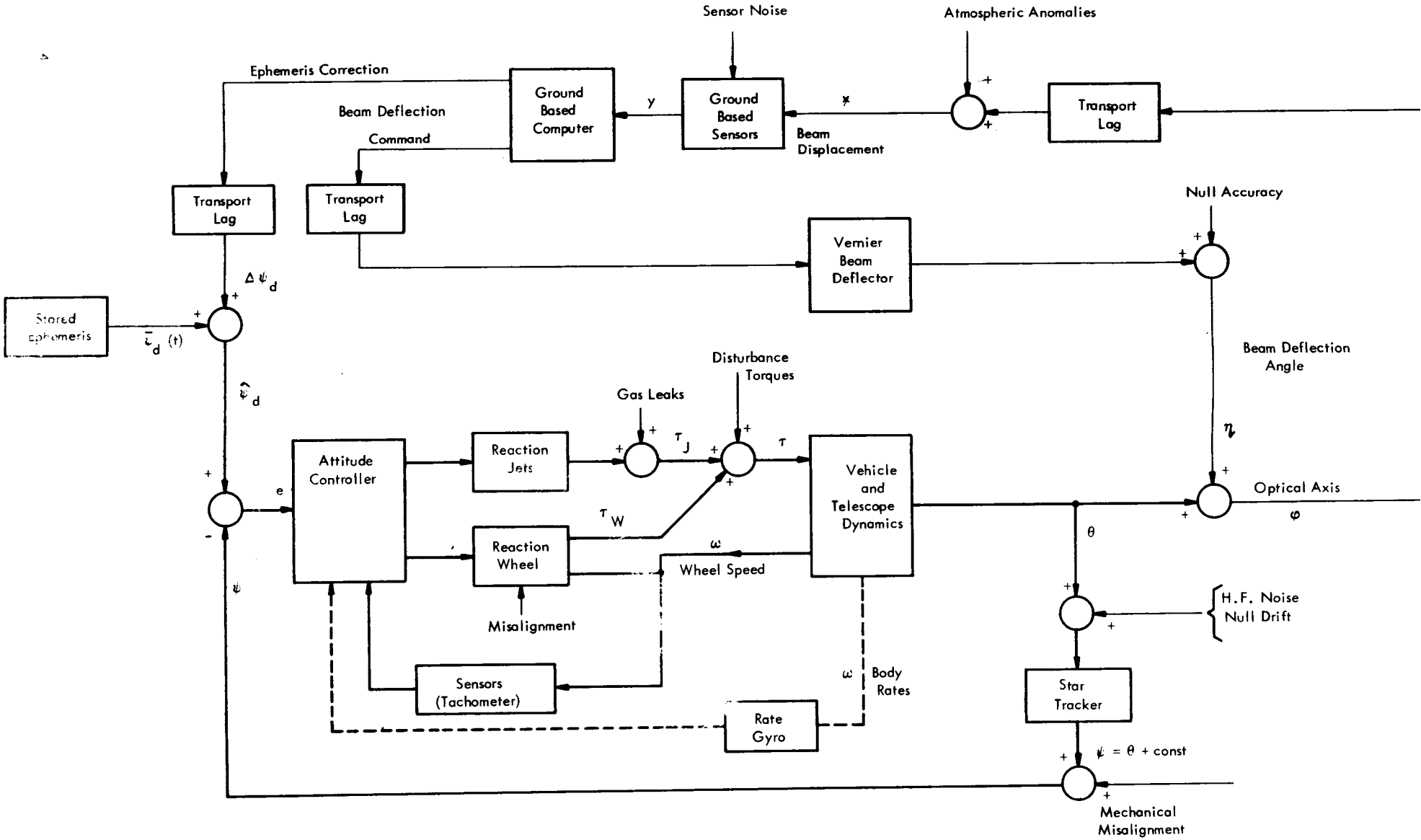

Fig. 1.1 - BLOCK DIAGRAM OF CONTROL SYSTEM FOR LASER BEAM POINTING

and disturbance torques due to gravity gradients, gas leaks and outgassing, and solar reflectivity unbalance. The effect of these "d-c" error and disturbance sources in current equipment are far more significant than the random torques (due primarily to micrometeoroid bombardment) on the attitude error. Nevertheless, in order to concentrate our attention on the purely random effects and the design problems pertaining thereto, we have neglected the d-c error sources. Although it is not immediately apparent, neglecting the d-c effects does not obviate the practical significance of the study: by proper design of the optical vernier control system, we have found that it is possible to counteract the d-c terms quite effectively; the random effects, on the other hand, pass through the vernier control system with very little attenuation. As a consequence, the total error at the receiver may be primarily due to the random disturbances on the spacecraft.

Since the purpose of the control system is to maintain the orientation of the optical axis within the field of view of the receiver for as long as possible, and thereby provide the longest time of uninterrupted communication, it would be desirable to design the control system to maximize the expected first passage time of the axis to the limits of the region in which communication can be maintained, or to maximize the half-life in this region. The theory for the design of an optimum system for these criteria, as noted earlier, is not yet available. Consequently, the design criterion we selected was the minimization of the stationary expectation of a quadratic form in the system state

$$V = E_s(x' Q x) = \lim_{T\to\infty} E\{ \frac{1}{T-t} \int_t^T x'(s)\, Q x(s)\, ds \mid z(\tau), \tau < t\} \qquad (1.1)$$

where z is the sensor output vector.

It is demonstrated (Sec. 3) that the controller which minimizes V for a linear time-invariant process is also linear and time-invariant. An expression for the transfer matrix $G(s)$ for the optimum controller was developed, and a digital computer program for the computation of this matrix of transfer functions was developed as a design aid. Although the performance criterion given by (1.1) is not precisely what should be optimized, it appears to be a reasonable performance criterion and has the advantage of being routinely applicable (with the aid of the computer program) to linear time-invariant systems of

arbitrarily high order, and explicitly accounting for the level of the disturbances and the sensor noise. These random quantities were assumed to be representable by Gaussian white noise with spectral densities on the basis of assumed (state-of-the-art) static accuracy and correlation time, as described in Section 4.

A three-axis dynamic model was assumed for the vehicle. In addition to the vehicle motion, a set of two solar paddles which move with respect to the vehicle were included. To describe the motion of the vehicle, a system of 11 first-order nonlinear differential equations were obtained. These, when linearized about a typical condition of motion, lead to a linear time-invariant system for which the optimum transfer function matrix was computed. The sensor package studied consisted of a set of star trackers measuring angular deviations from nominal motion and tachometers measuring the speeds of a set of three orthogonal reaction wheels.

To develop insight into the behavior of the closed-loop system without the complexity of an eleventh-order system, a single axis (third-order) version of the problem was considered in a preliminary study. For this simplified model, it was found that the optimum design described above, with typical parameter values leads to a steady-state $1\text{-}\sigma$ error of 0.09 $\widehat{\text{sec}}$. While this figure looks excellent, it should be remembered, that this accuracy is based on micrometeoroid bombardment being the only source of disturbance torque. A Monte-Carlo simulation was performed for the closed-loop process (which is fifth-order) to determine the half-life of the system. It was found that the pointing accuracy which can be maintained with a half-life of 30 minutes is in excess of 0.2 $\widehat{\text{sec}}$. On the other hand, the $1\text{-}\sigma$ pointing accuracy of 0.09 $\widehat{\text{sec}}$. is maintained with a half-life of under 4 minutes. The half-life was observed to increase very rapidly for permissible angular errors greater than about 3σ, but is quite small for pointing accuracy much under 1σ. In fact for very small angular position limits, the uncontrolled system is superior to the controlled system, which indicates that the performance criterion used is not very useful in this region.

The results of the preliminary investigation were verified with the more complicated dynamic situation, in which, for the assumed nominal motion, the yaw-axis dynamics (represented by a fifth-order model) were uncoupled from the dynamics for the coupled

pitch-roll axes (sixth-order model). The controller for the yaw-axis turned out to be third-order and gave a steady-state 1σ pointing accuracy of 0.127 $\overset{\frown}{\text{sec}}$. The pointing accuracy of 0.2 $\overset{\frown}{\text{sec}}$ was maintained for a half-life of over 10 minutes, but less than 30 minutes;* a pointing accuracy of 0.1 $\overset{\frown}{\text{sec}}$, however, is maintained with a half-life of only about 1 minute.

The controller for the roll-pitch axes turned out to be sixth-order and gave a steady-state 1σ pointing accuracy of 0.2 $\overset{\frown}{\text{sec}}$ which was maintained for approximately 30 minutes.

The authors would like to acknowledge the contributions of Mr. Maurice F. Hutton in programming the computer design algorithm and Mr. Sanford Welt in conducting the digital computer simulation of control system performance.

* Insufficient computer time was available to simulate ensembles having a half-life of of over 10 minutes.

2. REVIEW OF STOCHASTIC CONTROL THEORY

2.1 BACKWARD EQUATIONS

If one considers a deterministic system governed by the differential equation

$$\dot{x}(\tau) = f(x(\tau), u(\tau), \tau) \tag{2.1}$$

for which the cost functional can be expressed as

$$V(y, t) = \int_t^T L(x(\tau), u(\tau), \tau)\, d\tau \tag{2.2}$$

where $x(t) = y$, it is well-known [2] that if any feedback law is used to control the system, say

$$u(\tau) = \sigma(x(\tau))$$

then the cost which results for this feedback law satisfies the first-order partial differential equation

$$-\frac{\partial V}{\partial t} = L(y, \sigma(y), t) + \nabla V \cdot f(y, \sigma(y), t) \tag{2.3}$$

where ∇V denotes the gradient of V with respect to y. This is easily seen by differentiating both sides of (2.2) with respect to t.

For a system disturbed by additive white noise and characterized by

$$\dot{x}(\tau) = f(x(\tau), u(\tau)) + G(\tau)\,\xi(\tau) \tag{2.4}$$

where $\{\xi\}$ is a zero-mean white noise disturbance process with covariance matrix $\Sigma(t)\,\delta(t - \tau)$ one might expect that the cost functional defined by

$$V(y, t) = E\left\{\int_t^T L(x(\tau), u(\tau), \tau)\, d\tau \,\middle|\, x(t) = y\right\} \tag{2.5}$$

would also be governed by a partial differential equation, when a feedback law $u(\tau) = \sigma(x(\tau))$ is used. This is in fact true and V can be shown [3] to satisfy the second-order partial differential equation

$$-\frac{\partial V}{\partial t} = L(y, \sigma(y), t) + \nabla V \cdot f(y, \sigma(y), t) + \frac{1}{2}\nabla \cdot (G\Sigma G'\nabla V) \tag{2.6}$$

where the operator ∇ is again taken with respect to the components of y. This is one form of the "backward equation" which is so named because it involves the earlier time t and the state at this time rather than the later time T. Note that (2.6) is merely (2.3) with an additional term due to the presence of the noise. This term contains second partials of V with respect to y and thus stochastic problems require in general the solution of second order nonlinear partial differential equations. No general methods exist for obtaining such solutions analytically. The backward equation is actually much more general. Whenever a feedback law is used in (2.4), the equation can be written as

$$\dot{x}(\tau) = g(x(\tau), \tau) + G(\tau)\,\xi(\tau) \tag{2.7}$$

where $g(x, \tau) = f(x, \sigma(x), \tau)$. It turns out [1] that the conditional expectation of any function defined on the Markov process $\{x(\tau)\}$ generated by (2.7) satisfies a backward equation. That is the function

$$U(\tau, t, y) = E\{F(x(\tau)) | x(t) = y\} \tag{2.8}$$

satisfies the partial differential equation (backward equation)

$$\frac{\partial U}{\partial t} = \nabla U \cdot g + \frac{1}{2}\nabla \cdot [G\Sigma G'\nabla U] \tag{2.9}$$

Equation (2.6) can actually be obtained by using (2.9), since taking $\partial/\partial t$ of (2.5) gives

$$\frac{\partial V}{\partial t} = E\{L(x(t), \sigma(x(t)), t) | x(t) = y\} - \int_t^T \frac{\partial}{\partial t} E\{L | x(t) = y\}\, d\tau \tag{2.10}$$

Then, substituting the right-hand side of (2.9) for the expression inside the integral and noting that for any linear operation $\mathcal{L}_y$ defined in terms of the space variable y

$$\int_t^T \mathcal{L}_y [E\{L | x(t) = y\}]\, d\tau = \mathcal{L}_y [E\{\int_t^T L\, d\tau | x(t) = y\}] \tag{2.11}$$

we get (2.6) directly. It should be noted that V as defined in (2.5) is the conditional expectation of a functional defined on $\{x(\tau)\}$ over an interval rather than an ordinary function. Other important functionals on the process are also known to satisfy a backward equation. Some, which have been found useful in the study of stability of randomly perturbed systems are discussed in the next section.

2.2 STABILITY MEASURES

Just as in the study of deterministic systems, it is important to have a measure of system stability when studying randomly perturbed system. It is possible to define stability in probabilistic terms in such a way that the definition is applicable to deterministic systems.

Consider the function $q(t\ ,\ y)$ called the "confinement probability", defined as

$$q(t\ ,\ y) = \text{Prob}\ \{x(\tau) \in N \text{ for all } 0 \leq \tau \leq t \mid x(0) = y\} \tag{2.12}$$

where N is a finite region containing the origin. For a deterministic system the usual definition of stability of the origin corresponds to the following:

Definition - The origin of a deterministic system is stable if and only if for every neighborhood N of the origin, there exists a neighborhood M of the origin such that $q(\infty\ ,\ y) = 1$ for any y in M.

For random systems it is too much to ask for such a strong type of stability; however, the behavior of the confinement probability is still a good indicator of the stability of the system. Roughly speaking, the longer $q(t\ ,\ y)$ stays near one, the more stable the system.

It turns out [4] that $q(t\ ,\ y)$ is one of those functionals defined on the process $\{x(\tau)\}$ which satisfies the backward equation (2.9). Thus, the evolution of $q(t\ ,\ y)$ can be determined by solving (2.9) subject to the obvious boundary conditions $q(0\ ,\ y) = 1$ for all y inside the region N and $q(t\ ,\ y) = 0$ for all y on the boundary of N. Hence, for random systems, stability is no longer a property which is either present or absent, but there are degrees of system stability. In this regard we can measure stability by a quantity t_h called the "half life" of the system defined as the largest time such that $q(t\ ,\ 0) \geq \frac{1}{2}$ for all $t \leq t_h$. Since $q(t\ ,\ y)$ usually decreases monotonically with time, this is the time it takes for the confinement probability to diminish to one-half when the system starts at the origin.

Another measure of system stability is the "average first passage time" to the boundary of the set N. Let the random variable $T(y)$ denote the first time $x(\tau)$ reaches the boundary of N when $x(0)$ starts at the state y.

Let the density function of $T(y)$ be $r_y(\tau)$. Then since $T(y)$ is non-negative, the average first passage time is

$$T(y) = \int_0^\infty \tau\, r_y(\tau)\, d\tau \tag{2.13}$$

It has been shown [1] that $T(y)$ is related to the confinement probability by

$$T(y) = \int_0^\infty \tau\, q(\tau, y)\, d\tau \tag{2.14}$$

and it satisfies a modified form of the backward equation, namely

$$-1 = \nabla T \cdot g + \frac{1}{2} \nabla \cdot [G \Sigma G \nabla T] \tag{2.15}$$

We see from (2.14) that $T(y)$ is a weighted area under the time response of $q(t, y)$, and thus a number with physical meaning can replace the loose notion of keeping $q(t, y)$ as large as possible as long as possible.

2.3 STOCHASTIC OPTIMUM CONTROL

Perfect Sensor Observations - Consider the problem of designing a system with random disturbances such as that of (2.4) so that the cost given in (2.5) is minimized subject to the constraint that $u(\tau)$ be in a given set Ω for all $\tau \in [t, T]$. We assume here that the sensors used to measure the system state are perfect so that $x(\tau)$ can be determined exactly for $\tau \in [t, T]$. It is well-known [2] that when no disturbances are present the minimum cost $V^o(y, t)$ satisfies the Hamilton-Jacobi equation.

$$\frac{\partial V^o}{\partial t} = \min_{u(t) \in U} [L(y, u, t) + \nabla V \cdot f(y, u, t)] \tag{2.16}$$

The optimal feedback law is that $u^o \in U$ which minimizes the bracketed expression. This is of course a function of y and t and is expressed as $u^o(t) = k(y, \nabla V^o, T) = \sigma^o(y, t)$. Note that for the optimum deterministic system, the minimum cost V^o satisfies an equation of type (2.3) in which the right-side is minimized over the allowable controls. It turns out [3] that when disturbances are present the same is true but with respect to (2.6). More explicitly, V^o satisfies the stochastic Hamilton-Jacobi equation

$$-\frac{\partial V^{o}}{\partial t} = \min_{u(t)\in U} [L(y, u, t) + \nabla V \cdot f(y, u, t) + \frac{1}{2} \nabla \cdot (G\Sigma G \nabla V)] \qquad (2.17)$$

and the boundary condition $V(y, T) = 0$. As in the deterministic case the optimal feedback law is that $u^{o} \in U$ which minimizes the bracketed expression and is expressed as $u^{o}(t) = k(y, \nabla V^{o}, t) = \sigma^{o}(y, t)$. Thus, in order to solve the stochastic optimal control problem it is necessary to first solve the nonlinear second-order partial differential equation which results when u^{o} above is inserted for u in (2.17). This is a formidable task and it cannot be done in general.

In the special case of a system with linear dynamics, a quadratic cost functional and no input constraints, a solution is readily obtained. That is to say for the system

$$\dot{x}(\tau) = A(\tau)\, x(\tau) + B(\tau)\, u(\tau) + G(\tau)\, \xi(\tau) \qquad (2.18)$$

with $x(t) = y$ and

$$L(x(\tau), u(\tau), \tau) = \frac{1}{2} [x'(\tau)\, Q(\tau)\, x(\tau) + u'(\tau)\, R(\tau)\, u(\tau)] \qquad (2.19)$$

one finds [3] that the solution to (2.17) is

$$V^{o}(y, t) = y' M(t)\, y \qquad (2.20)$$

where $M(t)$ is a symmetric matrix which satisfies the matrix Riccati equation

$$-\dot{M} = A'M + MA + Q - MBR^{-1} B'M \qquad (2.21)$$

with $M(T) = 0$. The optimal control law is

$$u^{o}(t) = -R^{-1}(t)\, B'(t)\, M(t)\, y \qquad (2.22)$$

where we have been using $y = x(t)$. It is noted that this is exactly the same control law which results when no disturbances are present.

Noisy Sensor Observations - The problem becomes even more difficult when observations of the system state are mixed with noise and a satisfactory general theory of optimal control in this case is not yet available. However, as before in the special case of system (2.18), with noisy observations of the form

$$z(t) = H(t)\, x(t) + \eta(t) \qquad (2.23)$$

where $\{\eta(t)\}$ is a zero-mean white noise process with covariance matrix $\Gamma(t)\,\delta(t-\tau)$ and which is not correlated with the disturbance process $\{\xi(t)\}$, to minimize the quadratic cost functional

$$E\{\frac{1}{2}\int_t^T [x'(\tau)\,Q(\tau)\,x(\tau) + u(\tau)'\,R(\tau)\,u(\tau)]\,d\tau \mid z(\lambda) \text{ for all } \lambda \in [0, t]\} \tag{2.24}$$

it has been shown [3, 5] that the optimal control is that given in (2.22) with y equal to the conditional mean $\hat{x}(t)$ of the true state $x(t)$, given the data $z(\tau)$ for $\tau < t$; $\hat{x}(t)$ is obtained from the optimum Kalman filter [6]

$$\dot{\hat{x}}(t) = A(t)\,\hat{x}(t) + B(t)\,u(t) + P(t)\,H'(t)\,\Gamma^{-1}(t)[z(t) - H(t)\,\hat{x}(t)] \tag{2.25}$$

with $\hat{x}(0) = 0$ and where $P(t)$ satisfies the matrix Riccati equation

$$\dot{P} = AP + PA' + G\Sigma G' - PH'\Gamma^{-1}HP \tag{2.26}$$

with $P(0) = E\{x(0)\,x'(0)\}$ which must be known.

In the more general case where $\{\xi(t)\}$ are correlated such that

$$\text{Cov}\{\xi(t),\ \eta(\tau)\} = S(t)\,\delta(t-\tau) \tag{2.27}$$

then $\hat{x}(t)$ is obtained from

$$\dot{\hat{x}}(t) = A(t)\,\hat{x}(t) + B(t)\,u(t) + K(t)[z(t) - H(t)\,\hat{x}(t)] \tag{2.28}$$

with $\hat{x}(0) = 0$ where

$$K(t) = [P(t)\,H'(t) + G(t)\,S(t)]\,\Gamma^{-1}(t) \tag{2.29}$$

and $P(t)$ satisfies the matrix Riccati equation

$$\dot{P} = AP + PA' + G\Sigma G' - [PH' + GS]\,\Gamma^{-1}[HP + S'G'] \tag{2.30}$$

with $P(0) = E\{x(0)\,x'(0)\}$.

Thus again in the special case of a linear system, quadratic cost and no constraints, a general solution to the optimization problem is available even when the state sensor is noisy, provided it is linear in the state and the noise is additive. If the noise is not white then some additional complexities are introduced but a solution is available even then [7].

3. DESIGN FOR MINIMUM STEADY-STATE VARIANCE

Because the performance requirements for the fine-pointing attitude control problem are so stringent, it is essential that the controller be designed to optimize the performance of the closed-loop system. Ideally, it would be most desirable to use a design which maximizes the mean first-passage-time to the boundary of the angular region outside of which it is impossible to maintain communication. This would insure that the average length of the period of uninterrupted communication would be longest. The region within which it is possible to maintain communication, however, is not sharply defined, because the cross-sectional energy density profile of the beam does not drop sharply to zero, but rather decays gradually in a pattern approximating a Gaussian distribution. Thus as the beam deviates from the center of the receiver, the number of errors per unit time gradually increases. In other words a slight penetration into the "forbidden region" will not necessarily entail instantaneous interruption of communication. For this reason, it would seem feasible to design the control system to minimize the steady-state variance of the beam position from zero. This criterion would permit incursions into the forbidden region but would impose a heavy penalty for such incursions. Another reason for use of steady-state variance as the performance criterion is that it is the only performance criterion for which it is known how to perform the calculations required to accomplish the design.

In Section 2 we reviewed the result that the control system which minimizes the expected value of the integral of a quadratic form $x'Qx + u'Ru$ for a linear process $\dot{x} = Ax + Bu + G\xi$ given noisy measurements $z = Hx + \eta$, comprises the optimum controller for the deterministic process operating on the conditional mean $\hat{x}$. The block diagram for the combined filter which gives $\hat{x}$ and controller is shown in Figure 3.1. Wonham [3] has shown that the controller which minimizes

$$V = E_s(x'Qx + u'Ru) = \lim_{T-t\to\infty} \frac{1}{T-t} E\{ \int_t^T (x'Qx + u'Ru)\, d\tau \mid z(\tau), \tau < t \} \qquad (3.1)$$

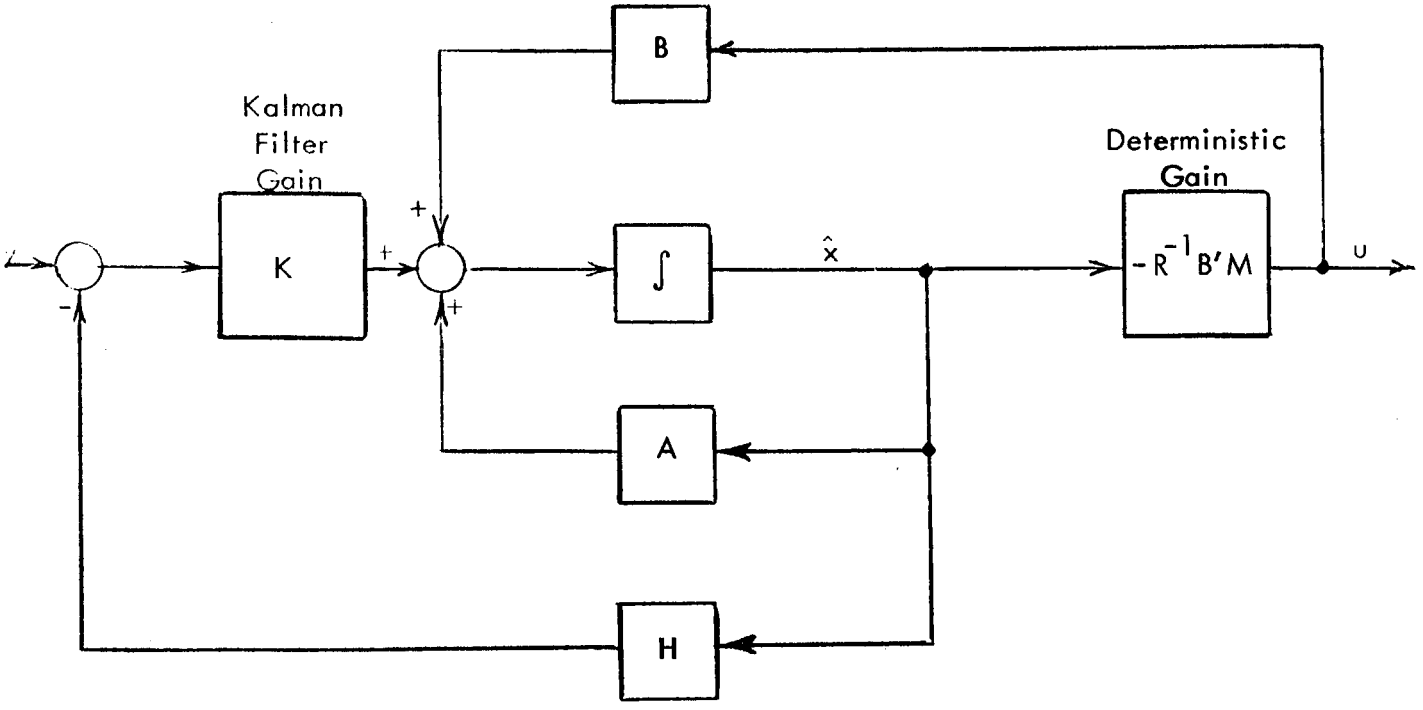

Figure 3.1 - Optimum Steady State Compensating Network
(Combining Estimator and Optimum Gain)

where Q , R , and A , B , G , H are constant matrices, has the same form as shown in Figure 3.1 , but K and M assume their asymptotic values, i.e., M is the solution to (2.21) with $\dot{M} = 0$ and K is given by (2.29) in which P is the solution to (2.30) with $\dot{P} = 0$. (If the process is controllable (observable) then a unique positive definite matrix M (P) exists [6] .) The minimum "asymptotic cost rate" in this case is given by (2.31) in which the asymptotic values of P and M are used.

The optimum controller for this problem is thus linear and time-invariant; it can be represented by the transfer-matrix $C(s)$ defined by

$$U(s) = - C(s)Z(s) \tag{3.2}$$

From Figure 3.1 it is seen that

$$C(s) = R^{-1}B'M\left[sI - \hat{A} + BR^{-1}B'M\right]^{-1}K \tag{3.3}$$

where

$$\hat{A} = A - KH \tag{3.4}$$

The term $u'Ru$ in the performance index (3.1) represents a penalty incurred for using large values of control, and is useful for limiting the total energy to be supplied by the actuator. In processes where the size of the power supply is a critical limiting factor, the use of a fairly large matrix as the control weighting matrix R would be appropriate. If ultimate performance is desired and one is willing to pay the price of the energy required, the matrix R should be made vanishingly small.

In a deterministic process ($\hat{x} = x$) however, omission of control weighting results in infinite gains from the state to the control and leads to the interpretation that the input is a series of impulses with infinite energy which reduces x to zero in an infinitesimal time (provided that the process is controllable).

In the stochastic case, on the other hand, it would appear, intuitively, that infinite control gains are not optimum even in the absence of control weighting, owing to the presence of noise in the observations. This intuition is reinforced by the configuration

of the optimum controller of Figure 3.1: as $R \to 0$, R^{-1} tends to infinity; however, because of the feedback through B, is is anticipated that the transfer function matrix $C(s)$ tends to a meaningful limiting form.

To investigate the nature of $C(s)$ as $R \to 0$, let

$$R = k^2 I \tag{3.5}$$

then, for $k^2 > 0$, the asymptotic form of (2.21) becomes

$$MA + A'M - \frac{1}{k^2} MBB'M + Q = 0 \tag{3.6}$$

the solution of which is expressed as a power series in k:

$$M = M_0 + kM_1 + k^2 M_2 + \ldots \tag{3.7}$$

On substituting (3.7) into (3.6) and equating (matrix) coefficients of like powers of k, it is found that (3.7) is a solution to (3.6) if

$$M_0 B = 0 \tag{3.8}$$

and

$$M_0 A + A'M_0 + Q - M_1 BB'M_1 = 0 \tag{3.9}$$

$$M_1 A + A'M_1 - M_2 BB'M_1 - M_1 BB'M_2 = 0$$

$$M_2 A + A'M_2 - M_1 BB'M_3 - M_3 BB'M_1 - M_2 BB'M_2 = 0$$

Pre-multiplying (3.9) by B', post-multiplying by B, and using (3.8) yields

$$B'M_1 B = (B'QB)^{1/2}$$

Thus, from (3.9) we have

$$B'M_1 = (B'QB)^{-1/2} B'\hat{Q} \tag{3.10}$$

where

$$\hat{Q} = Q + A'M_0$$

Hence M_0 is the solution to

$$\begin{aligned} 0 = {} & M_0 A[I - B(B'QB)^{-1}B'Q] + [I - QB(B'QB)^{-1}B']A'M_0 \\ & + Q - QB(B'QB)^{-1}B'Q - M_0AB(B'QB)^{-1}B'A'M_0 \end{aligned} \tag{3.11}$$

The gain of the deterministic control law is thus given by

$$\begin{aligned} R^{-1}B'M &= \frac{B'}{k^2}(M_0 + kM_1 + \dots) \\ &= \frac{1}{k}[(B'QB)^{-1/2}B'\hat{Q} + kB'M_2 + k^2B'M_3 + \dots] \end{aligned} \tag{3.12}$$

which, as expected, tends to infinity as k^{-1} with $k \to 0$. The transfer matrix $C(s)$ of (3.3), however, becomes

$$C(s) = [B'M_1 + O(k)][k(sI - \hat{A}) + BB'M_1 + O(k)]^{-1}K \tag{3.13}$$

The inverse of the second matrix on the right hand side of (3.13) can be written

$$k(sI - \hat{A}) + BB'\bar{M} = [kI + BB'\bar{M}(sI - \hat{A})^{-1}](sI - \hat{A}) \tag{3.14}$$

where

$$\bar{M} = M_1 + O(k)$$

Hence

$$\begin{aligned} C(s) &= B'\bar{M}(sI - \hat{A})^{-1}[kI + BB'\bar{M}(sI - \hat{A})^{-1}]^{-1}K + O(k^2) \\ &= B'L[kI + BB'L]^{-1}K + O(k^2) \end{aligned} \tag{3.15}$$

where

$$L = L(s) = \bar{M}(sI - \hat{A})^{-1} \tag{3.16}$$

Let

$$F = (kI + BB'L)^{-1}$$

Then

$$kF + BB'LF = I$$

or

$$(kI + B'LB)B'LF = B'L$$

Hence

$$B'LF = (kI + B'LB)^{-1}B'L$$

Thus

$$C(s) = [kI + B'\bar{M}(sI - \hat{A})^{-1}B]^{-1}B'\bar{M}(sI - \hat{A})^{-1}K + O(k^2)$$

Now, passing to the limit as $k \to 0$, we obtain

$$\begin{aligned} C(s) &= [B'M_1(sI - \hat{A})^{-1}B]^{-1}B'M_1(sI - \hat{A})K \\ &= [B'\hat{Q}(sI - \hat{A})^{-1}B]^{-1}B'\hat{Q}(sI - \hat{A})^{-1}K \qquad (3.17) \\ &= [W(s)B]^{-1}W(s)K \end{aligned}$$

where

$$W(s) = B'\hat{Q}(sI - \hat{A})^{-1} \qquad (3.18)$$

This is the required limiting form of $C(s)$.

If B is a nonsingular matrix, then $(WB)^{-1}W = B^{-1}$ and $C(s) = B^{-1}K$, independent of s, (where K is the estimator gain.) Hence, if it is possible to influence each state derivative directly, the optimum closed-loop system has the same dynamics as the optimum estimator; in other words, the optimum feedback network converts the original dynamic system into the optimum estimator of x if it is possible to do so.

Formula (3.17) for the transfer function $C(s)$ is not suitable for mechanical computation, because the calculation of $[W(s)B]^{-1}$ entails the inversion of a matrix of rational functions in s, and hence cannot readily be performed using only arithmetic operations. An effective algorithm for computing $C(s)$ is based on the relation of

$[W(s)B]^{-1}W(s)$ to the following $(n+k)\times(n+k)$ matrix

$$\Lambda(s) = \left[\begin{array}{c|c} sI - \hat{A} & B \\ \hline B'\hat{Q} & 0 \end{array}\right] \quad \begin{matrix} n \\ k \end{matrix} \qquad (3.19)$$

$$= sE - Z$$

where

$$Z = \left[\begin{array}{c|c} \hat{A} & -B \\ \hline -B'\hat{Q} & 0 \end{array}\right]$$

$$E = \left[\begin{array}{c|c} I & 0 \\ \hline 0 & 0 \end{array}\right]$$

It is readily established that

$$\Lambda^{-1}(s) = V(s) = \left[\begin{array}{c|c} V_{11} & V_{12} \\ \hline [W(s)B]^{-1}W(s) & V_{22} \end{array}\right] \qquad (3.20)$$

In other words, the lower left hand submatrix of $V(s) = \Lambda^{-1}(s)$ is the required term $[W(s)B]^{-1}W(s)$, which when postmultiplied by K yields $C(s)$.

By inspection of (3.19) it is seen that

$$V(s) = \frac{N(s)}{d(s)} = \frac{N_0 s^n + N_1 s^{n-1} + \ldots + N_{n-1}s + N_n}{d_1 s^{n-1} + d_2 s^{n-2} + \ldots + d_{n-1}s + d_n} \qquad (3.21)$$

where $N(s) = \text{adj}(sE - Z)$ and $d(s) = |sE - Z|$. The matrices N_j and the scalars d_j are numeric. The objective of the algorithm is the determination of N_j and d_j by use of only arithmetic operations. If (3.19) contained I instead of E, N_j and d_j could be found by the well-known algorithm of Souriau [8] . A modification of Souriau's algorithm is needed because E, not I, appears in (3.21). First, it is observed that

$$|sE - Z| I = (sE - Z)\,\text{adj}\,(sE - Z)$$

or

$$(d_1 s^{n-1} + \ldots d_n) I = (sE - Z)(N_0 + N_1 s^{n-1} + \ldots + N_n)$$

or, upon equating coefficients of s^j $(j = 0, \ldots, n)$

$$ZN_n = -d_n I \tag{3.22}$$

$$\begin{aligned} ZN_{n-1} &= EN_n - d_{n-1} I \\ &\vdots \\ ZN_2 &= EN_3 - d_2 I \\ ZN_1 &= EN_2 - d_1 I \\ ZN_0 &= EN_1 \end{aligned} \tag{3.23}$$

$$0 = EN_0 \tag{3.24}$$

Moreover

$$V(0) = \frac{N_n}{d_n} = -Z^{-1} = \frac{\text{adj}\,(-Z)}{|-Z|}$$

provided that Z^{-1} exists. It thus follows that

$$N_n = \text{adj}\,(-Z)$$
$$d_n = |-Z| \tag{3.25}$$

and these quantities can be determined algebraically by readily available computer programs. It is noted that

$$|Z| = \begin{vmatrix} \hat{A} & -B \\ -B'\hat{Q} & 0 \end{vmatrix} = |B'\hat{Q}\hat{A}^{-1}B|$$

(See [9] pp. 45 - 46). But $\hat{A} = A - KH$ is the matrix corresponding to the minimum variance estimator, which is known to be asymptotically stable if the process is observable [6]. Since asymptotic stability implies that $\hat{A}$ have eigenvalue with strictly negative real parts, $\hat{A}^{-1}$ exists for an observable process.

The existence of Z^{-1}, N_n, and d_n permits rewriting (3.23) as

$$N_{n-j} = Z^{-1}(EN_{n-j+1} - d_{n-j}I) \qquad j = 1, \ldots, n \tag{3.26}$$

$$d_0 = 0$$

as the recursive formula for computation of N_{j-1} in terms of N_j and d_{j-1}. Equation (3.25) serves as a check.

A similar recursive relation for the coefficients of $d(s) = |sE - Z|$ is obtained with the aid of the well-known relation

$$\frac{d\,|M(s)|}{ds} = \text{trace}\left[\frac{dM(s)}{ds}\,\text{adj}\,M(s)\right] \tag{3.27}$$

for any matrix $M(s)$. Applying this relation to $V(s) = sE - Z$ results in

$$(n-1)d_1 s^{n-2} + (n-2)d_2 s^{k-3} + \ldots + d_{n-1} = \text{trace}\,[E(N_0 s^n + N_1 s^{n-1} + \ldots + N_n)]$$

or, equating coefficients of like powers of s

$$\begin{aligned} 0 &= \text{trace}\,(EN_0) \\ 0 &= \text{trace}\,(EN_1) \\ d_1 &= \frac{1}{n-1}\,\text{trace}\,(EN_2) \\ &\vdots \\ d_{n-1} &= \text{trace}\,(EN_n) \end{aligned} \qquad (3.28)$$

Thus (3.26), (3.28) together with the starting condition (3.25) provide the required algorithm.*

Since the numerator of $V(s)$ given by (3.21) contains the term $N_0 s^n$ it might seem that the numerator of $[W(s)B]^{-1}W(s)$ is of higher degree than the denominator; this would imply that the controller, represented by $C(s)$, would be required to differentiate the sensor output, which would be an unacceptable design. Fortunately, however the lower left hand submatrix of N_0, in fact all terms except those in the lower right hand submatrix of N_0 are also zero, since the n-th degree cofactors of $\Lambda(s)$ all appear in the lower right hand positions of $V(s)$. Thus the numerator of $[W(s)B]^{-1}W(s)$ is of no higher degree than the denominator. In general, terms of degree $n-1$ will be present in $[W(s)B]^{-1}W(s)$, and hence there will be a direct path from the sensors to the control input. It should also

* A digital computer program for performing the calculation of the algorithm has been prepared.

be noted that the denominator of all terms of $C(s)$ will be of degree $n-1$ (or less**), and hence $C(s)$ can be realized by use of a system of at most $(n-1)$ st order, instead of requiring the n-th order system which is needed when control weighting is used. Since the required transfer function $C(s)$ is of lower degree than the order of the process controlled, it is evident that conditional mean $\hat{x}$ is not generated explicitly in the controller.

Several problems with the above method merit further attention. First, because no weighting is placed on u in the performance criterion, $E_s(u'u)$ is infinite in general because the numerator and the denominator of $C(s)$ are the same degree. Hence the "white" noise present in y gets through to u. This cannot be regarded as a practical difficulty: if it were, it would be necessary to dispose of all feedback systems with a direct path from the output to the input which are in common use. The reason why the apparent presence of "white" noise on u is no difficulty is that white noise is only a mathematical abstraction which is useful for design purposes but does not exist physically. A more accurate description of the physical situation would reveal that the noise has a spectrum which decays to zero for sufficiently high frequencies but is substantially flat at the frequencies of interest for the control system operation. With this representation, $E_s(u'u)$ remains finite. A more accurate noise model could probably be accomodated by use of well-known techniques, but the results should not differ materially from those obtained here and would entail more computational effort.

Another problem, which W.M. Wonham has pointed out in discussion and correspondence with the authors, is due to the formal derivation employed. Although the control law obtained with arbitrarily small (but nonzero) control weighting is known to exist and result in a closed-loop control system which is asymptotically stable when the process is observable and controllable, the same facts remain to be rigorously established when the control weighting vanishes .

The intuitive appeal of this design approach, however, has motivated its use in the current study.

** It can be shown, in fact, that the numerators and denominator of $C(s)$ are of degree $n-k$, where k is the rank of B.

4. CONTROL SYSTEM DESCRIPTION

4.1 VEHICLE DESCRIPTION

Based on information supplied by NASA/ERC and several discussions with NASA personnel, we arrived at a "conceptual" spacecraft having the appearance shown in Figure 4.1 . The vehicle comprises a heavy (1300 kg) central core, 2 m long and 1 m in radius, which contains the electronic equipment, sensors, power conditioning equipment, etc. The power for the entire system, including the laser transmitter, is derived from solar paddles which (by means of a separate control system) are kept oriented to the sun. Based on solar cells of improved efficiency* we calculated that a total area (in 2 panels) of about $24 m^2$, and weighing about 100 kg, would be required to provide the total power demand of about 2000 watts, which is a rough estimate of the total power requirement.

Extending from the vehicle body is a lightweight sunshield and optical structure weighing 100 lbs., 4 m in length and 0.5 m in radius.

This spacecraft orbits the planet under examination, which in this study was assumed to be Mars. For simplicity, it was assumed that the vehicle orbital plane coincides with the solar ecliptic plane and that the Earth and Mars also move in this plane. (This assumption is not necessary in practice, but without it the derivation of the linearized model would be more tedious.) It was also assumed that the spacecraft orbit around Mars is circular at an altitude of 400 km. The corresponding orbital period is 2.05 hours. Since Mars occludes the earth for nearly half the orbital period, one hour is all the time available for uninterrupted communication.

It would be desirable to maintain communication for as large a fraction of this time as possible by proper control system design.

* Current state-of-the-art [10] indicates an efficiency of about $50 m^2/kw$. Hence an improvement in efficiency by a factor of about 4 is assumed.

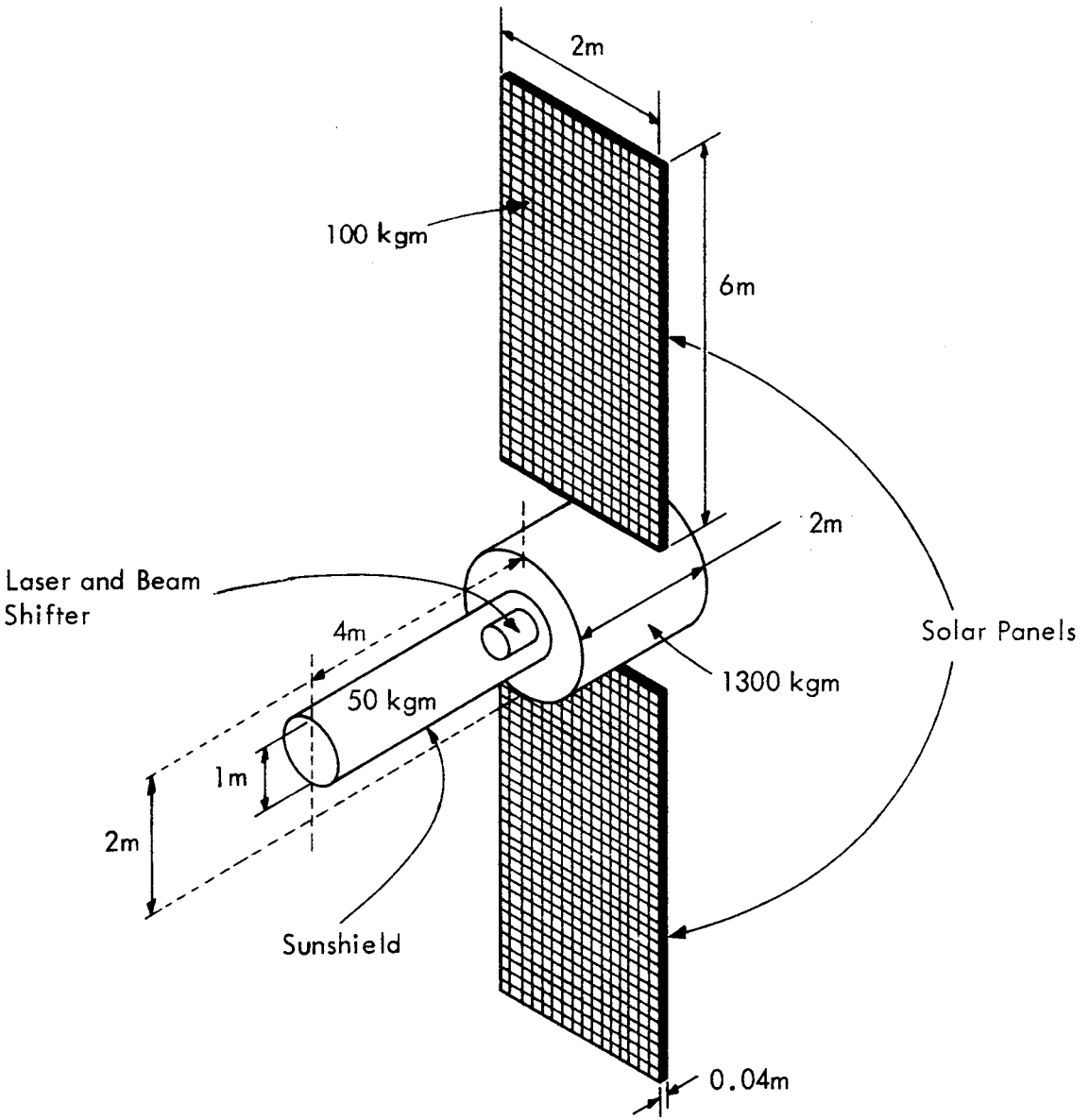

Fig. 4.11 - SCHEMATIC DIAGRAM OF LASER COMMUNICATION VEHICLE

The present study is concerned with the design and performance evaluation of the spacecraft attitude control system, the function of which is to maintain the mechanical axis pointed at the receiving telescope as closely as possible. The control system for the mechanical loop is shown by heavy lines in Figure 1.1. The system comprises the vehicle, the sensors (star-tracker and rate-sensors), the actuators, and the controller.

To derive the differential equations governing the spacecraft motion, the complete nonlinear equations of motion were derived. The state variables employed were the Euler angles of the body axes with respect to an inertially-fixed reference frame, the components of the vehicle angular velocity vector along the reference frame, the speeds of the reaction wheels, (see description below) and the speeds of the paddles. This results in an 11th order nonlinear system. These equations were then linearized about the assumed nominal motion described above to obtain an 11th order linear system. The details of the calculation are given in the Appendix and the resulting linear equations are given in Section 6.

4.2 ACTUATORS

A typical actuation system which could be used for the fine-pointing problem would comprise a momentum interchange device (in which angular momentum of the vehicle, in excess of that required to maintain the desired motion is transferred to another rotating device such as a reaction wheel or a control moment gyro) and a momentum discharge device such as reaction jets. In the absence of any mechanism for removal of momentum from the complete system, it is not possible to remove vehicle momentum indefinitely without causing the reaction wheel or control moment gyro to saturate. Consequently a momentum discharge device must be provided. In principle, it would be possible to use a momentum discharge device alone. This would be undesirable for two practical reasons. First, in order to remove system momentum it is necessary to discharge mass which must necessarily be carried in the vehicle in place of useful payload. Second, a reaction jet system which is operated frequently will invariably develop leaks which would have the effect of disturbance torques, the magnitude of which, in current state-of-the-art equipment could exceed the level of the disturbance torques due to other sources. The case in favor of using a dual system, however, is not entirely clear cut: the momentum interchange device must, of

course, have some weight in order to be effective. Moreover, with ion engines, it might be possible to obtain very precisely controlled torque levels at very high specific impulse. Such actuators could compare favorably or even be superior to the dual system. In view of the relative novelty of ion-engines, we have elected to consider the more conventional approach. Specifically, we have assumed that during the relatively short periods of precise control, only the momentum interchange device is operative. We have further assumed that reaction wheels, rather than control moment gyros are used. For each axis a pair of wheels, with axis coincident with the corresponding body axis was assumed, and each wheel of the pair was taken to have a mass of 5 kg, a radius of gyration of 10.61 cm, a thickness of 3 cm. This results in a moment of inertia of 0.1125 kg-m^2 about the axis of rotation, which would appear to be a reasonable size for the spacecraft considered here.

The wheels were assumed to be driven by ideal d-c torquers (no damping or other losses) having the dynamic relation

$$L = \alpha V + \beta \omega_w$$

where

L = delivered torque

V = applied control voltage

ω_w = reaction wheel speed, relative to body

The no-load speed ω_{NL} was taken as 100 rad/sec ($\approx$ 1000 rpm) and the time constant of the torquer driving the wheel was taken as 30 sec. The stall torque was taken as $T_s = -\beta \omega_{NL} = 0.375$ newton - m which was assumed to be developed with a control voltage of 25 v. As a consequence of these assumptions it is found that

$$\alpha = 1.5 \times 10^{-2} \text{ newton - m/v}$$

$$\beta = -3.75 \times 10^{-3} \text{ newton - m - sec/rad}$$

(See Appendix for calculation details)

4.3 SENSORS

Star-Tracker - The primary sensor of spacecraft motion is a 3-axis star tracker which can determine the vehicle attitude by determining the location of the images of fixed stars on a calibrated detecting surface, or by maintaining these fixed stars in the exact center of a movable optical field and then reading the position of the field with respect to the vehicle body axes. There are numerous methods for constructing such a sensor. Moreover, new mechanical configuarations are likely to be evolved during the next decade. For this reason, we did not consider any specific form of star tracker.

In every realization of the device, however, there will always be a number of errors inherent in the measurement of spacecraft attitude. As discussed in the Introduction, these errors may be grouped into two categories: static or d-c errors resulting from such factors as null uncertainty misalignment of sensor axes from vehicle body axis (i.e., uncertainty in the position of the sensor axes with respect to the body axes) and random errors due to noise. While, in present-day sensors the d-c errors are the principal sources of closed-loop system error, they have not been considered in the present study in order to focus attention on the effects of random errors. As previously noted, because of the presence of the optical vernier loop, the omission of d-c error sources is not entirely unrealistic.

The random errors in each star-tracker were modeled by "equivalent white noise". To obtain the spectral density of the equivalent white noise it was assumed that the actual noise consists of white noise passed through a first-order filter with a very short time constant equal to the tracker "correlation time", (the time required to process the data to achieve the specified static accuracy) and that the steady-state standard deviation σ of the output of this filter is equal to the nominal sensor accuracy. This has the effect of approximating the correlation of the output $\sigma^2 \exp(-|\tau|/T)/2$ by an impulse correlation function $\sigma^2 T\, \delta(\tau)$ of the same amplitude. The spectral density of the star-tracker noise is thus $\sigma^2 T$.

A typical star tracker would have a static accuracy of about 10 $\widehat{\text{sec}}$ and a correlation time of about 1 ms. Thus the spectral density of the equivalent white noise was calculated to be

$$\sigma^2_T = (10)^2 \times 10^{-3} \ \widehat{\text{sec}}^2 \ \text{sec}$$

$$= \left(\frac{10\,\pi}{3600 \times 180}\right)^2 \times \frac{10^{-3}}{60} \ \text{rad}^2 - \text{min}$$

$$= 3.9 \times 10^{-14} \ \text{rad}^2 - \text{min}$$

This is the numerical value used for the spectral density of the star-tracker equivalent white noise.

Tachometer - Since a reaction wheel actuator is normally equipped with a tachometer to measure its speed relative to the spacecraft, it was felt that the tachometer would serve as a useful sensor of the vehicle motion for control purposes. As in the case of the star-tracker, all the sources of error were represented as a single equivalent white noise source. The standard deviation σ was conservatively estimated at 30 rpm which is several percent of the highest anticipated operating speed. The correlation time was taken as 10 ms, corresponding to about one revolution of the tachometer at maximum speed. The use of this figure as a correlation time was verified with several engineers acquainted with tachometer error sources.

The resulting spectral density of the tachometer equivalent white noise is thus given by

$$\sigma^2_T = (30 \times 2\pi)^2 \times \frac{10^{-2}}{60} = 5.9 \left(\frac{\text{rad}}{\text{min}}\right)^2 - \text{min}$$

Rate - Gyro - In addition to tachometers, we considered using rate-gyros to measure spacecraft body rates. As for the other sensors, the errors were modeled by equivalent white noise. The steady-state accuracy was taken as σ = 3 millivolts, where the sensitivity is 260 millivolts/(degree/sec). The correlation time was taken as .01 sec. These figures are typical of the C70 2021 Series of Rate Gyros manufactured by General Precision. The resulting spectral density used is thus

$$\sigma^2_T = \left(\frac{3\pi}{260 \times 180}\right)^2 \times 60 \times 10^{-2} = 2.4 \times 10^{-8} \left(\frac{\text{rad}}{\text{min}}\right)^2 - \text{min}$$

4.4 DISTURBANCE TORQUES

There are two types of disturbance torques on the vehicle. The first type is due to purely random natural phenomena. The principal disturbance in this class results from the bombardment of the vehicle by micrometeoroids; the effect of this bombardment on the vehicle motion is not negligible, and hence the design of a control system to counteract the effects of this disturbance is not merely an academic exercise. Gas leaks are another source of random torques.

The second type of disturbance torques is that caused by non random phenomena, such as thermal distortion, gravity gradient, etc. In principle, such torques could be completely counteracted in the control system design by programming equal and opposite control torques. For practical reasons, however, the feedback mechanism of the control system would be relied upon to provide the appropriate counter-torques. Although these disturbance torques are estimated below for the sake of completeness, it is emphasized that the effects of these torques is not the main concern of this investigation.

Random Process Torques

Micrometeoroid Bombardment - According to an analysis of Mariner IV data [11] the flux of particles in the vicinity of Mars can be expressed as

$$\Phi = \alpha m^{\beta} \text{ particles/m}^2 \text{ sec } (\pi \text{ steradian})$$

where α and β are constants and m is the particle mass. The zodiacal dust experiment on board Mariner IV counted particles whose momenta were larger than $m = 1.96 \times 10^{-3}$ dyne-sec. Assuming that all particles have the same velocity $v = 10^5$ cm/sec., we find that the lower limit on particle mass is $m_1 = 1.96 \times 10^{-8}$ gm. We also assume an upper limit on particle mass of 1 gm, $\Phi = 1.8 \times 10^{-4}$ particles/m^2 sec. (π steradian), and $\beta = -0.6$. Thus the upper limit on particle momentum is $m_2 = 10^5$ dyne-sec.

Using the same approach as that of Section 2 of [12] we find that the value of α does not affect the micrometeoroid momentum probability distribution which has a mean $\overline{m}$,

$$\bar{m} = \frac{\beta}{\beta+1} \frac{m_2^{\beta+1} - m_1^{\beta+1}}{m_2^{\beta} - m_1^{\beta}} = .397 \text{ dyne-sec}$$

and a variance

$$\theta^2 = \frac{\beta}{\beta+2} \frac{m_2^{\beta+2} - m_1^{\beta+2}}{m_2^{\beta} - m_1^{\beta}} - \bar{m}^2 = 1 \times 10^5 \text{ (dyne-sec)}^2$$

Thus, the momentum bombardment process striking the symmetric vehicle is assumed to be zero-mean white noise with variace $\sigma^2 \delta(t)$ where [12]

$$\sigma^2 = 4\Phi\theta^2 = 7.2 \times 10^{-3} \text{ (dyne-sec)}^2/\text{cm}^2 - \text{sec}$$

To convert this momentum process to an angular-acceleration white noise disturbance process with variance $c^2\delta(t)$ we use (5.24) in [1] with $A = 12\ \text{m}^2$, $r = 3.8$ m, $J = 100$ n - m- min^2 and obtain

$$c^2 = r^2 A\sigma^2/J^2$$

$$= 1.8 \times 10^{-12} \text{ (rad/min)}^2 - \text{min}$$

Gas Leaks - It would appear reasonable to model the random torques due to gas leaks by a Poisson step process, i.e. a random step process with Poisson-distributed transition times and normally-distributed transition levels.

A crude estimate of the magnitude of the parameters of the gas leak process was obtained from Mariner IV data [1]: it was estimated that the average transition rate was 0.02/hr and the standard deviation of the amplitude of torque was 4 dyne-cm.

If reaction wheel control is used for the laser vehicle, we can expect similar torques from this source, allowing for the less frequent use of the gas jets (for removing momenta from reaction wheels) and the larger size of the vehicle.

It is noted that gas leaks are not a natural phenomenon; their magnitude depends on the quality of the valves and other hardware used in the system. Hence, the numerical values of the parameters describing the gas leak process can be made arbitrarily small de-

pending on care exercised in the fabrication of the system. It would be of interest to determine the quality of equipment actually needed either to accomplish the desired objective or to make the effects of the gas leaks insignificant relative to micrometeoroids which physically cannot be eliminated.

Deterministic Torques

Gravity Gradient - A significant deterministic disturbance torque is that caused by the gradient of the gravitational field of Mars. The magnitude of this torque can be estimated by assuming that the vehicle in orbit about Mars can be represented by two equal point masses connected by a massless rod. Based on this assumption we find that the maximum gravity gradient torque is approximated by

$$T_{mg} = gI/R$$

where g is the local Martian gravitational acceleration, R is the radius of Mars and I is the moment of inertia of the object. Using data which is representative of the laser communication vehicle: weight (Earth) = 3000 lb, radius of gyration = 1 meter, we find that

$$T_{mg} = 1.5 \times 10^{4} \text{ dyne-cm}$$

which corresponds to an angular acceleration of about 10^{-6} rad/sec^2.

Aerodynamic - Another significant deterministic disturbance torque is the aerodynamic torque due to lift and drag forces acting on the vehicle as it moves through the atmosphere of Mars. Although this torque is a function of the angle of attack of the vehicle, its maximum value can be approximated by

$$T_{ma} = \frac{1}{2} \delta v^2 sS(C_{L\alpha} + C_D)/I$$

where δ is the density of the Martian atmosphere, v is the orbital velocity, s is the distance between the center of mass and center of pressure of the vehicle, S is reference area, C_D is the drag coefficient, and $C_{L\alpha}$ is related to the lift coefficient of the vehicle. From [13] we find that at a height of 200 km, δ is approximately 0.5×10^{-15} gms/cm^3. Using this figure and the following representative values:

$$\text{Weight} = 3000 \text{ lb}$$

$$\text{Radius of gyration} = 1 \text{ m}$$

$$C_{L\alpha} + C_D = 2$$

$$S = 100\pi/4 \text{ m}^2$$

$$s = 5 \text{ m}$$

$$v = 24 \times 10^3 \text{ m/sec}$$

we find that

$$T_{ma} = 0.8 \times 10^3 \text{ dyne-cm}$$

Because of the exponential variation of density with altitude, the aerodynamic torque is a very sensitive function of the vehicle orbit.

Thermal Distortion - As the communication vehicle orbits Mars maintaining an approximately constant orientation towards the sun, thermal distortion of materials will cause a change in the vehicle shape which can be interpreted as the effect of additional disturbance torques which will, of course, depend on the type of materials used in the vehicle. Three techniques might be applicable to compensate for these thermal distortions: 1) If the thermal distortion can be predicted to sufficient accuracy, the vehicle might be designed to have an inherent shift of center of gravity which will be essentially "equalized" naturally as the vehicle reaches the Martian orbital environment; 2) Compensating elements with inverse thermal characteristics to those of the principal components might be added to the vehicle to counteract the thermal expansion of the principal parts; 3) Any biases caused by thermal distortion could possibly be estimated by an appropriate filter in the attitude control system.

Magnetic Induction - Interaction of the moving vehicle with the magnetic field of Mars is another source of disturbance torque which is essentially deterministic. This interaction results in eddy current torques as well as torques caused by the interaction of Mars' magnetic field with magnetic fields internal to the vehicle. Clearly these torques will also be a sensitive function of the type and configuration of materials used in the vehicle. However,

it has been found from Mariner IV data [11] that the magnetic field of Mars is not more than 0.001 that of Earth. Thus, it would appear that electromagnetic torques will not be a major source of disturbance torques.

Internal Moving Parts - The normal functioning of the communication vehicle will involve the motion of parts of the vehicle: solar panels, antennas, or the beam shifter. The motion of these objects is another source of disturbance torques. The effect of this motion is incorporated directly into the dynamic equations of the vehicle as discussed in the Appendix.

Reflectivity Unbalance - A numerical estimate of the disturbance torque due to solar reflectivity unbalance can be obtained from our analysis of a segment of Mariner IV telemetry data [1]. It was found that a bias of 20 dyne-cm could be attributed to reflectivity unbalance. Since the laser communication vehicle may have a surface area an order of magnitude or two greater than that of Mariner IV, the same care as was exercised in the design of Mariner IV could result in torques as large as 2000 dyne-cm from this source.

5. SINGLE-AXIS STUDY

To gain insight into the structure of the fine-pointing attitude control system we have considered the control of a single-axis under the assumption that the solar panels do not deviate from their nominal motion. We have assumed that the momentum interchange device for the single axis is a reaction wheel driven by a d-c torquer. Three different sensor configurations were examined: star tracker and tachometer, star tracker and rate gyro, and a combination of star tracker, tachometer, and rate gyro. The characteristics of these components are given in Sections 4.2 and 4.3 .

The equations of motion of the vehicle and reaction wheel are

$$J\ddot{\theta} = L + \xi \tag{5.1}$$

$$I_w(\dot{\omega}_w + \ddot{\theta}) = -L \tag{5.2}$$

where the center of mass of the wheel coincides with the center of mass of the vehicle, J is the moment of inertia of the vehicle, I_w is the moment of inertia of the wheel, θ is the angular position of the vehicle, ω_w is the angular velocity of the wheel with respect to the vehicle, L is the control torque, and ξ is an external distrubance torque caused by micrometeoroid bombardment. We assume that the control torque is provided by an electric motor,

$$L = \alpha u + \beta\omega_w \tag{5.3}$$

where α and β are constants and u is the applied voltage.

If we define the state vector x as

$$x = \begin{bmatrix} \omega \\ \omega_w \\ \theta \end{bmatrix}$$

where ω is the angular velocity of the vehicle, then (5.1) - (5.3) become

$$\dot{x} = Ax + Bu + G\xi \tag{5.4}$$

where

$$A = \begin{bmatrix} 0 & \beta/J & 0 \\ 0 & (-\beta/J)(J/I_w + 1) & 0 \\ 1 & 0 & 0 \end{bmatrix}, \quad B = \begin{bmatrix} \alpha/J \\ (-\alpha/J)(1 + J/I_w) \\ 0 \end{bmatrix}, \quad G = \begin{bmatrix} 1/J \\ -1/J \\ 0 \end{bmatrix} \tag{5.5}$$

Note that (5.4) and (5.5) could also be obtained from the complete 3-axis dynamics of Section 6 by assuming that the solar panels do not deviate from their nominal motion (i.e., $\lambda_4 = \lambda_5 \equiv 0$), and that no reaction jet control is used. To correspond to the numerical values of the previous section we have

$$\beta/J = 10^{-4}, \quad \frac{\alpha}{J} = 2 \times 10^{-2}, \quad [1 + J/I_w] = 2 \times 10^{4}, \quad 1/J = 2 \tag{5.6}$$

where the disturbance ξ is zero-mean white noise with variance $\sigma^2\delta(t)$, $\sigma^2 = 1.8 \times 10^{-12}$ $(\text{rad/min}^2)^2$ - min., as computed in Section 4.4.

A controller for system (5.4) was designed using the performance criterion of Section 3, $\overline{W} = E_s[x'Qx]$, where

$$Q = \begin{bmatrix} q_2^2 & 0 & 0 \\ 0 & 0 & 0 \\ 0 & 0 & q_1^2 \end{bmatrix} \tag{5.7}$$

Note that the performance criterion serves to minimize the expected vehicle position and velocity deviations, without regard to the velocity attained by the reaction wheel. The performance of the single axis was determined for each of the above sensor configurations.

5.1 STAR TRACKER AND TACHOMETER

We assume that the measurements available to the controller are angular position,

provided by a star tracker, and angular velocity of the reaction wheel, provided by a tachometer. Thus, the measurement vector $z = [z_1 \ , \ z_2]$ is given by

$$z = Hx + \eta \tag{5.8}$$

where

$$H = \begin{bmatrix} 0 & 1 & 0 \\ 0 & 0 & 1 \end{bmatrix} \tag{5.9}$$

and $\{\eta\}$ is zero-mean white noise with covariance matrix

$$\Sigma_\eta = \begin{bmatrix} \sigma_w^2 & 0 \\ 0 & \sigma_\theta^2 \end{bmatrix} \delta(t) \ , \qquad \begin{aligned} \sigma_w^2 &= 5.915 \left(\frac{\text{rad}}{\text{min}}\right)^2 \text{- min.} \\ \sigma_\theta^2 &= 3.9 \times 10^{-14} \ (\text{rad})^2 \text{ - min.} \end{aligned} \tag{5.10}$$

Using the nomenclature of Section 3 we find that

$$K = \begin{bmatrix} -.0955 \times 10^{-12} & 6.7 \\ .0653 \times 10^{-12} & -2.56 \\ -.0169 \times 10^{-12} & 3.66 \end{bmatrix} , \quad \hat{A} = \begin{bmatrix} 0 & 10^{-4} & -6.7 \\ 0 & -2 & 2.56 \\ 1 & .0169 \times 10^{-12} & -3.66 \end{bmatrix} , \quad \hat{Q} = \begin{bmatrix} q_2^2 & 0 & q_1 q_2 \\ 0 & 0 & 0 \\ 0 & 0 & q_1^2 \end{bmatrix} \tag{5.11}$$

where the off-diagonal term in $\hat{Q}$ is the contribution of $A' M_0$ and where

$$P = \begin{bmatrix} .961 \times 10^{-12} (\text{rad/min})^2 & -.565 \times 10^{-12} (\text{rad/min})^2 & .262 \times 10^{-12} (\text{rad}^2/\text{min}) \\ -.565 \times 10^{-12} (\text{rad/min})^2 & .386 \times 10^{-12} (\text{rad/min})^2 & -.0997 \times 10^{-12} (\text{rad}^2/\text{min}) \\ .262 \times 10^{-12} (\text{rad}^2/\text{min}) & -.0997 \times 10^{-12} (\text{rad}^2/\text{min}) & .1429 \times 10^{-12} (\text{rad})^2 \end{bmatrix} \tag{5.12}$$

is the asymptotic solution to the variance equation (2.21), obtained by numerical integration.

The elements of the weighting matrix Q were obtained as follows: because the angular position accuracy is of critical importance to the fine pointing system a significant weighting was assigned to deviations in angular position: a ratio $q_1/q_2 = 10$ was selected.

A number of other weighting ratios were also examined, and the influence of the weighting ratio on the performance of the resulting control system will be discussed below.

From (3.17) we find that, for $q_1/q_2 = 10$, we have

$$U(s) = -[G_1(s) \ , \ G_2(s)]\ Z(s) \tag{5.13}$$

where

$$G_1(s) = \frac{(-50 \times 10^{-12})(0.3s^2 + 1.7s + 2.8)}{s(s + 14)}$$

$$G_2(s) = 50\frac{43s^2 + 154s + 233}{s(s + 14)} \tag{5.14}$$

If we represent the controller by the dynamic system

$$\dot{q} = \bar{F}q + \bar{G}z \tag{5.15}$$

where

$$\bar{F} = \begin{bmatrix} 0 & 0 \\ 0 & -14 \end{bmatrix} \ , \quad \bar{G} = \begin{bmatrix} 10 \times 10^{-12} & -832.143 \\ -135 \times 10^{-12} & 23232.143 \end{bmatrix} \tag{5.16}$$

then

$$u = \bar{K}q + \bar{L}z \tag{5.17}$$

where

$$\bar{K} = [1 \ , \ 1] \quad , \quad \bar{L} = [15 \times 10^{-12} \ , \ -2150] \tag{5.18}$$

The closed-loop system shown in Figure 5.1, is given by

$$\begin{bmatrix} \dot{x} \\ \hline \dot{q} \end{bmatrix} = \left[\begin{array}{c|c} A + B\bar{L}H & B\bar{K} \\ \hline \bar{G}H & \bar{F} \end{array}\right] \begin{bmatrix} x \\ \hline q \end{bmatrix} + \left[\begin{array}{c|c} G & B\bar{L} \\ \hline 0 & \bar{G} \end{array}\right] \begin{bmatrix} \xi \\ \hline \eta \end{bmatrix} = \tilde{A} \begin{bmatrix} x \\ \hline q \end{bmatrix} + \tilde{B} \begin{bmatrix} \xi \\ \hline \eta \end{bmatrix} \tag{5.19}$$

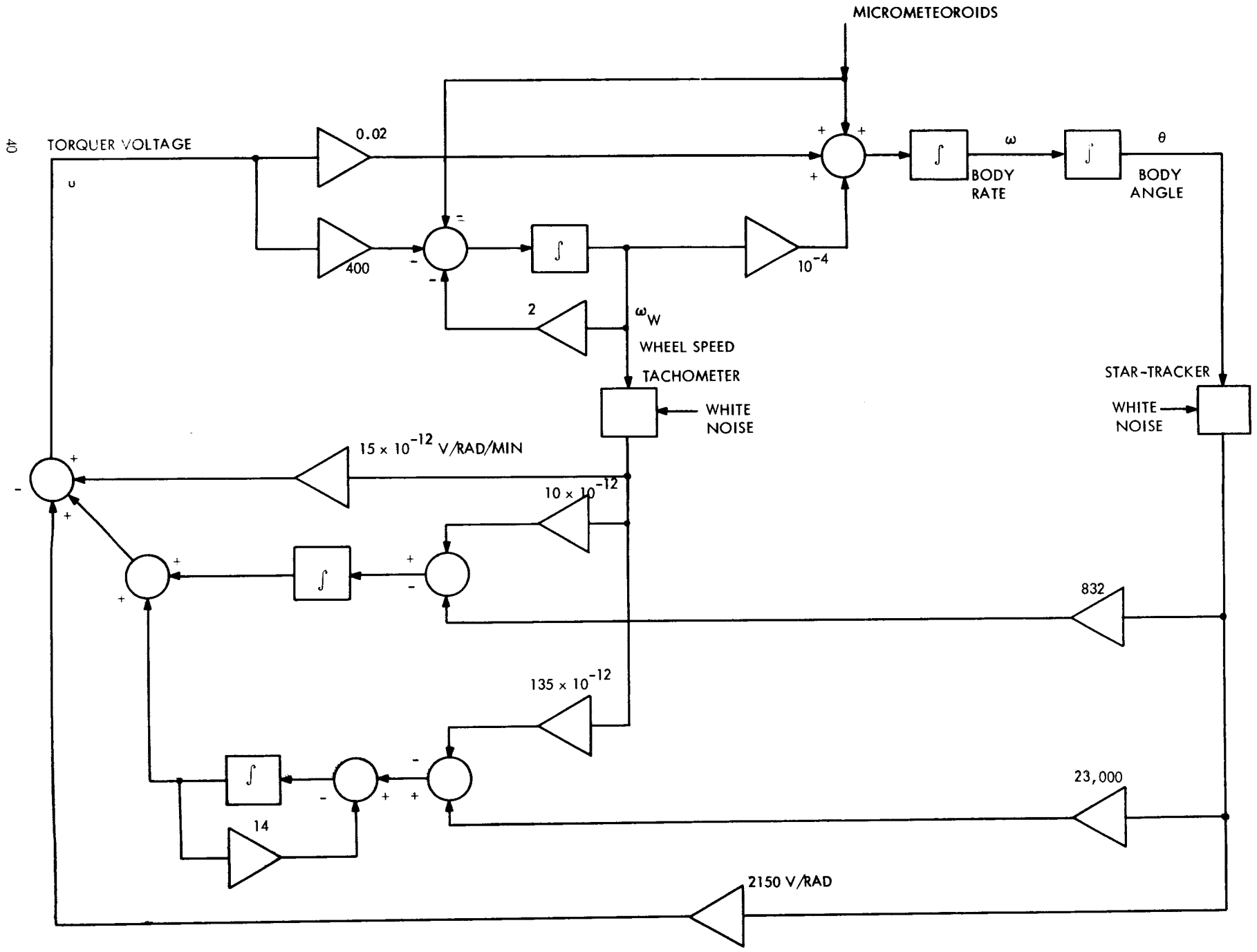

SINGLE-AXIS CONTROL SYSTEM - STAR-TRACKER AND TACHOMETER

FIGURE 5.1

where

$$\tilde{A} = \begin{bmatrix} 0 & 10^{-4} & -43 & 2 \times 10^{-2} & 2 \times 10^{-2} \\ 0 & -2 & 86 \times 10^{4} & -4 \times 10^{4} & -4 \times 10^{2} \\ 1 & 0 & 0 & 0 & 0 \\ 0 & 10^{-11} & -832.143 & 0 & 0 \\ 0 & -1.35 \times 10^{-10} & 23232.143 & 0 & -14 \end{bmatrix} \tag{5.20}$$

and

$$\tilde{B} = \begin{bmatrix} 1 & 30 \times 10^{-14} & -43 \\ -1 & -60 \times 10^{-10} & 86 \times 10^{4} \\ 0 & 0 & 0 \\ 0 & 10 \times 10^{-12} & -832.143 \\ 0 & -1.35 \times 10^{-10} & 23232.143 \end{bmatrix} \tag{5.21}$$

It is of interest to compare the response to random distrubances of the uncontrolled vehicle with the response of the closed-loop system designed above. Since the $\{\xi, \eta\}$ process is white noise, the output of the closed-loop system is a Markov process with covariance matrix $M_c(t)$ which satisfies

$$\dot{M}_c = \tilde{A} M_c + M_c \tilde{A}' + \tilde{B} \Sigma \tilde{B}' \quad , \quad M_c(0) = 0 \tag{5.22}$$

where

$$\Sigma = \begin{bmatrix} \sigma^2 & 0 & 0 \\ 0 & \sigma_w^2 & 0 \\ 0 & 0 & \sigma_\theta^2 \end{bmatrix} \tag{5.23}$$

Sinilarly, the open-loop (uncontrolled) system has the covariance matrix M_0 ,

$$\dot{M}_0 = AM_0 + M_0A' + BB'\sigma^2 \quad , \quad M_0(0) = 0 \tag{5.24}$$

Figure 5.2 contains a comparison of the 1-1 components of M_c and M_0 . The figure indicates that during a 30 minute interval the closed-loop system maintains the angular position of the vehicle to an accuracy which represents an improvement of several orders of magnitude compared with that of the uncontrolled system. Note that $M_c(t)$ reaches a steady-state whereas $M_0(t)$ is monotonically increasing. At the end of the 30 minute interval the angular position standard deviation of the open-loop system is 26.8 $\widehat{\text{sec}}$ whereas that of the controlled system is .089 $\widehat{\text{sec}}$. Thus the linear closed-loop system using a star tracker and tachometer achieves a significant improvement in steady-state angular position accuracy for the single-axis subject to micrometeoroid bombardment. It is interesting to note, however, that as indicated in Figure 5.3, for small values of time the angular position variance of the uncontrolled system is lower than that of the closed-loop system.

Using a digital computer simulation we investigated the performance of the single-axis controller for various values of the parameter $\lambda = q_1/q_2$. Table 5.1 indicates the variation with λ of steady-state vehicle angular position variance P_θ and steady-state vehicle angular velocity variance P_ω .

TABLE 5.1

STEADY - STATE PERFORMANCE

λ	P_θ in rad^2	P_ω in rad^2/min^2
5	$.282 \times 10^{-12}$	$.299 \times 10^{-11}$
10	$.187 \times 10^{-12}$	$.363 \times 10^{-11}$
50	$.149 \times 10^{-12}$	$.141 \times 10^{-10}$
100	$.146 \times 10^{-12}$	$.271 \times 10^{-10}$

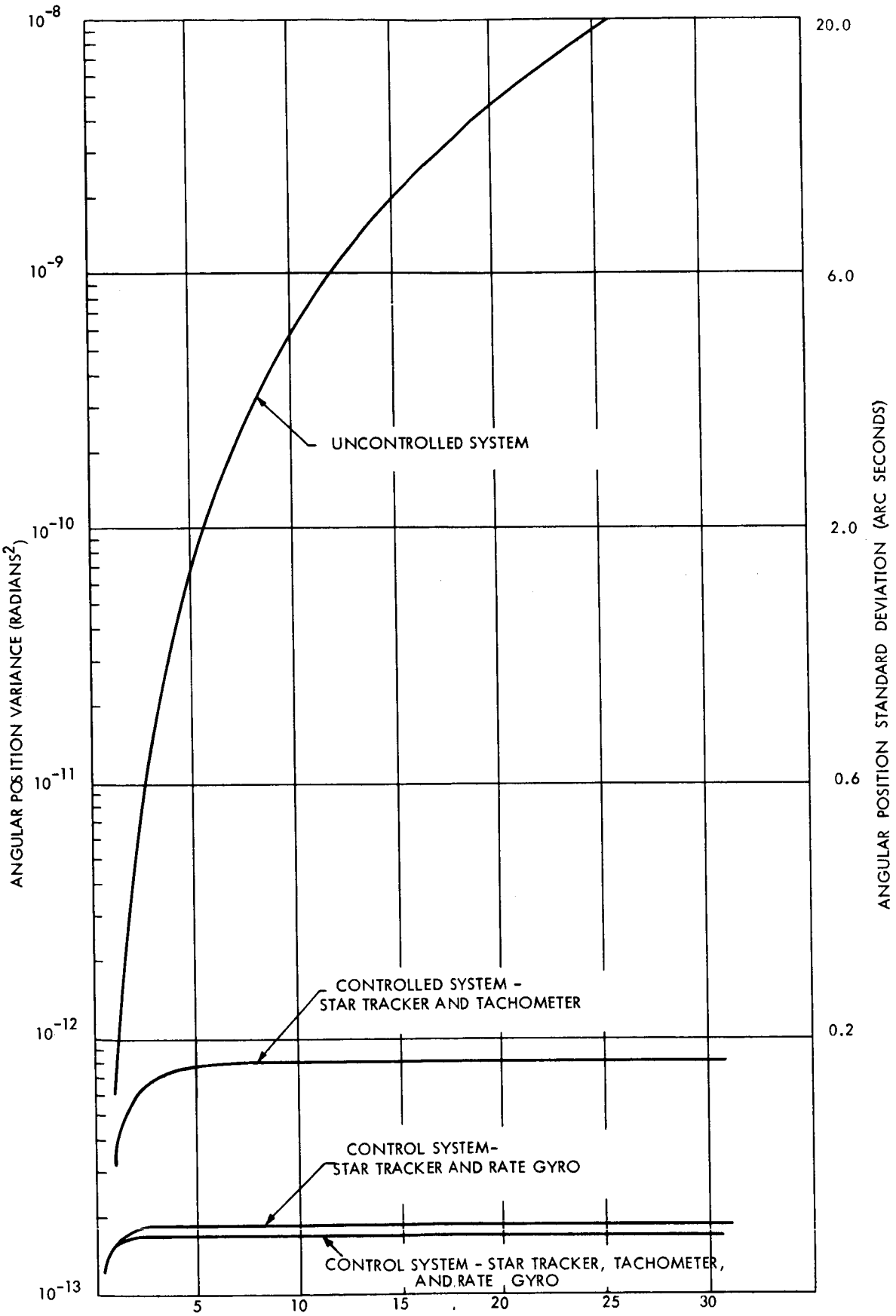

SINGLE AXIS ANGULAR POSITION VARIANCE
FIGURE 5.2

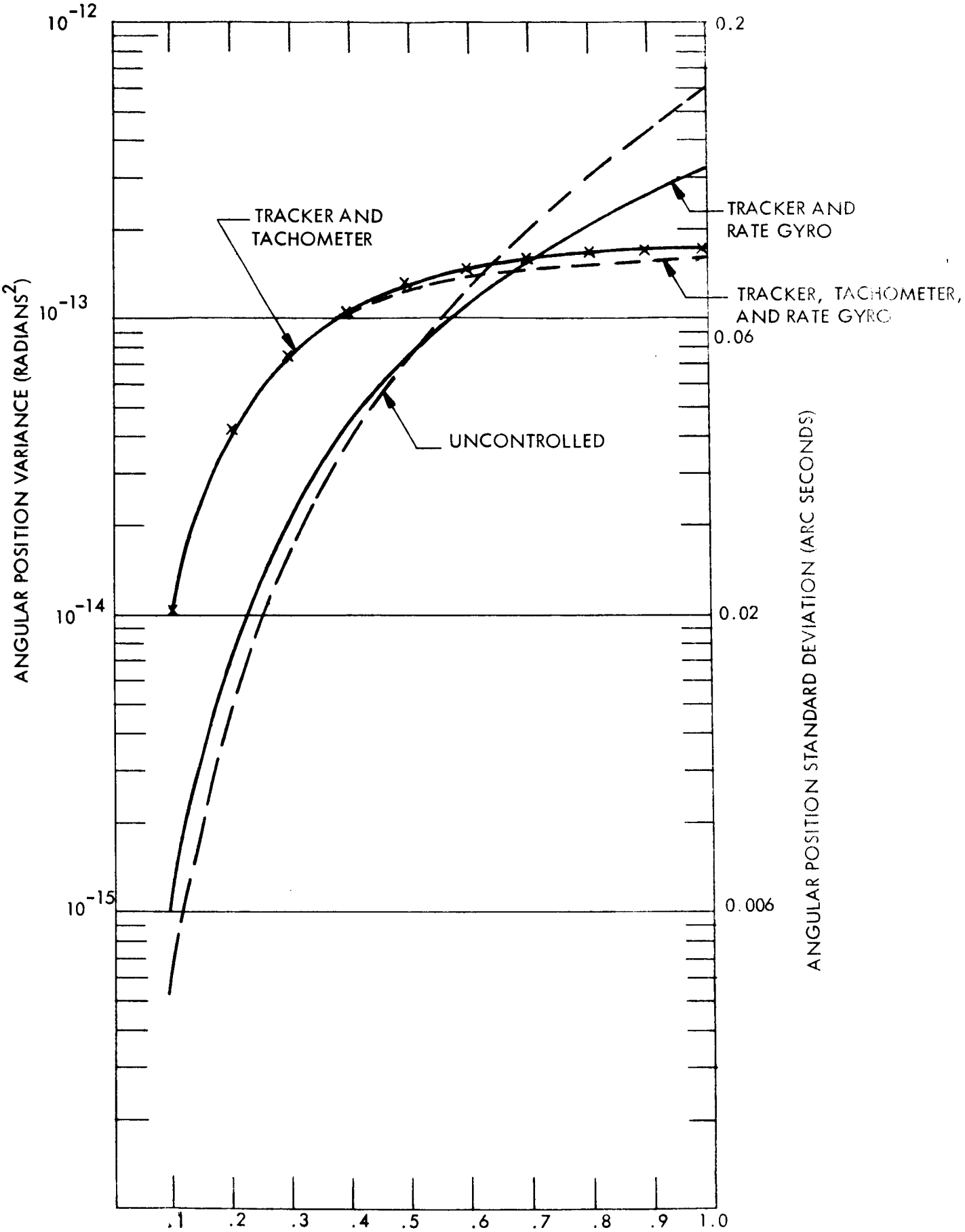

SINGLE AXIS ANGULAR POSITION VARIANCE

FIGURE 5.3

Since larger values of λ indicate a larger weighting assigned to position errors compared to velocity errors, one would expect that this would be reflected in lower steady-state position variance and higher steady-state velocity variance for large values of λ. Thus the monotonic variation of P_θ and P_ω with λ shown in Table 5.1 is to be expected.

Table 5.2 indicates the variation of the steady-state vehicle angular position variance P_θ and steady-state vehicle angular velocity variance P_ω with changes in sensor accuracies: $\sigma_1^2 \delta(t)$, the variance of the star tracker and $\sigma_2^2 \delta(t)$, the variance of the tachometer.

TABLE 5.2

STEADY-STATE PERFORMANCE

σ_1^2/σ_{10}^2	σ_2^2/σ_{20}^2	P_θ in rad^2	P_ω in rad^2/min^2
.1	.1	$.105 \times 10^{-12}$	$.771 \times 10^{-11}$
1	1	$.187 \times 10^{-12}$	$.363 \times 10^{-11}$
10	10	$.925 \times 10^{-12}$	$.913 \times 10^{-11}$

$\sigma_{10}^2 = 3.9 \times 10^{-14} (rad)^2 - min.$

$\sigma_{20}^2 = 5.915 \left(\frac{rad}{min}\right)^2 - min.$

Table 5.1 and 5.2 indicate that the closed-loop steady-state performance is relatively insensitive to variations in performance weighting and to variations in sensor accuracy.

A series of Monte-Carlo simulation runs for $\lambda = 10$ was made to determine the dependence of half-life on angular position limits. The results obtained are given in Figure 5.4 . Note that for a position limit of $1\sigma = \sqrt{.187 \times 10^{-12}} = .432 \times 10^{-6}$ rad , the half-life is only about 2.5 minutes. It is thus quite evident that it is not possible to maintain the steady-state 1σ error for a very long time. The curve marked "Closed-Loop Upper Bound " in Figure 5.4 was determined by using the probability

$$P\{ |\theta(T)| \leq B \mid \theta(t_0) = 0 \} \tag{5.25}$$

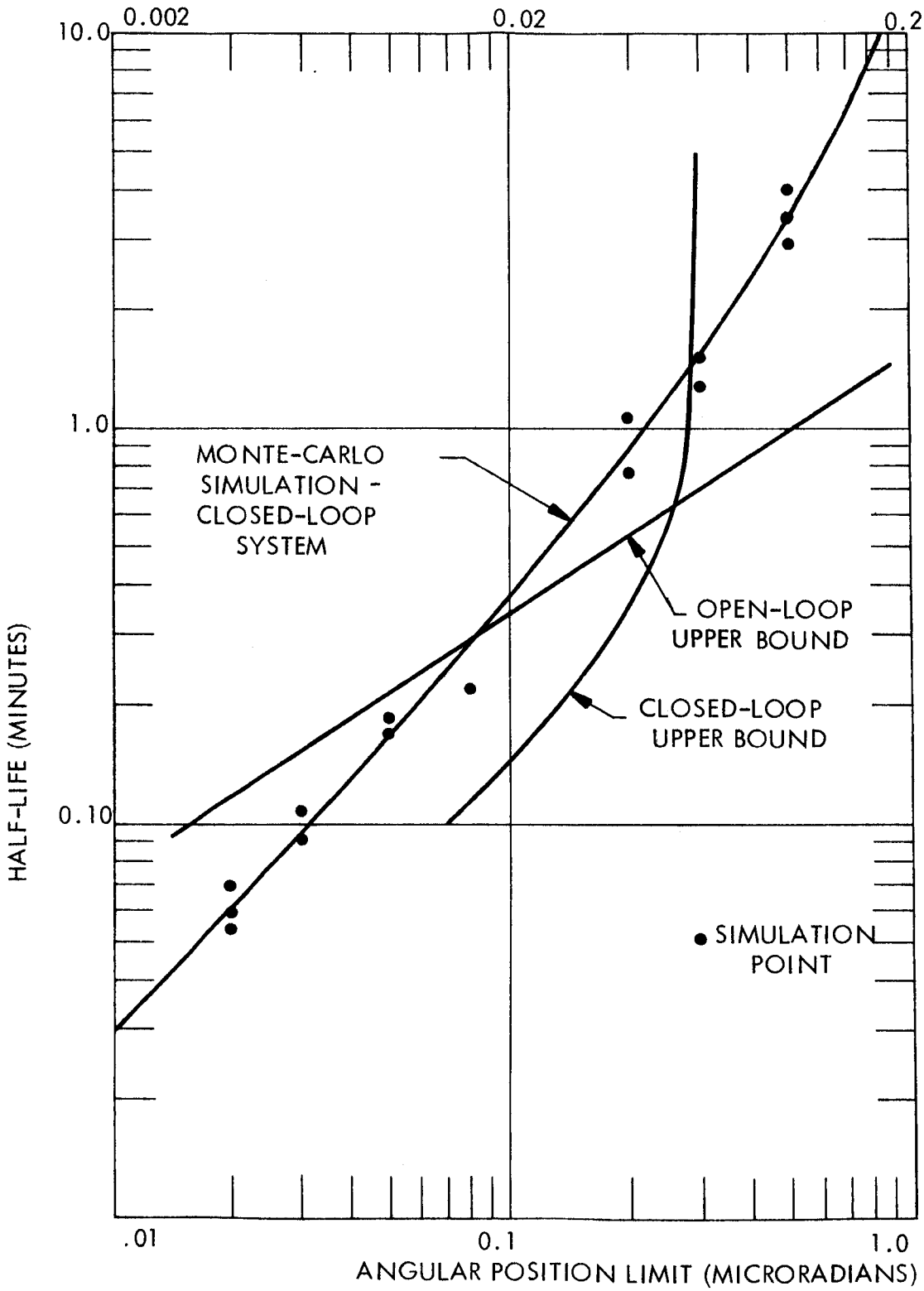

HALF- LIFE OF SINGLE-AXIS
FIGURE 5.4

as an upper bound on the confinement probability

$$q(T,0) = P\{\,|\theta(\tau)| \le B \text{ for all } t_0 \le \tau \le T \mid \theta(t_0) = 0\} \qquad (5.26)$$

Thus since the output process is Gaussian we find that

$$P\{|\theta(T)| \le B\} = \text{erf}\,(B/\sqrt{2}\,\sigma_\theta(T)) \qquad (5.27)$$

where $\sigma_\theta^2(T)$ is the angular position variance for the closed-loop system. The "upper bound" curve is drawn by using (5.27) and the data of Figures 5.2 and 5.3 . The fact that the "upper bound" falls below the half-life curve given by the Monte-Carlo simulation, indicates that the random number generator used in the Monte-Carlo simulation program generates random numbers whose properties do not conform with those required to properly simulate the white-noise acting on the closed-loop system. After an investigation of this problem it was found that the random number generator does indeed provide a poor approximation to white noise.

The curve labeled "Open-Loop Upper Bound" was obtained by treating the open-loop system as a double-integrator and using Figure 7-8 of [1]. Note that for small angular position limits the open-loop upper bound indicates a larger half-life than does the closed-loop upper bound. This is similar to the situation described above in reference to Figure 5.3.

5.2 STAR TRACKER AND RATE GYRO

We assume that the measurements available to the controller are angular position, provided by a star tracker, and angular velocity of the body provided by a rate gyro. Thus, the measurement vector $z = [z_1 , z_2]$ is given by (5.8) where

$$H = \begin{bmatrix} 1 & 0 & 0 \\ 0 & 0 & 1 \end{bmatrix} \qquad (5.28)$$

and $\{\eta\}$ in (5.8) is zero-mean white noise with covariance matrix

$$\Sigma_\eta = \begin{bmatrix} \sigma_\omega^2 & 0 \\ 0 & \sigma_\theta^2 \end{bmatrix} \delta(t) \quad , \quad \begin{aligned} \sigma_\omega^2 &= 2.41 \times 10^{-8} \left(\frac{\text{rad}}{\text{min}}\right)^2 \text{ - min.} \\ \sigma_\theta^2 &= 3.9 \times 10^{-14} (\text{rad})^2 \text{ - min.} \end{aligned} \tag{5.29}$$

Using the nomenclature of Section 3 we find that

$$K = \begin{bmatrix} .2278 \times 10^{-4} & 2.1482 \\ -.1656 \times 10^{-4} & -1.1958 \\ .3476 \times 10^{-4} & .655 \end{bmatrix}, \quad \hat{A} = \begin{bmatrix} -.2278 \times 10^{-4} & 10^{-4} & -2.1482 \\ .1656 \times 10^{-4} & -2 & 1.1958 \\ 1 & 0 & -.6555 \end{bmatrix},$$

$$\hat{Q} = \begin{bmatrix} q_2^2 & 0 & q_1 q_2 \\ 0 & 0 & 0 \\ 0 & 0 & q_1^2 \end{bmatrix} \tag{5.30}$$

where, again, the off diagonal term in $\hat{Q}$ is the contribution of $A' M_0$.

To compare the performance of the closed-loop system using star tracker and rate gyro with that of the system using star tracker and tachometer, the performance weighting $\lambda = q_1/q_2 = 10$ was chosen. From (3.17) we find that $U(s)$ is given by (5.14) where

$$\begin{aligned} G_1(s) &= 10^{-5}\left[+287 + \frac{221}{s} - \frac{1535}{s + 10.655} \right] \\ G_2(s) &= +435 + \frac{201}{s} - \frac{2896}{s + 10.655} \end{aligned} \tag{5.31}$$

If we represent the controller by the dynamic system (5.15) where

$$\bar{F} = \begin{bmatrix} 0 & 0 \\ 0 & -10.655 \end{bmatrix}, \quad \bar{G} = \begin{bmatrix} -221 \times 10^{-5} & -201 \\ 1535 \times 10^{-5} & 2896 \end{bmatrix} \tag{5.32}$$

then the control u is given by (5.17) where

$$\bar{K} = [1 \ , \ 1] \quad , \quad \bar{L} = [-287 \ , \ -435] \tag{5.33}$$

The closed-loop system employing the star tracker and rate gyro as sensors is shown in Figure 5.5 and is given by (5.19) where

$$\tilde{A} = \begin{bmatrix} -576 \times 10^{-7} & 10^{-4} & -8.7 & .02 & .02 \\ 1.151 & -2 & 1.74 \times 10^{5} & -400 & -400 \\ 1 & 0 & 0 & 0 & 0 \\ -221 \times 10^{-5} & 0 & -201 & 0 & 0 \\ 1535 \times 10^{-5} & 0 & 2896 & 0 & -10.65 \end{bmatrix} \tag{5.34}$$

and

$$\tilde{B} = \begin{bmatrix} 1 & -576 \times 10^{-7} & -8.7 \\ -1 & 1.151 & 1.74 \times 10^{5} \\ 0 & 0 & 0 \\ 0 & -221 \times 10^{-5} & -201 \\ 0 & 1535 \times 10^{-5} & 2896 \end{bmatrix} \tag{5.35}$$

The closed-loop variance shown in Figures 5.2 and 5.3 was obtained by using (5.34) and (5.35) and numerically integrating (5.22). From Figure 5.2 it is seen that after approximately 10 minutes, the tracker-rate gyro system provides a 4-fold improvement in steady state angular position variance compared with the tracker-tachometer system. In the time interval from 0 to 1 minute the tracker-rate gyro system also provides an improvement in closed-loop angular position variance.

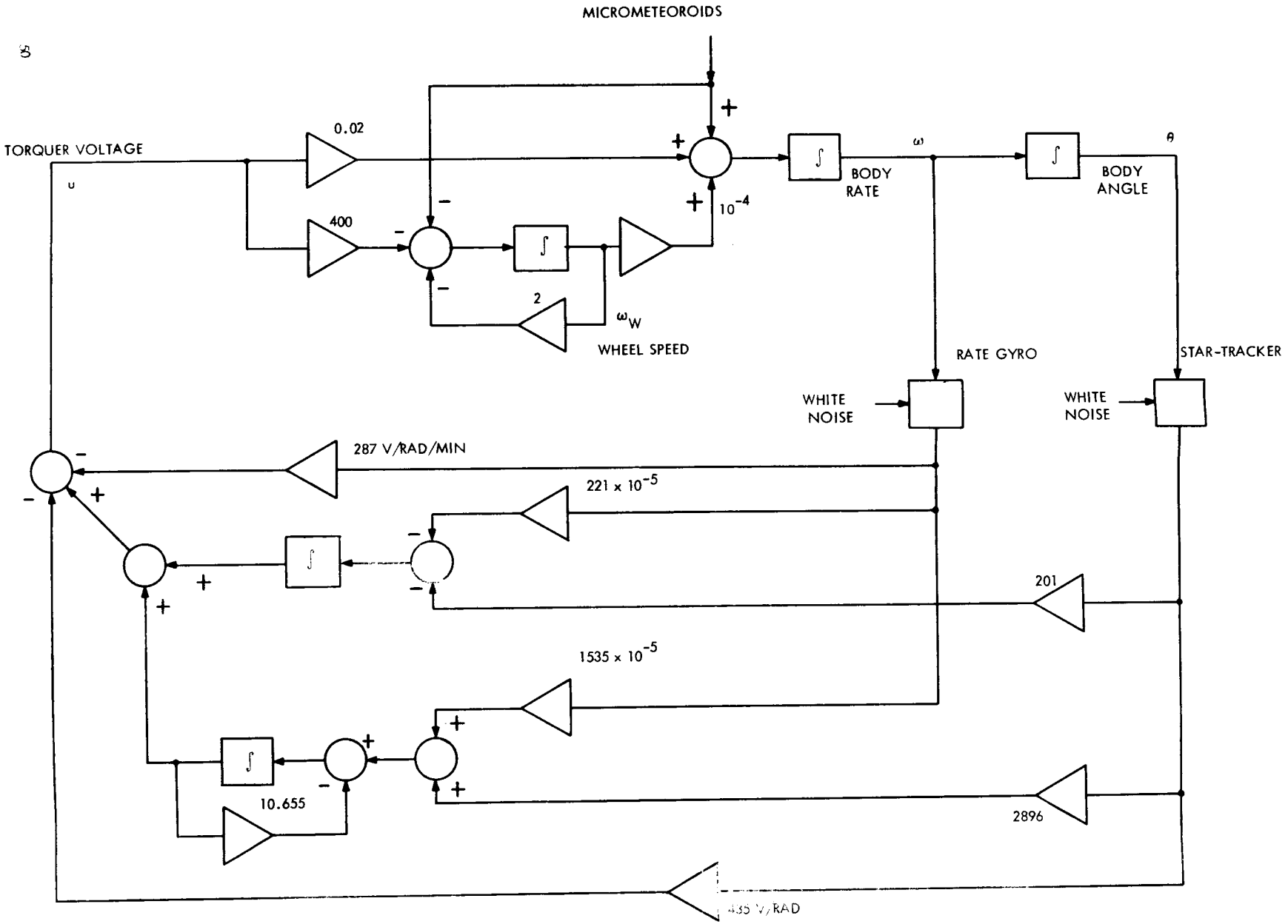

SINGLE-AXIS CONTROL SYSTEM - STAR-TRACKER AND RATE GYRO

FIGURE 5.5

5.3 STAR TRACKER, TACHOMETER, AND RATE GYRO

We assume that three sensors are used to measure the three state variables of the single axis. The measurement vector $z = [z_1, z_2, z_3]$ again is given by (5.8) where

$$H = \begin{bmatrix} 1 & 0 & 0 \\ 0 & 1 & 0 \\ 0 & 0 & 1 \end{bmatrix} \tag{5.36}$$

and $\{\eta\}$ in (5.8) is zero-mean white noise with covariance matrix

$$\Sigma_\eta = \begin{bmatrix} \sigma_\omega^2 & 0 & 0 \\ 0 & \sigma_w^2 & 0 \\ 0 & 0 & \sigma_\theta^2 \end{bmatrix} \delta(t) \quad , \quad \begin{aligned} \sigma_\omega^2 &= 2.41 \times 10^{-8} \text{ (rad/min)}^2 \text{ - min.} \\ \sigma_w^2 &= 5.915 \text{ (rad/min)}^2 \text{ - min.} \\ \sigma_\theta^2 &= 3.9 \times 10^{-14} \text{ (rad)}^2 \text{ - min.} \end{aligned} \tag{5.37}$$

Again using the nomenclature of Section 3 we find that

$$K = \begin{bmatrix} .405 \times 10^{-4} & -.095 \times 10^{-12} & 6.8 \\ -.234 \times 10^{-4} & .065 \times 10^{-12} & -2.54 \\ .109 \times 10^{-4} & -.168 \times 10^{-13} & 3.7 \end{bmatrix},$$

$$\hat{A} = \begin{bmatrix} -.405 \times 10^{-4} & 10^{-4} & -6.8 \\ .234 \times 10^{-4} & -2 & 2.54 \\ 1 & +.168 \times 10^{-13} & -3.7 \end{bmatrix}, \quad \hat{Q} = \begin{bmatrix} q_2^2 & 0 & q_1 q_2 \\ 0 & 0 & 0 \\ 0 & 0 & q_1^2 \end{bmatrix} \tag{5.38}$$

To facilitate comparison with the two previous cases the performance weighting $\lambda = q_1/q_2 = 10$ was chosen and from (3.17) it was found that

$$U(s) = -[G_1(s), G_2(s), G_3(s)]\, Z(s) \tag{5.39}$$

where

$$G_1(s) = 10^{-4}\left[74.8 + \frac{35.1}{s} - \frac{670}{s+13.7}\right]$$

$$G_2(s) = 10^{-12}\left[-13.15 - \frac{8.65}{s} + \frac{103}{s+13.7}\right] \qquad (5.40)$$

$$G_3(s) = 2190 + \frac{497}{s} - \frac{22,700}{s+13.7}$$

If we represent the controller by the dynamic system (5.15) where

$$\bar{F} = \begin{bmatrix} 0 & 0 \\ 0 & -13.7 \end{bmatrix}, \qquad \bar{G} = \begin{bmatrix} -35.1 \times 10^{-4} & 8.65 \times 10^{-12} & -497 \\ 670 \times 10^{-4} & -103 \times 10^{-12} & 22,700 \end{bmatrix} \qquad (5.41)$$

then the control u is given by (5.17) where

$$\bar{K} = [1, 1], \qquad \bar{L} = [-74.8 \times 10^{-4}, +13.15 \times 10^{-12}, -2190] \qquad (5.42)$$

The closed-loop system employing the three sensors is shown in Figure 5.6 and is given by (5.19) where

$$\tilde{A} = \begin{bmatrix} -149.6 \times 10^{-6} & 10^{-4} & -43.8 & .02 & .02 \\ 2.99 & -2 & 8.76 \times 10^{5} & -400 & -400 \\ 1 & 0 & 0 & 0 & 0 \\ -35.1 \times 10^{-4} & 8.65 \times 10^{-12} & -497 & 0 & 0 \\ 670 \times 10^{-4} & -103 \times 10^{-12} & 22,700 & 0 & -13.7 \end{bmatrix} \qquad (5.43)$$

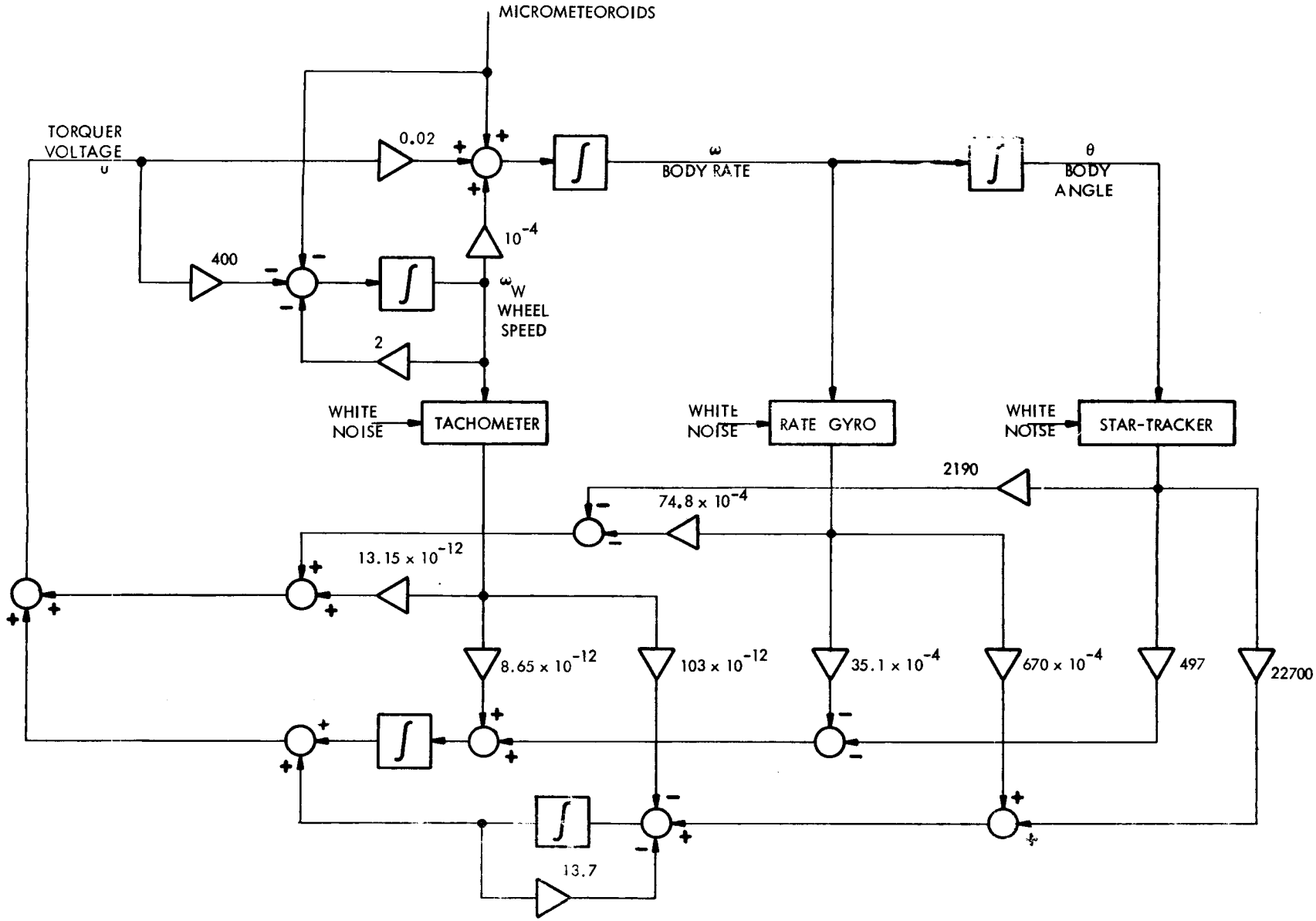

SINGLE-AXIS CONTROL SYSTEM- STAR-TRACKER, TACHOMETER, AND RATE GYRO
FIGURE 5.6

$$\tilde{B} = \begin{bmatrix} 1 & -149.6 \times 10^{-6} & 26.3 \times 10^{-14} & -43.8 \\ -1 & 2.99 & -52.6 \times 10^{-10} & 8.76 \times 10^{5} \\ 0 & 0 & 0 & 0 \\ 0 & -35.1 \times 10^{-4} & 8.65 \times 10^{-12} & -497 \\ 0 & 670 \times 10^{-4} & -103 \times 10^{-12} & 22700 \end{bmatrix} \tag{5.44}$$

Again the closed-loop variance shown in Figures 5.2 and 5.3 was obtained by using (5.43) and (5.44) and numerically integrating (5.22). From Figure 5.3 it is seen that in the time interval from 0 to 1 minute the tachometer controls the performance and the closed-loop variance resulting from the use of the three sensors is quite close to the closed-loop variance that results from the use of the star-tracker and tachometer alone. From Figure 5.2 it is seen that in the steady-state the rate gyro controls the performance and the closed-loop variance resulting from the use of the three sensors is quite close to the closed-loop variance that results from the use of the star-tracker and rate gyro alone.

6. MULTIPLE AXIS STUDY

6.1 ASSUMPTIONS FOR SPACECRAFT DYNAMICS

The state variables employed to describe the vehicle motion in 3 dimensions are the following:

ω_a , ω_b , ω_c	:	vehicle body rates
ω_1 , ω_2 , ω_3	:	speeds of reaction wheels 1, 2, 3, respectively, relative to body.
θ_1 , θ_2 , θ_3	:	Euler angles of spacecraft body axes, relative to a fixed inertial coordinate system.
ω_4 , ω_5	:	Angular rates of solar paddles relative to body.

The control variables employed are

V_1 , V_2 , V_3	:	voltages on reaction wheels 1, 2, 3 respectively.

The only disturbance torques considered were those due to micrometeoroid bombardment.

Since satisfactory operation of the control system implies that the state variables can differ only by very small amounts from the values they should have under ideal (nominal) conditions, it is reasonable to linearize the equations about this nominal motion and thus obtain a set of linear perturbation equations for which the control system is to be designed. The reaction wheel control voltages V_i thus are the sum of the voltages V_{iN} required to maintain the nominal motion, and the additional correction voltages u_i which depend on the perturbations of the state variables from their nominal conditions.

To simplify the linearization, it was assumed that all planets move in a single (ecliptic) plane which coincides with the plane of the spacecraft orbit around Mars. The nominal motion of the spacecraft is assumed to be that in which the axis a through the telescope is maintained in the ecliptic plane pointed to the Earth's center; the axis b about which the paddles rotate is maintained normal to the ecliptic plane, and the third axis c maintained normal to the first two.

For this assumed nominal motion it is found* that perturbations in rotation about the axis normal to the ecliptic plane is independent of perturbations in rotations about the nominally in-plane axes. As a consequence, it was possible to separate the design for the former from that of the latter.

6.2 DESIGN FOR AXIS NORMAL TO ORBITAL PLANE

Dynamics - The five component state vector $x = \{ x_1, \ldots, x_5 \}$ is used to describe the motion about the axis normal to the orbital (ecliptic) plane. The state variables are defined as follows:

$$
\begin{aligned}
x_1 &= \omega_b - \omega_{bN} : && \text{deviation in body rate from nominal} \\
x_2 &= \omega_2 - \omega_{2N} : && \text{deviation in wheel speed from nominal} \\
x_3 &= \theta_1 - \theta_{1N} : && \text{angular error} \\
x_4 &= \omega_4 - \omega_{4N} \\
x_5 &= \omega_5 - \omega_{5N} \Big\} && : \text{deviation of paddle speeds from nominal}
\end{aligned}
\qquad (6.1)
$$

In terms of these state variables, and using the physical parameter (size, mass, etc.) of Section 4 it is found that the motion about the axis normal to the orbital plane is given by

$$\dot{x} = Ax + Bu + G\xi \qquad (6.2)$$

where u is the voltage input to the reaction wheel, and ξ is the white noise equivalent** of the micrometeoroid bombardment process. Using minutes as the unit of time, meters for length, and kilograms for mass, it is found that the matrices in (6.2) are:

$$
A = \begin{bmatrix}
0 & 1.091 \times 10^{-4} & 0 & 0.4365 & -0.4365 \\
0 & -2.000 & 0 & -0.4365 & 0.4365 \\
1 & 0 & 0 & 0 & 0 \\
0 & -1.091 \times 10^{-4} & 0 & -27.71 & 0.4365 \\
0 & 1.091 \times 10^{-4} & 0 & 0.4365 & -27.71
\end{bmatrix} \qquad (6.3)
$$

* For details of calculation, see Appendix. Deviations from nominal values of state variables are designated by λ_i ($i = 1, 2, \ldots, 11$).

** See Section 4.

$$B' = [0.0262, \quad -479.9, \quad 0, \quad -0.0262, \quad 0.0262] \tag{6.4}$$

$$G = \begin{bmatrix} 1.746 & 0 \\ -1.746 & 0 \\ 0 & 0 \\ -1.746 & 109 \\ 1.746 & -109 \end{bmatrix} \tag{6.5}$$

On the basis of the preliminary investigation described in the previous section, it was felt that the sensors combination of a star-tracker and a reaction wheel tachometer provide nearly as good performance as obtained by addition of a rate gyro, and this was the sensor package studied for this application. The observation equation corresponding to this set of sensors is

$$z = Hx + \eta \tag{6.6}$$

where z and η are each two-component vectors with

z_1 = tachometer output

z_2 = star-tracker output

η_1 = tachometer equivalent white noise

η_2 = star-tracker equivalent white noise

The matrix H is

$$H = \begin{bmatrix} 0 & 1 & 0 & 0 & 0 \\ 0 & 0 & 1 & 0 & 0 \end{bmatrix}$$

(For convenience, the scale factors of the star-tracker and tachometer were taken as unity - volts/rad and volts/rad/min, respectively).

Control System Design - The technique described in Section 3 was used to design the controller. The performance criterion, was the same as used in the preliminary design study, namely

$$E_s(x'Qx) = E_s(x_1^2 + 100\, x_3^2) \tag{6.7}$$

consequently the weighting matrix Q was taken as

$$Q = \begin{bmatrix} 1 & 0 & 0 & 0 & 0 \\ 0 & 0 & 0 & 0 & 0 \\ 0 & 0 & 100 & 0 & 0 \\ 0 & 0 & 0 & 0 & 0 \\ 0 & 0 & 0 & 0 & 0 \end{bmatrix}$$

The controller was designed with the aid of digital computer programs developed for this purpose. Since the controller has two inputs: from the star-tracker and from the tachometer and one putput: the reaction wheel control voltage, the controller is represented by two transfer functions $G_1(s) = -U(s)/Z_1(s)$ and $G_2(s) = -U(s)/Z_2(s)$. These transfer functions have been determined to be

$$\begin{aligned} G_1(s) &= -10^{-10}\ \frac{.695\, s^3 + 18.135\, s^2 + 188\, s + 277}{s^3 + 44.4\, s^2 + 467\, s + .765} \\ G_2(s) &= 10^4\ \frac{.369\, s^3 + 12.13\, s^2 + 50.37\, s + 55.17}{s^3 + 44.4\, s^2 + 467\, s + .765} \end{aligned} \tag{6.8}$$

The resulting third-order transfer function matrix is synthesized by the use of three integrators. The closed-loop block diagram (plant, sensors, and controller) is shown in Fig. 6.1.

Performance Evaluation - The performance of the closed-loop system of Fig. 6.1 was simulated using the MARKOV simulation program to determine the dependence of half-life upon the angular position limits. The results, shown in Fig. 6.2, indicate that for an angular

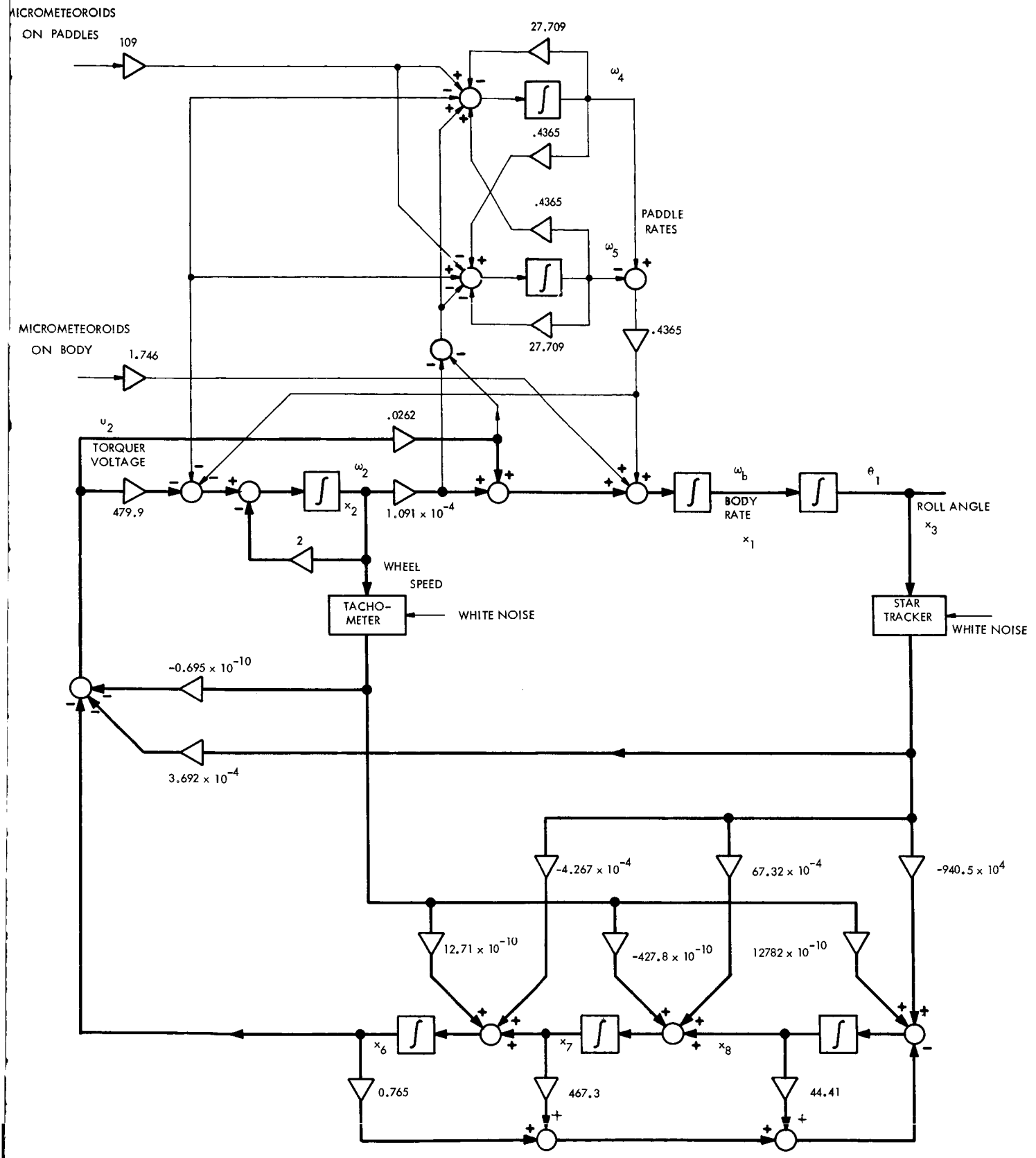

YAW AXIS CLOSED-LOOP CONTROL SYSTEM

FIGURE 6.1

position limit of $1\sigma = .618 \times 10^{-6}$ rad = .124 arc seconds the half-life is only about 2 minutes. Thus, it is difficult to stay within the steady-state 1σ error for more than 2 minutes. The curve marked "upper bound" in Fig. 6.2 was obtained by using the closed-loop variance shown in Fig. 6.3 and the expression (5.27). The crossing of the two curves in Fig. 6.2 is again caused by the imperfect random number generator used in the MARKOV simulation program.

It is interesting to note that these results agree closely with those shown in Fig. 5.4 for the single-axis approximation. The half-life indicated in Fig. 6.2 is slightly lower than that indicated in Fig. 5.4; this can be attributed to the presence of the solar paddles which were not included in the design of Section 5.1.

6.3 DESIGN FOR AXES IN ORBITAL PLANE

Dynamics - The six component state vector $x = \{x_1, \ldots, x_6\}$ is used to describe the motion about the two axes which are nominally in the orbital plane of spacecraft motion. The state variables in this case are defined as follows:

$x_1 = \omega_a - \omega_{aN}$ = deviation of rate about body axis nominally oriented toward earth

$x_2 = \omega_c - \omega_{cN}$ = deviation of rate about third body axis

$x_3 = \omega_1 - \omega_{1N}$ = deviation from nominal of axis a reaction wheel speed

$x_4 = \omega_3 - \omega_{3N}$ = deviation from nominal of axis c reaction wheel speed

$x_5 = \theta_2 - \theta_{2N}$ = angular error about axis nominally earth oriented

$x_6 = \theta_3 - \theta_{3N}$ = angular error about third axis

In terms of these state variables, the linearized dynamic equations take the form

$$\dot{x} = Ax + Bu + G\xi \tag{6.9}$$

where

u_i = control voltage on reaction wheel i ($i = 1, 3$)

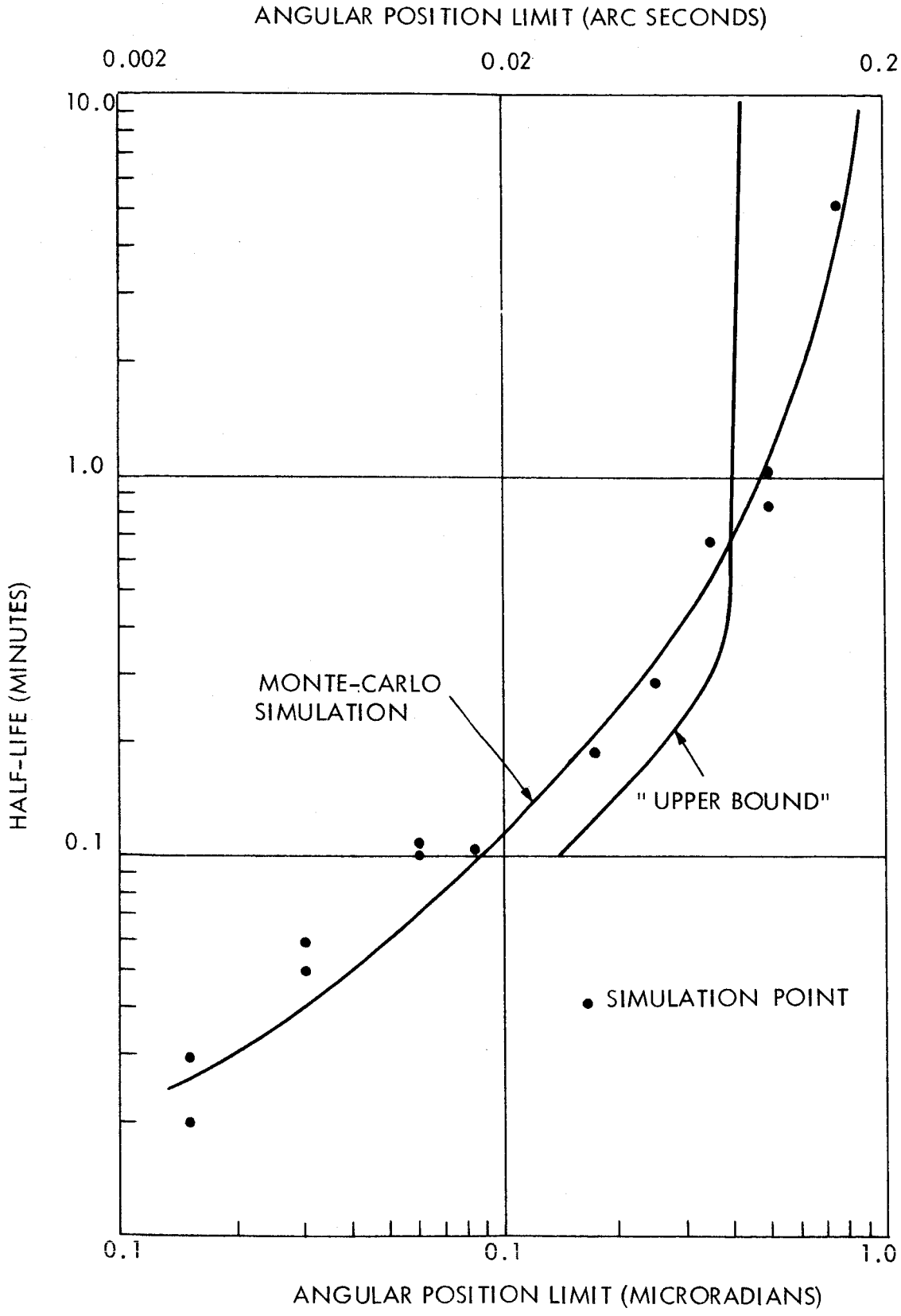

HALF-LIFE OF YAW AXIS
FIGURE 6.2

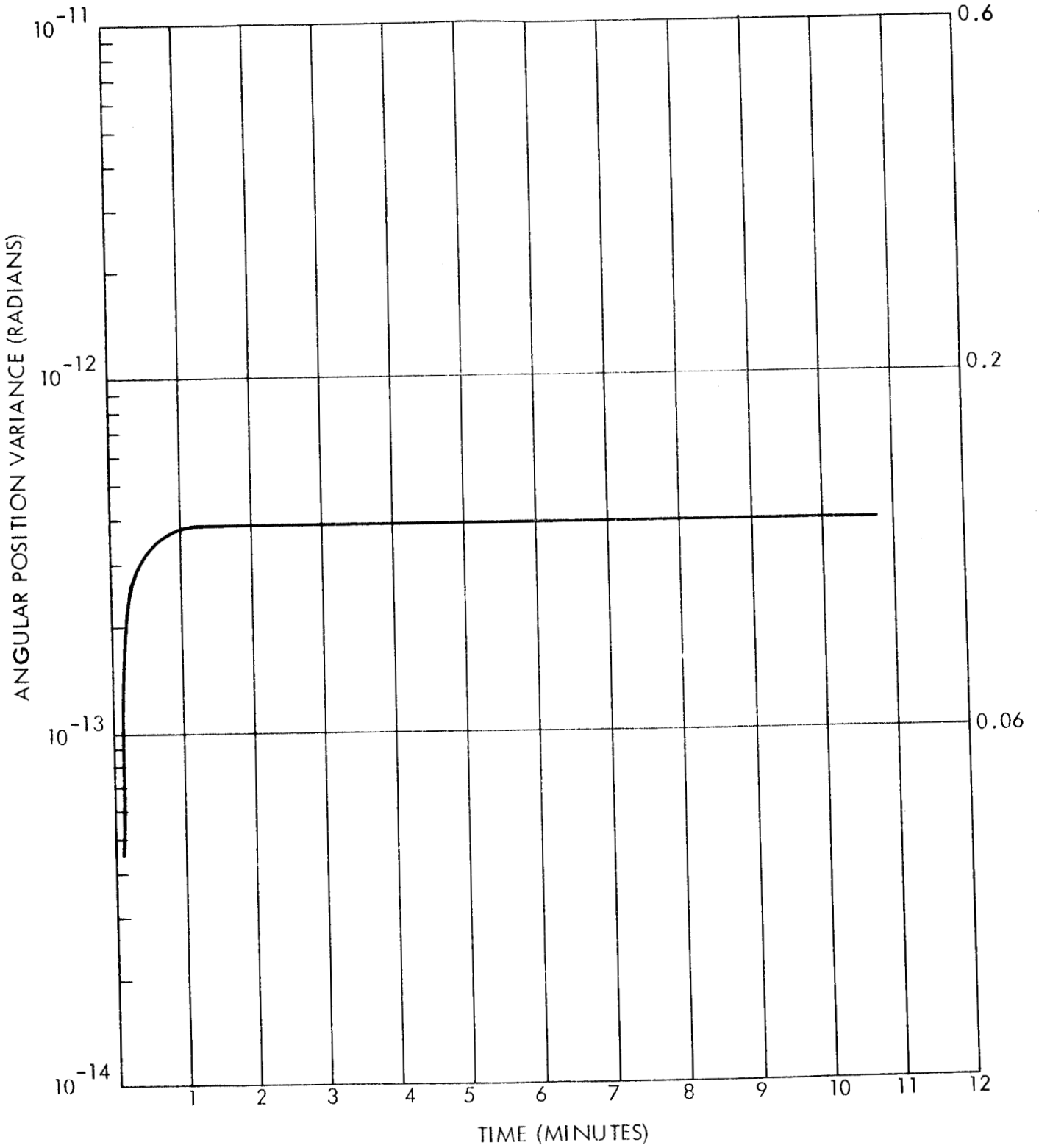

CLOSED-LOOP ANGULAR POSITION VARIANCE FOR YAW AXIS

FIGURE 6.3

and the matrices A, B, and G are given by:

$$A = \begin{bmatrix} -.1235 \times 10^{-10} & 4.552 \times 10^{-6} & .4992 \times 10^{-4} & 1.639 \times 10^{-10} & 0 & 0 \\ -1.502 \times 10^{-7} & -0.73 \times 10^{-11} & .093 \times 10^{-10} & .3838 \times 10^{-4} & 0 & 0 \\ .1235 \times 10^{-10} & -4.552 \times 10^{-6} & -2 & -1.639 \times 10^{-10} & 0 & 0 \\ 1.502 \times 10^{-7} & 0.73 \times 10^{-11} & -.093 \times 10^{-10} & -2 & 0 & 0 \\ 0 & 1 & 0 & 0 & 0 & -.35 \times 10^{-5} \\ 1 & 0 & 0 & 0 & .35 \times 10^{-5} & 0 \end{bmatrix} \tag{6.10}$$

$$B = \begin{bmatrix} .012 & 1.8 \times 10^{-8} \\ 1.8 \times 10^{-8} & .0092 \\ -597.96 & -1.8 \times 10^{-8} \\ -1.8 \times 10^{-8} & -479.9 \\ 0 & 0 \\ 0 & 0 \end{bmatrix}, \quad \xi = \begin{bmatrix} T_a \\ \hline T_c \end{bmatrix} \tag{6.11}$$

$$G = \begin{bmatrix} .0799 & .122 \times 10^{-5} \\ .122 \times 10^{-5} & .614 \\ -.0799 & -.122 \times 10^{-5} \\ -.122 \times 10^{-5} & -.614 \\ 0 & 0 \\ 0 & 0 \end{bmatrix}, \quad \Sigma = \begin{bmatrix} 1.8 \times 10^{-12} & 0 \\ 0 & 1.8 \times 10^{-12} \end{bmatrix} \tag{6.12}$$

where T_a is the torque about the a axis, T_c is the torque about the c axis, and $\sigma_a^2 = \sigma_c^2 = 1.8 \times 10^{-12}$.

The underlined terms in the above matrices represent the principal paths and correspond to the dynamics of the simplified model studied in the previous section. The remaining terms represent the effects of cross-axis coupling. These cross-coupling terms are quite small, but since we don't know whether they are negligible, we have included them in the design study.

The sensors for this pair of axes again were assumed to consist of star-trackers and reaction wheel tachometers. Accordingly, the observation equation is

$$z = Hx + \eta \tag{6.13}$$

where

z_1 = measurement of ω_1

z_2 = measurement of ω_3

z_3 = measurement of θ_2

z_4 = measurement of θ_3

the H matrix is

$$H = \begin{bmatrix} 0 & 0 & 1 & 0 & 0 & 0 \\ 0 & 0 & 0 & 1 & 0 & 0 \\ 0 & 0 & 0 & 0 & 1 & 0 \\ 0 & 0 & 0 & 0 & 0 & 1 \end{bmatrix} \tag{6.14}$$

and

η_1 = tachometer noise

η_2 = tachometer noise

η_3 = star-tracker noise

η_4 = star-tracker noise

$$\Gamma = \begin{bmatrix} 5.915 & 0 & 0 & 0 \\ 0 & 5.915 & 0 & 0 \\ 0 & 0 & 3.9 \times 10^{-14} & 0 \\ 0 & 0 & 0 & 3.9 \times 10^{-14} \end{bmatrix} \tag{6.15}$$

Control System Design - It was found that (3.11) did not have a unique solution for the two-axis design. This may be caused by the fact that the system (6.9) with A and B matrices given by (6.10) and (6.11) is not completely controllable. Thus the theory of Section 3 may not be directly applicable to the design of the two-axis controller. Another cause of the problem may have been the ill-conditioning of the coefficient matrices of (3.11) which may have caused numerical errors.

For this reason values of $k = .1, .01,$ and $.001$ in (3.5) were chosen and solutions $M(k)$ to (3.6) were obtained with

$$Q = \begin{bmatrix} 1 & 0 & 0 & 0 & 0 \\ 0 & 1 & 0 & 0 & 0 \\ 0 & 0 & 0 & 0 & 0 \\ 0 & 0 & 0 & 0 & 0 \\ 0 & 0 & 0 & 100 & 0 \\ 0 & 0 & 0 & 0 & 100 \end{bmatrix} \tag{6.16}$$

These solutions were substituted into (3.7), truncated after the third term, and the resulting 3 equations were solved for $M_0 = \tilde{M}_0$ which was taken as an initial approximation to the actual value of M_0. Using $\tilde{M}_0$ as an initial condition, (3.11) (with the left side replaced by $\dot{M}_0$) was integrated until a "steady-state" was reached. It was found that, although some terms in the resulting M_0 were close to those of $\tilde{M}_0$, others were not. Because of this discrepancy it was decided to choose the value of $k = .001$ and to proceed with the design using performance index (2.19) with Q given by (6.16) and

$$R = \begin{bmatrix} 10^{-16} & 0 \\ 0 & 10^{-16} \end{bmatrix} \tag{6.17}$$

Hence, in agreement with the design philosophy of Section 3, very little penalty was assigned to the use of control.

The controller was again designed with the aid of digital computer programs developed for this purpose. Since the controller has four inputs, from the two star trackers and the two reaction wheel tachometers, and two outputs, the two reaction wheel control voltages, the controller is represented by the dynamic system

$$\dot{\hat{x}} = A\hat{x} + Bu + K(z - H\hat{x}) \tag{6.18}$$

$$u = -\frac{B'M}{k^2} \tag{6.19}$$

where M is the solution of (2.21) with $\dot{M} = 0$,

$$M = \begin{bmatrix} .201\times10^{4} & .154\times10^{-1} & .405\times10^{-6} & .369\times10^{-6} & -.985\times10^{-3} & .910\times10^{3} \\ .154\times10^{-1} & .178\times10^{1} & .309\times10^{-6} & .303\times10^{-4} & .114\times10^{1} & .693\times10^{-2} \\ .405\times10^{-1} & .309\times10^{-6} & .814\times10^{-6} & .742\times10^{-11} & -.198\times10^{-7} & .183\times10^{-1} \\ .369\times10^{-6} & .303\times10^{-4} & .742\times10^{-11} & .573\times10^{-9} & .967\times10^{-6} & .167\times10^{-6} \\ -.985\times10^{-3} & .114\times10^{1} & -.198\times10^{-7} & .967\times10^{-6} & .179\times10^{2} & -.454\times10^{-3} \\ .910\times10^{3} & .693\times10^{-1} & .183\times10^{-1} & .167\times10^{-6} & -.454\times10^{-3} & .427\times10^{3} \end{bmatrix} \tag{6.20}$$

K is given by (2.29) in which P is the solution of (2.30) with $\dot{P} = 0$,

$$K = \begin{bmatrix} -.892\times10^{-15} & -.130\times10^{-18} & .204\times10^{-4} & .543 \\ -.179\times10^{-18} & -.402\times10^{-13} & .417\times10^{1} & .161\times10^{-4} \\ .482\times10^{-15} & .907\times10^{-19} & -.931\times10^{-5} & -.445\times10^{-1} \\ .907\times10^{-19} & .261\times10^{-13} & -.125\times10^{1} & -.341\times10^{-5} \\ -.614\times10^{-19} & -.823\times10^{-14} & .289\times10^{1} & .109\times10^{-4} \\ -.293\times10^{-15} & -.225\times10^{-19} & .109\times10^{-4} & .104\times10^{1} \end{bmatrix} \tag{6.21}$$

and A, B, and H are given by (6.10), (6.11), and (6.14), respectively.

The resulting sixth-order controller is synthesized by the use of six integrators. The closed-loop block diagram (plant, sensors, and controller) is shown in Figure 6.4 . It is interesting to note that in comparing the characteristic equation of this sixth-order controller with that of the fourth-order controller which was obtained by using a design based on M_0, it was found that four of the six roots of the former were close to the four roots of the latter and that the remaining two roots of the former appeared to be close to a pair of the latter. It thus seems that the controller with $k = 0$ has a fourth-order characteristic polynomial but requires six integrators for its realization.

Performance Evaluation - The performance of the closed-loop system of Figure 6.4 was simulated using the MARKOV simulation program to determine the dependence of half-life upon the angular position limits. The curve marked "Monte-Carlo Simulation" in Figure 6.5 was obtained by determining the first time that each member of an ensemble of trajectories escaped from the region

$$R = \{ \theta_2 , \theta_3 : |\theta_2| < B, |\theta_3| < B \} \tag{6.22}$$

The curve indicates that for an angular position limit $B = .6 \times 10^{-6}$ rad. $= .12$ arc seconds the half-life is about 5.5 minutes. Thus there is a probability of only 1/2 that the trajectory of the closed-loop system will remain inside the region R (with $B = .12$ arc seconds) for more than 5.5 minutes. The curve marked "upper bound" in Figure 6.5 was obtained by using the closed-loop variance shown in Figure 6.6 and the expression (5.27). The "hump" in the upper bound curve is caused by using the variance labeled "Pitch Axis" for $0 \leq t \leq 2.4$ minutes and then using the variance labeled "Roll Axis" for $2.4 \leq t$ in the expression (5.27). It is interesting to note that, as in the case of the single-axis controller of Section 6.2, these results agree closely with those shown in Figure 5.4 for the single-axis approximation.

FOLDOUT FRAME 1

FOLDOUT FRAME 2

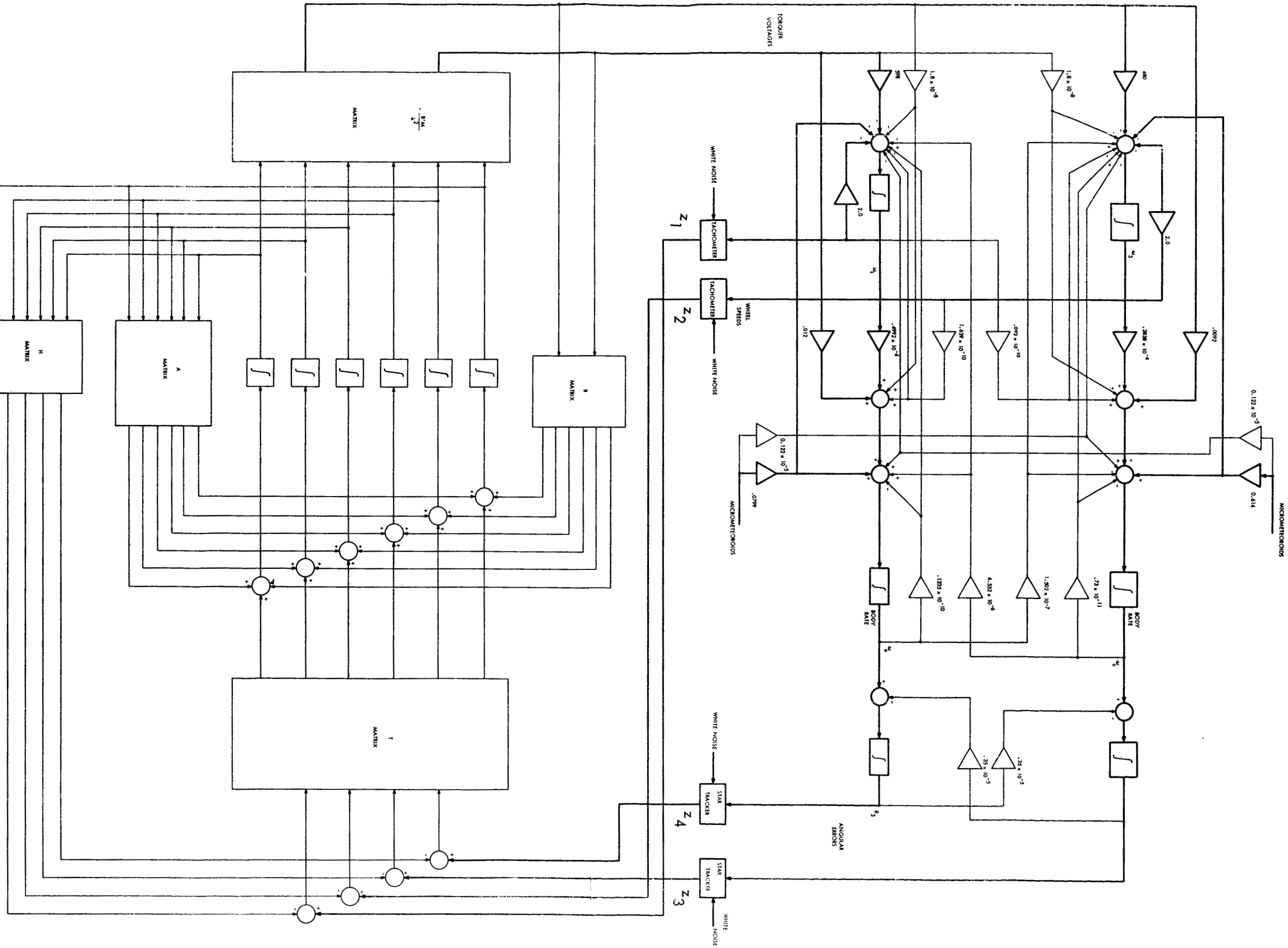

ROLL-PITCH AXES CLOSED-LOOP CONTROL SYSTEM
FIGURE 6.4

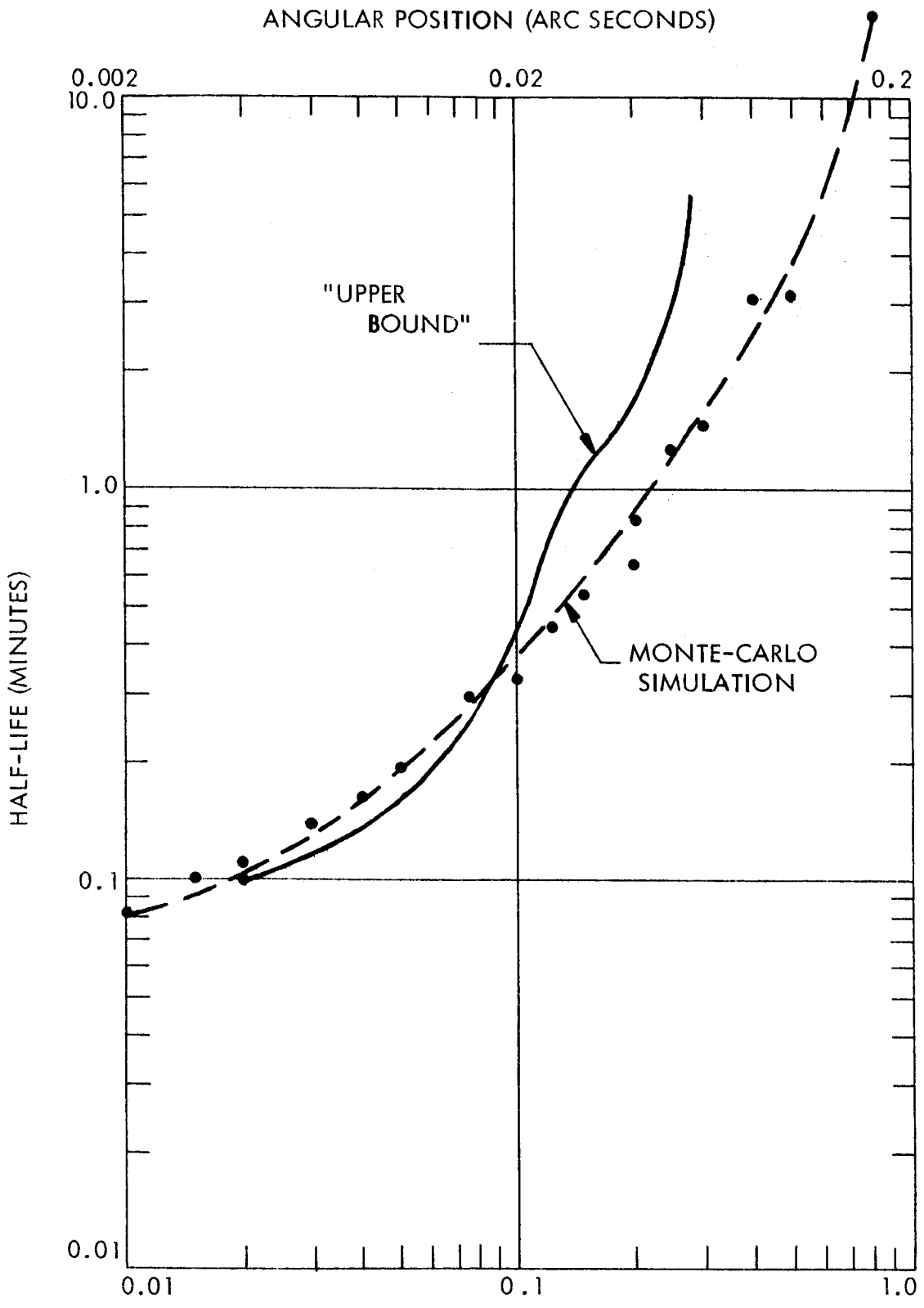

HALF-LIFE OF ROLL AND PITCH AXIS

FIGURE 6.5

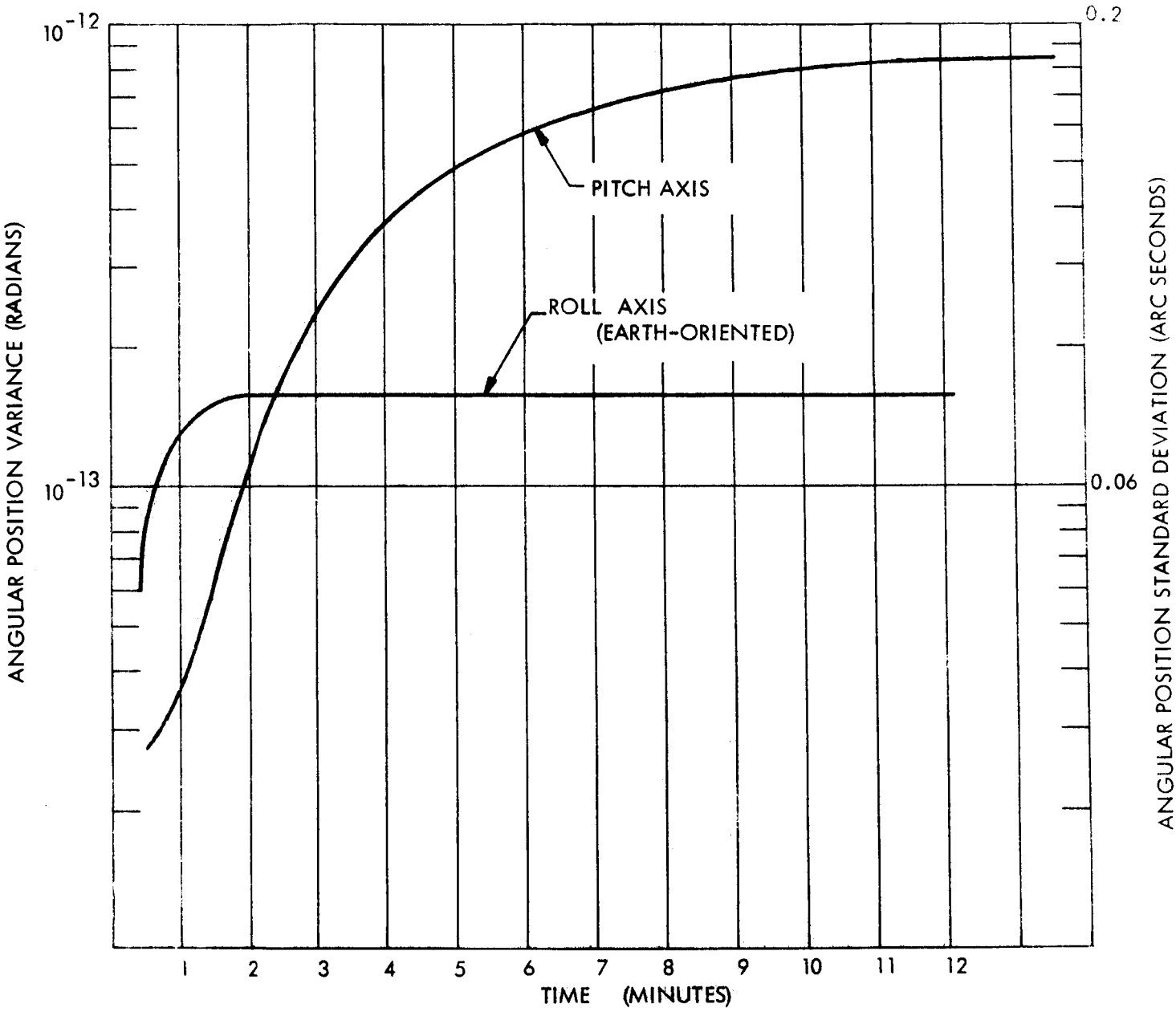

CLOSED LOOP ANGULAR POSITION VARIANCE
FOR ROLL AND PITCH AXES

FIGURE 6.6

7. CONCLUSIONS AND RECOMMENDATIONS

On the basis of the results achieved in Sections 5 and 6 above it is our conclusion that minimization of the steady-state variance is an effective technique for the design of an accurate fine-pointing control system. From the computer simulations of control system performance it was found that the "minimum steady-state variance" criterion yielded results which would be consistent with a "maximum confinement probability" criterion.

The fact that for the single-axis approximation the uncontrolled system has a lower angular position variance for small values of time than did the closed-loop system indicates that a combination of passive and active control might be considered for future fine-pointing control systems.

A number of problems regarding the design of control systems in the presence of random perturbations require further study. A more complete study of the fine pointing problem for a spacecraft should take into account a more detailed treatment of the system dynamics, for example, the flexibility of the telescope sunshield which was neglected in our investigation.

A significant source of random disturbances which was neglected in the present study is the random bias torque caused by the difference between the actual and nominal values of deterministic torques and the imperfections in the vehicle or control system construction. The principal random bias torques are those caused by misalignment of actuators and by solar reflectivity unbalance. These disturbances result in forcing terms of known form but of unknown magnitude appearing in the equations of motion of the vehicle. For example, the dynamics of the vehicle may be written as

$$\dot{x} = f(x) + k$$

where k is an unknown constant. The attitude control system can be designed to take these bias torques into account by treating k as an additional state variable. We may thus augment the system dynamics as follows

$$\dot{x} = f(x) + y$$
$$\dot{y} = 0, \quad y(0) = k$$

and estimate the state variable y as well as x.

Although our study was based on a fixed vehicle configuration it might be possible at an early stage in the design of a future communication vehicle to optimize the spacecraft configuration according to a suitable design criterion. This parameter optimization problem is essentially nonlinear and would probably require an iterative numerical solution on a digital computer.

As mentioned in Section 6 the question of existence and uniqueness of solutions to (3.11) is of critical importance for the application of the design technique of Section 3 based on minimizing the steady-state variance in the absence of control weighting. This problem requires further study.

Another problem requiring further attention is that of maximizing the expected first passage time to the boundary of a set given that the initial state is inside the set. It would be of interest to determine the relation between the control law based on this criterion and that which is obtained by minimizing the steady-state variance.

As mentioned in Section 5.1, it is essential that the algorithm used to provide the simulation of a random excitation properly model the characteristics of the noise used in the theoretical study. Thus the improvement of noise generation algorithms also deserves further study.

APPENDIX
VEHICLE DYNAMICS

In order to design the attitude control system and subsequently simulate its performance, it is necessary to have a fairly accurate model of the vehicle dynamics, including possible cross axis coupling terms. For this purpose we assume that the principal moving parts in the vehicle are the following:

1) The vehicle body and telescope rigidly mounted thereon.

2) Three double reaction wheels (nominally aligned with the vehicle principal axes and centered at the center of mass) torqued by d.c. torquers with "ideal" characteristics.

3) Two solar panels (nominally aligned with one of the principal axes orthogonal to the mechanical axis of the telescope). Additional panels or other moving parts can be treated in a similar manner.

The mechanical axis of the telescope is taken as one of the vehicle principal axes.

The vehicle state is defined by the following vector

$$y = \{\underbrace{\omega_a, \omega_b, \omega_c}_{\text{body rates}}, \underbrace{\omega_1, \omega_2, \omega_3}_{\substack{\text{reaction wheel}\\ \text{speeds (relative}\\ \text{to body)}}}, \underbrace{\theta_1, \theta_2, \theta_3}_{\substack{\text{Euler angles}\\ \text{with respect to}\\ \text{inertial reference}\\ \text{system}}}, \underbrace{\omega_4, \omega_5}_{\substack{\text{Solar paddle}\\ \text{rates relative}\\ \text{to body}}}\}$$

The control variables are assumed to be the quantities in the control vector

$$v = \{\underbrace{V_1, V_2, V_3}_{\substack{\text{voltages}\\ \text{applied to}\\ \text{reaction}\\ \text{wheel torquers}}}, \underbrace{T_{ra}, T_{rb}, T_{rc}}_{\substack{\text{reaction jet}\\ \text{torques}}}\}$$

Nonlinear Equations of Motion

The nonlinear differential equations of motion relating the state variables to the control variables are derived in this section.

Consider a vehicle with N moving parts and let the first N_0 parts have relative motions with respect to the main body which are completely known as functions of time. The remaining $N_0 + 1, \ldots N$ parts are connected to the main body (but not to any other part) via some constraint. We will use the following notation:

$\mathbb{I}_0$ = inertia tensor of the main body relative to a set of axes $(\underline{\xi}_a, \underline{\xi}_b, \underline{\xi}_c)$ passing through the center of mass of the main body and fixed in the main body (i.e., origin of body axis system is at c.m. of main body)

$\mathbb{I}_t$ = inertia tensor of $t^{\underline{th}}$ part relative to axes passing through the center of mass of the $t^{\underline{th}}$ part and aligned with $(\underline{\xi}_a, \underline{\xi}_b, \underline{\xi}_c)$

$\underline{r}_t$ = vector from origin of body axes to c.m. of $t^{\underline{th}}$ part.

$\underline{\omega}_t$ = angular velocity $t^{\underline{th}}$ part relative to body axes.

$\underline{\omega}$ = angular velocity of main body relative to some fixed inertial axes.

$\underline{R}^*$ = vector from the origin of the inertial system to the origin of the body axes system.

m_0 = mass of main body

m_t = mass of $t^{\underline{th}}$ part

$M = \sum_{t=0}^{N} m_t$ = mass of composite body

$\underline{R} = \frac{1}{M} \sum_{t=1}^{N} m_t \underline{r}_t$ = vector from origin of body axes to c.m. of the composite body.

$\underline{\tilde{T}}_t$ = the external torque applied to the $t^{\underline{th}}$ body (for $t = 0$ this refers to main body)

$\underline{T}_{tj}$ = interaction torque of $t^{\underline{th}}$ body due to $j^{\underline{th}}$ body (note $T_{tj} = -T_{jt}$)

We can write the equation of motion of each body separately as*

$$\frac{d}{dt}[\mathbb{I}_0 \underline{\omega}] = \underline{\tilde{T}}_0 + \sum_{i=1}^{N} \underline{T}_{0t} \tag{1}$$

* Roberson, R.E. "Attitude Control of Satellites and Space Vehicles", Chapter of book "Advances in Space Science" pp. 351-436. Academic Press.

for the main body and

$$\frac{d}{dt}[\mathbb{I}_1(\underline{\omega}+\underline{\omega}_1)+m_1\underline{r}_1\times\underline{\dot{r}}_1]=\underline{\tilde{T}}_1+\sum_{j=1}^{N_0}\underline{T}_{1j}-\underline{T}_{01}-m_1\underline{r}_1\times\frac{d^2}{dt^2}(\underline{R}^*) \tag{2}$$

for the i^{th} body with $i = 1, \ldots N$

Note $\underline{T}_{ij} = \underline{0}$ for $i \geq N_0 + 1$

Sum eq. (2) for $i = 1, \ldots N_0$ and add to (1) to give

$$\frac{d}{dt}[\mathbb{I}_0\underline{\omega}+\sum_{i=1}^{N_0}\{\mathbb{I}_i(\underline{\omega}+\underline{\omega}_i)+m_i\underline{r}_i\times\underline{\dot{r}}_i\}]$$

$$=\underline{\tilde{T}}_0+\sum_{i=1}^{N_0}\underline{T}_i+\sum_{i=N_0+1}^{N}\underline{T}_{0i}+\sum_{i=1}^{N_0}\sum_{j=1}^{N_0}\underline{T}_{ij}-\sum_{i=1}^{N_0}m_i\underline{r}_i\times\frac{d^2\underline{R}^*}{dt^2}$$

but $\sum_{i=1}^{N_0}\sum_{j=1}^{N_0}\underline{T}_{ij}=\underline{0}$ since $T_{ij}=-T_{ji}$ so the equations governing the unknown motions are

$$\frac{d}{dt}[\mathbb{I}_0\underline{\omega}+\sum_{i=1}^{N_0}\{\mathbb{I}_i(\underline{\omega}+\underline{\omega}_i)+m_i\underline{r}_i\times\underline{\dot{r}}_i\}]$$

$$=\underline{\tilde{T}}_0+\sum_{i=1}^{N_0}\underline{\tilde{T}}_i+\sum_{i=N_0+1}^{N}\underline{T}_{0i}-\sum_{i=1}^{N_0}m_i\underline{r}_i\times\frac{d^2\underline{R}^*}{dt^2} \tag{3}$$

and

$$\frac{d}{dt}[\mathbb{I}_i(\underline{\omega}+\underline{\omega}_i)+m_i\underline{r}_i\times\underline{\dot{r}}_i]=\underline{\tilde{T}}_i-\underline{T}_{0i}-m_i\underline{r}_i\times\frac{d^2\underline{R}^*}{dt^2} \tag{4}$$

To determine $\frac{d^2\underline{R}^*}{dt^2}$ the equations governing rectilinear motion would have to be solved in general. i.e.

$$M\frac{d^2}{dt^2}(\underline{R}^*+\underline{R})=\underline{F}+\sum_{i=1}^{N}\underline{F}_i$$

and

$$m_i\frac{d^2}{dt^2}[\underline{R}^*+\underline{r}_i]=\underline{F}_i-\underline{F}_{0i}$$

However, if the composite body is moving in a uniform force field so that the forces acting at the origin and at each body m_i are the same then by defining

$$\underline{\bar{R}}^* \triangleq \underline{R} + \underline{R}^* = \text{the vector from the origin of the inertial system to the c.m. of the composite body}$$

we can replace $\underline{R}^*$ in (3) and (4) by

$$\underline{R}^* = \underline{\bar{R}}^* - \underline{R}$$

and the quantities $\frac{d^2}{dt^2}(\underline{\bar{R}}^*)$ may be eliminated provided the torques due to the uniform force field are eliminated from the $\underline{T}_0$ and $\underline{T}_i$ terms. (i.e., the rotational effect of a uniform force field cancels out so it may be neglected from the start).

We will assume that motion is in a uniform force field so (3) and (4) become

$$\frac{d}{dt}\left[\mathbb{I}_0\underline{\omega} + \sum_{i=1}^{N_0}\{\mathbb{I}_i(\underline{\omega}+\underline{\omega}_i) + m_i\underline{r}_i\times\dot{\underline{r}}_i\}\right] = \underline{\tilde{T}}_0 + \sum_{i=1}^{N_0}\underline{\tilde{T}}_i + \sum_{i=N_0+1}^{N}\underline{T}_{0i} + \sum_{i=1}^{N_0} m_i\underline{r}_i\times\frac{d^2}{dt^2}(\underline{R}) \tag{5}$$

and

$$\frac{d}{dt}\left[\mathbb{I}_i(\underline{\omega}+\underline{\omega}_i) + m_i\underline{r}_i\times\dot{\underline{r}}_i\right] = \underline{\tilde{T}}_i - \underline{T}_{0i} + m_i\underline{r}_i\times\frac{d^2}{dt^2}(\underline{R}) \tag{6}$$

$$\text{for } i = N_0+1, \ldots N$$

Rotational Motion Only

When all the centers of mass are rigidly fixed in the main body, then the motion of each part with respect to the main body can only be a rotation about its individual mass center. Since all time derivatives in equations (5) and (6) are time rate of changes as viewed from the inertial reference frame from [14]

$$\frac{d}{dt}[\underline{a}(t)]_{\text{inertial}} = \frac{d}{dt}[\underline{a}(t)]_{\text{body}} + \underline{\omega}_{\text{body}}\times\underline{a}(t) \tag{7}$$

we have $\dot{\underline{r}}_i = \underline{\omega} \times \underline{r}_i$ and $\dot{\underline{R}} = \underline{\omega} \times \underline{R}$ so eq. (5) becomes

$$\frac{d}{dt}\left[\mathbb{I}_0 \underline{\omega} + \sum_{i=1}^{N_0} \{\mathbb{I}_i (\underline{\omega} + \underline{\omega}_i) + m_i \underline{r}_i \times \underline{\omega} \times \underline{r}_i\}\right] \tag{8}$$

$$= \underline{\tilde{T}}_0 + \sum_{i=1}^{N_0} \underline{T}_i + \sum_{i=N_0+1}^{N} \underline{T}_{0i} + \sum_{i=1}^{N_0} m_i \underline{r}_i \times \frac{d}{dt}(\underline{\omega} \times \underline{R})$$

Using $$\underline{a} \times \underline{b} \times \underline{c} = (\underline{a} \cdot \underline{c})\underline{b} - (\underline{a} \cdot \underline{b})\underline{c} = [\underline{a}^T \underline{c} I - \underline{c}\underline{a}^T]\underline{b} \tag{9}$$

we get $$m_i (\underline{r}_i \times \underline{\omega} \times \underline{r}_i) = m_i [\underline{r}_i^T \underline{r}_i I - \underline{r}_i \underline{r}_i^T] \underline{\omega} \triangleq \mathbb{J}_i \underline{\omega} \tag{10}$$

Again applying (7) gives

$$\frac{d}{dt}(\underline{\omega} \times \underline{R}) = \dot{\underline{\omega}} \times \underline{R} + \underline{\omega} \times (\underline{\omega} \times \underline{R}) \tag{11}$$

and thus from (9),

$$m_i \underline{r}_i \times \dot{\underline{\omega}} \times \underline{R} = m_i [\underline{r}_i^T \underline{R} I - \underline{R}\underline{r}_i^T] \dot{\underline{\omega}} \triangleq \mathbb{A}_i \dot{\underline{\omega}} \tag{12}$$

Inserting (10), (11) and (12) into (8) gives

$$\frac{d}{dt}\left[\mathbb{I}_0 \underline{\omega} + \sum_{i=1}^{N_0} (\mathbb{I}_i + \mathbb{J}_i)\underline{\omega} + \sum_{i=1}^{N_0} \mathbb{I}_i \underline{\omega}_i\right]$$

$$= \underline{\tilde{T}}_0 + \sum_{i=1}^{N_0} \underline{\tilde{T}}_i + \sum_{i=N_0+1}^{N} \underline{T}_{0i} + \sum_{i=1}^{N_0} \mathbb{A}_i \dot{\underline{\omega}} + \sum_{i=1}^{N_0} m_i \underline{r}_i \times [\underline{\omega} \times (\underline{\omega} \times \underline{R})]$$

and upon using (7) this becomes

$$[\mathbb{I}_0 + \sum_{i=1}^{N_0} (\mathbb{I}_i + \mathbb{J}_i)]\,\dot{\underline{\omega}} + \underline{\omega} \times [\mathbb{I}_0 + \sum_{i=1}^{N_0} (\mathbb{I}_i + \mathbb{J}_i)]\,\underline{\omega}$$

$$+ \sum_{i=1}^{N_0} [\mathbb{I}_i\,\dot{\underline{\omega}}_i + (\underline{\omega} + \underline{\omega}_i) \times \mathbb{I}_i\,\underline{\omega}_i] \tag{13}$$

$$= \underline{\tilde{T}}_0 + \sum_{i=1}^{N_0} \underline{\tilde{T}}_i + \sum_{i=N_0+1}^{N} \underline{T}_{0i} + \sum_{i=1}^{N_0} \mathbb{A}_i\,\dot{\underline{\omega}} + \sum_{i=1}^{N_0} m_i\,\underline{r}_i \times [\underline{\omega} \times (\underline{\omega} \times \underline{R})]$$

Now from (9) we write

$$m_i\,\underline{r}_i \times [\underline{\omega} \times (\underline{\omega} \times \underline{R})] = m_i\,[\underline{r}_i^T\,(\underline{\omega} \times \underline{R})\,I - (\underline{\omega} \times \underline{R})\,\underline{r}_i^T]\,\underline{\omega}$$

but note that

$$\underline{\omega} \times \mathbb{A}_i\,\underline{\omega} = m_i\,[\underline{\omega} \times (\underline{r}_i^T\,\underline{R}\,I - \underline{R}\,\underline{r}_i^T)\,\underline{\omega}]$$

$$= m_i\,[(\underline{r}_i^T\,\underline{R})\,\underbrace{(\underline{\omega} \times \underline{\omega})}_{0} - (\underline{r}_i^T\,\underline{\omega})\,(\underline{\omega} \times \underline{R})]$$

thus $\quad m_i\,\underline{r}_i \times [\underline{\omega} \times (\underline{\omega} \times \underline{R})] = \underline{\omega} \times \mathbb{A}_i\,\underline{\omega} + m_i\,[\underline{r}_i \cdot (\underline{\omega} \times \underline{R})]\,\underline{\omega}$

also let $\quad \mathbb{L}_i \triangleq \mathbb{I}_i + \mathbb{J}_i - \mathbb{A}_i$

and $\quad \mathbb{I} \triangleq \mathbb{I}_0 + \sum_{i=1}^{N_0} \mathbb{L}_i$

so (13) becomes

$$\mathbb{I}\,\dot{\underline{\omega}} + \underline{\omega} \times \mathbb{I}\,\underline{\omega} = \underline{\tilde{T}}_0 + \sum_{i=1}^{N_0} \underline{\tilde{T}}_i + \sum_{i=N_0+1}^{N} \underline{T}_{0i}$$

$$- \sum_{i=1}^{N_0} \mathbb{I}_i\,\dot{\underline{\omega}}_i + (\underline{\omega} + \underline{\omega}_i) \times \mathbb{I}_i\,\underline{\omega}_i - m_i\,[\underline{r}_i \cdot (\underline{\omega} \times \underline{R})]\,\underline{\omega} \tag{14}$$

Note: When $N_0 = N$, then $\sum_{i=1}^{N_0} m_i [\underline{r}_i \cdot (\underline{\omega} \times \underline{R})] = M\underline{R} \cdot \underline{\omega} \times \underline{R} = 0$

For rotational motion only (4) becomes similarly

$$\frac{d}{dt}[\mathbb{I}_i (\underline{\omega} + \underline{\omega}_i) + m_i \underline{r}_i \times \underline{\omega} \times \underline{r}_i] = \underline{\tilde{T}}_i - \underline{T}_{0i} + m_i \underline{r}_i \times \frac{d}{dt}[\underline{\omega} \times \underline{R}]$$

so $$\frac{d}{dt}[(\mathbb{I}_i + \mathbb{J}_i)\underline{\omega} + \mathbb{I}_i \underline{\omega}_i] = \underline{\tilde{T}}_i - \underline{T}_{0i} + \mathbb{A}_i \dot{\underline{\omega}} + m_i \underline{r}_i \times [\underline{\omega} \times (\underline{\omega} \times \underline{R})]$$

thus

$$[\mathbb{I}_i + \mathbb{J}_i - \mathbb{A}_i]\dot{\underline{\omega}} + \underline{\omega} \times [\mathbb{I}_i + \mathbb{J}_i]\underline{\omega} + \mathbb{I}_i \dot{\underline{\omega}}_i + (\underline{\omega} + \underline{\omega}_i) \times \mathbb{I}_i \underline{\omega}_i$$

$$= \underline{\tilde{T}}_i - \underline{T}_{0i} + \underline{\omega} \times \mathbb{A}_i \underline{\omega} + m_i [\underline{r}_i \cdot (\underline{\omega} \times \underline{R})] \underline{\omega}$$

so

$$\mathbb{L}_i \dot{\underline{\omega}} + \underline{\omega} \times \mathbb{L}_i \underline{\omega} + \mathbb{I}_i \dot{\underline{\omega}}_i + (\underline{\omega} + \underline{\omega}_i) \times \mathbb{I}_i \underline{\omega}_i = \underline{\tilde{T}}_i - \underline{T}_{0i} + m_i [\underline{r}_i \cdot (\underline{\omega} \times \underline{R})] \underline{\omega} \tag{15}$$

$$\text{for } i = N_0 + 1, \ldots N$$

In order to complete the description of the vehicle attitude motion we must describe the orientation with respect to the fixed inertial reference axes.

It has been found most convenient to define the Euler angles θ_1, θ_2, θ_3 as the angles shown in Figure A1. Here the body having a set of body axis directions indicated by x', y', z' is originally aligned with a set of inertial axes indicated by x, y, z. The body is first rotated about the z direction through an angle θ_1, as shown. It is next rotated about the resulting x' axis (denoted by ξ) thus specifying θ_2 as shown and finally it is rotated about the resulting z' axis thus specifying θ_3 as shown. Note that z denotes the direction of the z' axis after the first rotation and η' denotes the direction of y' after the second rotation.

We will consider the case in which the vehicle body axes $\underline{\xi}_a$, $\underline{\xi}_b$ and $\underline{\xi}_c$ are

$$\underline{\xi}_a = z', \quad \underline{\xi}_b = x', \quad \underline{\xi}_c = y' \tag{16}$$

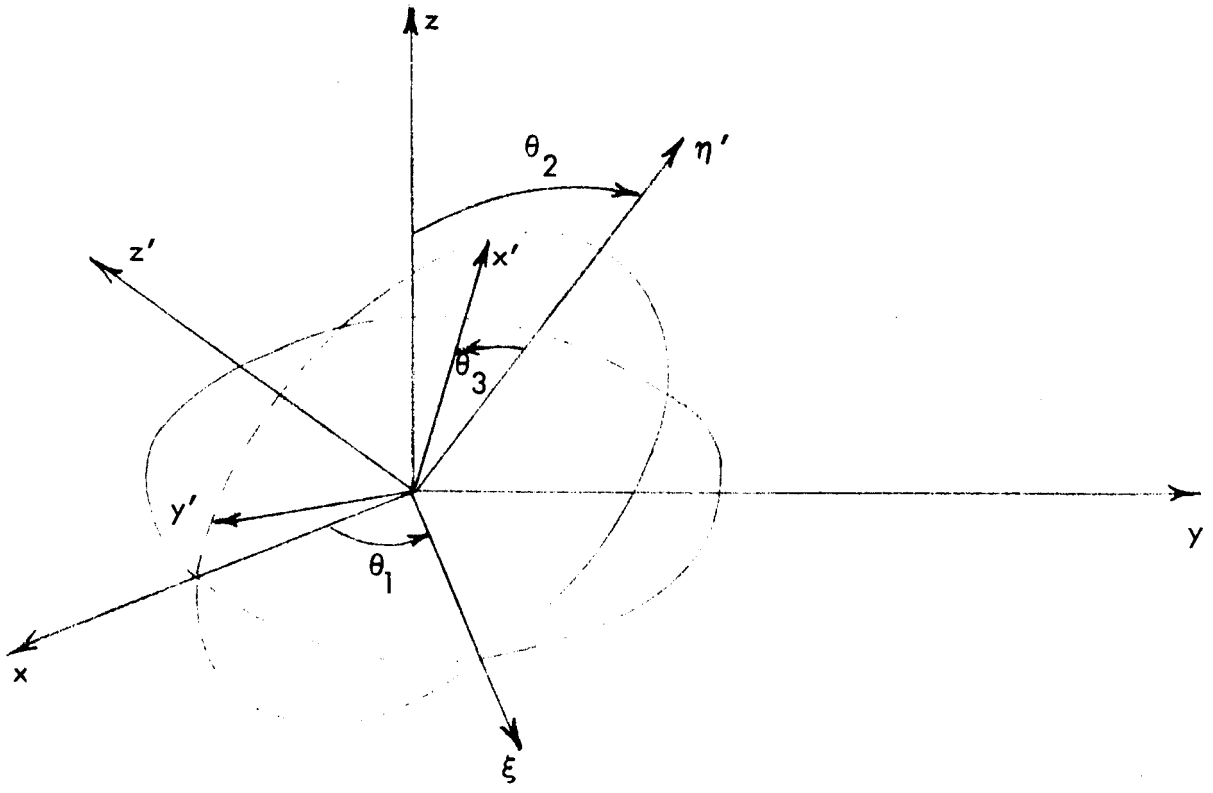

FIGURE A-1 DEFINITION OF EULER ANGLES

With the correspondence of (16) we find that

$$\begin{bmatrix} \omega_a \\ \omega_b \\ \omega_c \end{bmatrix} = \begin{bmatrix} \sin\theta_2 & 0 & 1 \\ \cos\theta_2 \cos\theta_3 & \sin\theta_3 & 0 \\ -\cos\theta_2 \sin\theta_3 & \cos\theta_3 & 0 \end{bmatrix} \begin{bmatrix} \dot{\theta}_1 \\ \dot{\theta}_2 \\ \dot{\theta}_3 \end{bmatrix} \tag{17}$$

so that

$$\begin{bmatrix} \dot{\theta}_1 \\ \dot{\theta}_2 \\ \dot{\theta}_3 \end{bmatrix} = \begin{bmatrix} 0 & \dfrac{\cos\theta_3}{\cos\theta_2} & -\dfrac{\sin\theta_3}{\cos\theta_2} \\ 0 & \sin\theta_3 & \cos\theta_3 \\ 1 & -\tan\theta_2 \cos\theta_3 & \tan\theta_2 \sin\theta_3 \end{bmatrix} \begin{bmatrix} \omega_a \\ \omega_b \\ \omega_c \end{bmatrix} \tag{18}$$

Let us now apply equations (14), (15) and (18) to give the dynamic equations governing the motion of a space vehicle having three independent reaction wheels used to control vehicle attitude and two banks of solar batteries in the shape of paddles which can rotate independently about a fixed axis through their respective mass centers (Fig. A1) in order to track the Sun.

We note that all these parts are of the second type since their motions with respect to the main body are not completely known time functions so $N_0 = 0$ and $\mathbb{I} = \mathbb{I}_0$. Let $\underline{a}_i$ for $i = 1, \ldots 5$ be the unit vector in the direction of the rotational axis of each moving part so $\underline{\omega}_i = \omega_i \underline{a}_i$. If we denote by I_{ai} the moment of inertia of each part about its axis $\underline{a}_i$ and choose $\underline{b}_i$ and $\underline{c}_i$ such that $\underline{a}_i$, $\underline{b}_i$, $\underline{c}_i$ forms a right-handed orthonormal set for each $i = 1, \ldots 5$ and letting I_{bi} and I_{ci} be the moments of inertia of the $i^{\underline{th}}$ body about $\underline{b}_i$ and $\underline{c}_i$ respectively we can write

$$\mathbb{I}_i = I_{ai} \underline{a}_i \underline{a}_i^T + I_{bi} \underline{b}_i \underline{b}_i^T + I_{ci} \underline{c}_i \underline{c}_i^T \quad \text{for } i = 1, \ldots 5 \tag{19}$$

Note - For the reaction wheels (i.e., $i = 1, 2, 3$) $I_{bi} = I_{ci}$.

The interaction torques can be resolved in the directions $\underline{a}_i$, $\underline{b}_i$ and $\underline{c}_i$ as $\underline{T}_{0i} = T^a_{0i}\underline{a}_i + T^b_{0i}\underline{b}_i + T^c_{0i}\underline{c}_i$. Also when an electric motor provides the torques to rotate the wheels or the battery panels then

$$T^a_{0i} = \alpha_i V_i(t) + \beta_i \omega_i(t) \tag{20}$$

where $V_i(t)$ are applied voltages.

We finally note that since the reaction wheels are mounted inside the main body they have no externally applied torques. Thus, $\underline{\tilde{T}}_i = \underline{0}$ for $i = 1, 2, 3$. The battery panels may have external torques applied. Under these conditions eq. (14) becomes

$$\mathbb{I}_0 \dot{\underline{\omega}} = -\underline{\omega} \times \mathbb{I}_0 \underline{\omega} + \underline{\tilde{T}}_0 + \sum_{i=1}^{5} [T^a_{0i}\underline{a}_i + T^b_{0i}\underline{b}_i + T^c_{0i}\underline{c}_i] \tag{21}$$

and premultiplying (15) by $\underline{b}_i^T$ gives

$$\underline{b}_i^T [\mathbb{L}_i \dot{\underline{\omega}} + \underline{\omega} \times \mathbb{L}_i \underline{\omega} + \mathbb{I}_i \dot{\underline{\omega}}_i + (\underline{\omega} + \underline{\omega}_i) \times \mathbb{I}_i \underline{\omega}_i]$$

$$= \underline{b}_i \cdot \underline{\tilde{T}}_i - T^b_{0i} + m_i [\underline{r}_i \cdot (\underline{\omega} + \underline{R})] \underline{b}_i \cdot \underline{\omega}$$

so

$$T^b_{0i} = \underline{b}_i \cdot \underline{\tilde{T}}_i - \underline{b}_i^T [\mathbb{L}_i \dot{\underline{\omega}} + \underline{\omega} \times \mathbb{L}_i \underline{\omega} + \mathbb{I}_i \dot{\underline{\omega}} + (\underline{\omega} + \underline{\omega}_i) \times \mathbb{I}_i \underline{\omega}_i - m_i \underline{r}_i \cdot (\underline{\omega} \times \underline{R}) \underline{\omega}] . \tag{22}$$

Similarly, premultiplying (15) by $\underline{c}_i^T$ gives

$$T^c_{0i} = \underline{c}_i \cdot \underline{\tilde{T}}_i$$

$$- \underline{c}_i^T [\mathbb{L}_i \dot{\underline{\omega}} + \underline{\omega} \times \mathbb{L}_i \underline{\omega} + \mathbb{I}_i \dot{\underline{\omega}}_i + (\underline{\omega} + \underline{\omega}_i) \times \mathbb{I}_i \underline{\omega}_i - m_i \underline{r}_i \cdot (\underline{\omega} \times \underline{R}) \underline{\omega}] \tag{23}$$

When (19), (20), (22) and (23) are inserted into (21) and the orthogonality of $\underline{a}_i$, $\underline{b}_i$ and $\underline{c}_i$ is used, we find

$$
\begin{aligned}
&[\mathbb{I}_0 + \sum_{i=1}^{5} (\underline{b}_i \underline{b}_i^T + \underline{c}_i \underline{c}_i^T) \mathbb{L}_i]\, \dot{\underline{\omega}} = -\underline{\omega} \times \mathbb{I}_0 \underline{\omega} + \tilde{\underline{T}}_0 \\
&\quad + \sum_{i=1}^{5} (\alpha_i V_i + \beta_i \omega_i) \underline{a}_i + \sum_{i=4}^{5} (\underline{b}_i \underline{b}_i^T + \underline{c}_i \underline{c}_i^T) \tilde{\underline{T}}_i \\
&\quad - \sum_{i=1}^{5} (\underline{b}_i \underline{b}_i^T + \underline{c}_i \underline{c}_i^T) [\underline{\omega} \times \mathbb{L}_i \underline{\omega} + \underline{\omega} \times \underline{a}_i I_{ai} \omega_i - m_i \underline{r}_i \cdot (\omega \times \underline{R})\, \underline{\omega}]
\end{aligned}
\tag{24}
$$

Note that for each i (15) gives a vector equation. However, the motion of each part is constrained to be about the axis $\underline{a}_i$ so there is really only one degree of freedom for each i, not three. We can reduce (15) to a scalar equation by premultiplying by $\underline{a}_i^T$. Using (19) and the orthogonality of $\underline{a}_i$, $\underline{b}_i$, $\underline{c}_i$ we get

$$
\begin{aligned}
I_{ai} \dot{\omega}_i = &-\underline{a}_i^T [\mathbb{L}_i \dot{\underline{\omega}} + \underline{\omega} \times \mathbb{L}_i \underline{\omega} + \underline{\omega} \times \underline{a}_i I_{ai} \omega_i] \\
&-\beta_i \omega_i + m_i [\underline{\rho}_i \cdot (\underline{\omega} \times \underline{R})] (\underline{a}_i \cdot \underline{\omega}) + \underline{a}_i \cdot \tilde{\underline{T}}_i - \alpha_i V_i
\end{aligned}
\tag{25}
$$

In order to obtain the complete state differential equations (24) must be solved for $\dot{\underline{\omega}}$ which is then inserted into (25). The expression for $\dot{\underline{\omega}}$, the resulting equations (25), and (18) are then the state equations.

In order to proceed further we must be more specific about the physical structure of the system. Let us define the body axes $\underline{\xi}_a$, $\underline{\xi}_b$, $\underline{\xi}_c$ as the three principle axes of the main body then $\mathbb{I}_0$ becomes a diagonal matrix with diagonal elements I_{a0}, I_{b0}, I_{c0}. We will assume that the three reaction wheels are essentially aligned with these body axes so

$$
\begin{aligned}
\underline{a}_1 &= \underline{\xi}_a + \underline{\epsilon}_1 \\
\underline{a}_2 &= \underline{\xi}_b + \underline{\epsilon}_2 \\
\underline{a}_3 &= \underline{\xi}_c + \underline{\epsilon}_3
\end{aligned}
$$

where $\underline{\epsilon}_i$ are error vectors with small components.

We will make the following additional assumptions regarding the construction of the vehicle.

1) The c.m. of the composite vehicle is located very near the body axis origin (i.e., $\underline{R}$ is a small vector representing the error in centering the system).

2) The c.m.'s of the reaction wheels lie essentially on the coordinate axes so that

$$\underline{r}_1 = r_1 \underline{\xi}_a + \underline{\epsilon}_4$$

$$\underline{r}_2 = r_2 \underline{\xi}_b + \underline{\epsilon}_5$$

$$\underline{r}_3 = r_3 \underline{\xi}_c + \underline{\epsilon}_6$$

where $\underline{\epsilon}_i$ are small error vectors and r_i is the distance from the c.m. of the $i^{\underline{th}}$ wheel to the origin.

3) Let $\underline{\xi}_a$ denote the roll axis of the vehicle we will assume that $\underline{r}_4$ and $\underline{r}_5$ lie essentially along the $\underline{\xi}_b$ or yaw axis (i.e., perpendicular to the roll axis) so that

$$\underline{r}_4 = r_4 \underline{\xi}_b + \underline{\epsilon}_7$$

$$\underline{r}_5 = r_5 \underline{\xi}_b + \underline{\epsilon}_8$$

4) The pivot axes of the solar panels are essentially aligned with $\underline{\xi}_b$ axis (see Fig. A2) so that

$$\underline{a}_4 = \underline{\xi}_b + \underline{\epsilon}_9 \;, \quad \underline{b}_4 = \begin{bmatrix} \cos\delta \\ 0 \\ \sin\delta \end{bmatrix} + \underline{\epsilon}_9 \;, \quad \underline{c}_4 = \begin{bmatrix} \sin\delta \\ 0 \\ -\cos\delta \end{bmatrix} + \underline{\epsilon}_9 \tag{26}$$

where the angle δ is indicated in Fig. A-2 and $\underline{\epsilon}$ terms are small. Similarly

$$\underline{a}_5 = -\underline{\xi}_b + \underline{\epsilon}_{10} \;, \quad \underline{b}_5 = -\begin{bmatrix} \cos\delta \\ 0 \\ \sin\delta \end{bmatrix} + \underline{\epsilon}_{10} \;, \quad \underline{c}_5 = -\begin{bmatrix} \sin\delta \\ 0 \\ -\cos\delta \end{bmatrix} + \underline{\epsilon}_{10} \tag{27}$$

Note that when $\delta = 0$, $\underline{b}_4$ is essentially aligned with $\underline{\xi}_a$ and $\underline{c}_4$ with $-\underline{\xi}_c$.

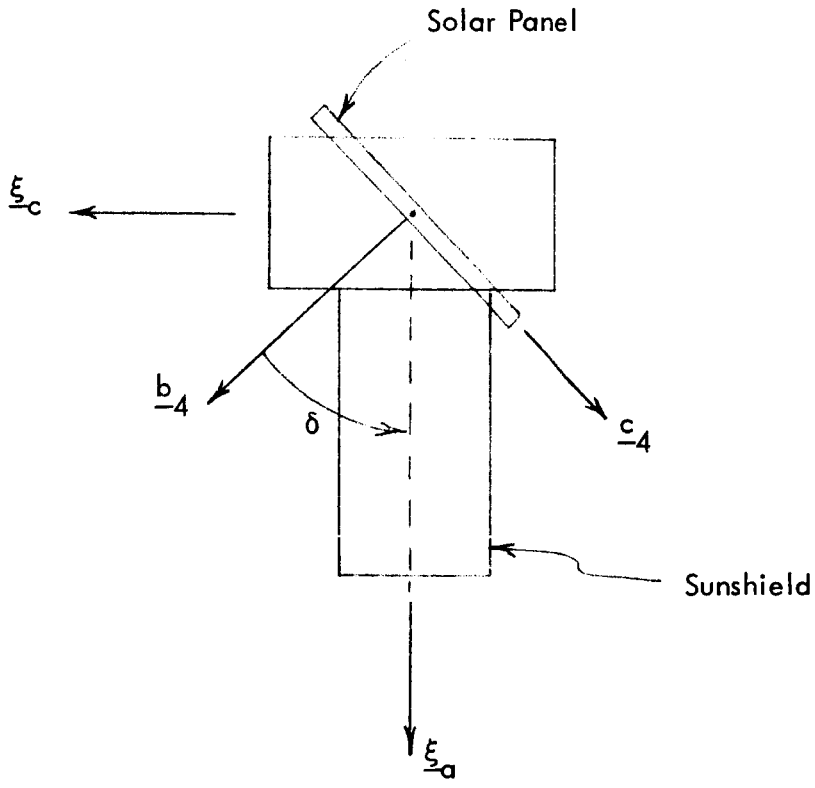

FIGURE A-2 NOMINAL ALIGNMENT OF SOLAR PANELS

Using these assumptions and neglecting the small error terms we find that $A_i = 0$ so $\mathbb{I}_i = \mathbb{I}_i + \mathbb{J}_i$ and if we define the matrix $\Sigma^{-1} \triangleq \mathbb{I}_0 + \sum_{i=1}^{5} (\underline{b}_i \underline{b}_i^T + \underline{c}_i \underline{c}_i^T)\mathbb{I}_i$ we obtain

$$\Sigma^{-1} = \begin{bmatrix} \hat{\Sigma}_{11} & 0 & \hat{\Sigma}_{13} \\ 0 & \hat{\Sigma}_{22} & 0 \\ \hat{\Sigma}_{13} & 0 & \hat{\Sigma}_{33} \end{bmatrix}$$

so

$$\Sigma = \frac{1}{\hat{\Sigma}_{11}\hat{\Sigma}_{33} - \hat{\Sigma}_{13}^2} \begin{bmatrix} \hat{\Sigma}_{33} & 0 & -\hat{\Sigma}_{13} \\ 0 & \dfrac{\hat{\Sigma}_{11}\hat{\Sigma}_{33} - \hat{\Sigma}_{13}^2}{\hat{\Sigma}_{22}} & 0 \\ -\hat{\Sigma}_{13} & 0 & \hat{\Sigma}_{11} \end{bmatrix}$$

where

$$\hat{\Sigma}_{11} = I_{a0} + \sum_{i \neq 1}^{5} m_i r_i^2 + I_{b3} + I_{c2} + (I_{b4} + I_{b5})\cos^2\delta + (I_{c4} + I_{c5})\sin^2\delta$$

$$\hat{\Sigma}_{22} = I_{b0} + I_{b1} + I_{c3} + m_1 r_1^2 + m_3 r_3^2$$

$$\hat{\Sigma}_{33} = I_{c0} + I_{b2} + I_{c1} + \sum_{i \neq 3}^{5} m_i r_i^2 + (I_{b4} + I_{b5})\sin^2\delta + (I_{a4} + I_{c5})\cos^2\delta$$

$$\hat{\Sigma}_{13} = (I_{b4} + I_{b5} - I_{c4} - I_{c5})\sin\delta\cos\delta$$

When the assumptions and the expression for Σ are used in (24) we obtain

$$\begin{bmatrix} \dot{\omega}_a \\ \dot{\omega}_b \\ \dot{\omega}_c \end{bmatrix} = \Sigma \begin{bmatrix} -\omega_b\omega_c f_2 - \omega_a\omega_b \hat{\Sigma}_{13} + \omega_c f_3 - \omega_b\omega_3 I_{a3} + \alpha_1 V_1 + \beta_1\omega_1 + (\tilde{T}_{0a} + \tilde{T}_{4a} + \tilde{T}_{5a}) \\ \text{---------- ---------- ---------- ---------- ---------- ----------} \\ -\omega_a\omega_c (I_{a0} - I_{c0} + I_{a1} - m_1 r_1^2 - I_{c1} + m_3 r_3^2 + I_{b3} - I_{a3}) + \omega_a\omega_3 I_{a3} \\ -\omega_c\omega_1 I_{a1} + \beta_2\omega_2 + \beta_4\omega_4 - \beta_5\omega_5 + \alpha_2 V_2 + \alpha_4 V_4 - \alpha_5 V_5 + \tilde{T}_{0b} \\ \text{---------- ---------- ---------- ---------- ---------- ----------} \\ -\omega_a\omega_b f_1 + \omega_a\omega_c \hat{\Sigma}_{13} - \omega_a f_3 + \omega_b\omega_1 I_{a1} + \beta_3\omega_3 + \alpha_3 V_3 + (\tilde{T}_{0c} + \tilde{T}_{4c} + \tilde{T}_{5c}) \end{bmatrix} \tag{28}$$

where

$$f_1 = I_{b0} - I_{a0} + I_{b1} - I_{a1} + I_{a2} - I_{c2} + I_{a4} + I_{a5} - (I_{b4} + I_{b5}) \cos^2\delta$$
$$-(I_{c4} + I_{c5}) \sin^2\delta + m_1 r_1^2 - m_2 r_2^2 - m_4 r_4^2 - m_5 r_5^2$$

$$f_2 = I_{c0} - I_{b0} + I_{b2} - I_{a2} + I_{a3} - I_{c3} - I_{a4} - I_{a5} + (I_{c4} + I_{c5}) \cos^2\delta$$
$$+ (I_{b4} + I_{b5}) \sin^2\delta + m_2 r_2^2 - m_3 r_3^2 + m_4 r_4^2 + m_5 r_5^2$$

$$f_3 = \omega_2 I_{a2} + \omega_4 I_{a4} - \omega_5 I_{a5}$$

while from (25) we obtain

$$\dot{\omega}_1 = -\dot{\omega}_a - \omega_b\omega_c \frac{(I_{c1} - I_{b1})}{I_{a1}} - \frac{\beta_1}{I_{a1}} \omega_1 - \frac{\alpha_1}{I_{a1}} V_1$$

$$\dot{\omega}_2 = -\dot{\omega}_b - \omega_a\omega_c \frac{(I_{c2} - I_{b2})}{I_{a2}} - \frac{\beta_2}{I_{a2}} \omega_2 - \frac{\alpha_2}{I_{a2}} V_2$$

$$\dot{\omega}_3 = -\dot{\omega}_c - \omega_a\omega_b \frac{(I_{c3} - I_{b3})}{I_{a3}} - \frac{\beta_3}{I_{a3}} \omega_3 - \frac{\alpha_3}{I_{a3}} V_3 \tag{29}$$

$$\dot{\omega}_4 = -\dot{\omega}_b - \omega_a\omega_c \frac{I_{b4} - I_{c4}}{I_{a4}} (\cos^2\delta - \sin^2\delta) + (\omega_a^2 - \omega_c^2) \frac{I_{b4} - I_{c4}}{I_{c4}} \sin\delta\cos\delta$$

$$- \frac{\beta_4}{I_{a4}} \omega_4 - \frac{\alpha_4}{I_{a4}} V_4 + \frac{\tilde{T}_{4b}}{I_{a4}}$$

$$\dot{\omega}_5 = \dot{\omega}_b + \omega_a\omega_b \frac{I_{b5} - I_{c5}}{I_{a5}} (\cos^2\delta - \sin^2\delta) - (\omega_a^2 - \omega_c^2) \frac{I_{b5} - I_{c5}}{I_{a5}} \sin\delta\cos\delta$$

$$- \frac{\beta_5}{I_{a5}} \omega_4 - \frac{\alpha_5}{I_{a5}} V_5 + \frac{\tilde{T}_{4b}}{I_{a5}}$$

When the expressions for $\dot{\omega}_a$, $\dot{\omega}_b$ and $\dot{\omega}_c$ from (28) are inserted into the equations (29), the resulting equations together with (28) and (18) are the complete state differential equations of the system. They are

$$\dot{\omega}_a = \Sigma_{11}\Gamma_1(y, V, T) + \Sigma_{13}\Gamma_3(y, V, T)$$

$$\dot{\omega}_b = \Sigma_{22}\Gamma_2(y, V, T)$$

$$\dot{\omega}_c = \Sigma_{13}\Gamma_1(y, V, T) + \Sigma_{33}\Gamma_3(y, V, T)$$

$$\dot{\omega}_1 = -\Sigma_{11}\Gamma_1(y, V, T) - \Sigma_{13}\Gamma_3(y, V, T) - \omega_b\omega_c \frac{(I_{c1} - I_{b1})}{I_{a1}} - \frac{\beta_1}{I_{a1}} \omega_1 - \frac{\alpha_1}{I_{a1}} V_1$$

$$\dot{\omega}_2 = -\Sigma_{22}\Gamma_2(y, V, T) - \omega_a\omega_c \frac{(I_{c2} - I_{b2}}{I_{a2}} - \frac{\beta_2}{I_{a2}} \omega_2 - \frac{\alpha_2}{I_{a2}} V_2$$

$$\dot{\omega}_3 = -\Sigma_{13}\Gamma_1(y, V, T) - \Sigma_{33}\Gamma_3(y, V, T) - \omega_a\omega_b \frac{I_{c3} - I_{b3}}{I_{a3}} - \frac{\beta_3}{I_{a3}} \omega_3 - \frac{\alpha_3}{I_{a3}} V_3$$

$$\dot{\theta}_1 = \omega_b \frac{\cos\theta_3}{\cos\theta_2} - \omega_c \frac{\sin\theta_3}{\cos\theta_2}$$

$$\dot{\theta}_2 = \omega_b \sin\theta_3 + \omega_c \cos\theta_3$$

$$\dot{\theta}_3 = \omega_a - \omega_b \tan\theta_2 \cos\theta_3 + \omega_c \tan\theta_2 \sin\theta_3$$

$$\dot{\omega}_4 = -\Sigma_{22}\Gamma_2(y, V, T) - \omega_a\omega_c \frac{I_{b4} - I_{c4}}{I_{a4}} (\cos^2\delta - \sin^2\delta)$$

$$+ (\omega_a^2 - \omega_c^2) \frac{I_{b4} - I_{c4}}{I_{a4}} \sin\delta \cos\delta + \frac{\tilde{T}_{4b} - \beta_4\omega_4 - \alpha_4 V_4}{I_{a4}}$$

$$\dot{\omega}_5 = \Sigma_{22}\Gamma_2(y, V, T) + \omega_a\omega_c \frac{I_{b5} - I_{c5}}{I_{a5}} (\cos^2\delta - \sin^2\delta)$$

$$- (\omega_a^2 - \omega_c^2) \frac{I_{b5} - I_{c5}}{I_{a5}} \sin\delta \cos\delta - \frac{\tilde{T}_{5b} + \beta_5\omega_5 + \alpha_5 V_5}{I_{a5}} \qquad (30)$$

where

$$\Gamma_1(y, V, T) = -\omega_b\omega_c f_2 - \omega_a\omega_b \hat{\Sigma}_{13} + \omega_c(\omega_2 I_{a2} + \omega_4 I_{a4} - \omega_5 I_{a5})$$

$$- \omega_b\omega_3 I_{a3} + \alpha_1 V_1 + \beta_1\omega_1 + (\tilde{T}_{0a} + \tilde{T}_{4a} + \tilde{T}_{5a})$$

$$\Gamma_2(y, V, T) = -\omega_a\omega_c [I_{a0} - I_{c0} + I_{a1} - m_1 r_1^2 - I_{c1} + m_3 r_3^2 + I_{b3} - I_{a3}]$$

$$+ \omega_a\omega_3 I_{a3} - \omega_c\omega_1 I_{a1} + \hat{\rho}_2\omega_2 + \hat{\rho}_4\omega_4 - \hat{\rho}_5\omega_5 + \alpha_2 V_2$$

$$+ \alpha_4 V_4 - \alpha_5 V_5 + \tilde{T}_{0b}$$

$$\Gamma_3(y, V, T) = -\omega_a\omega_b f_1 + \omega_b\omega_c \hat{\Sigma}_{13} + \omega_a [-\omega_2 I_{a2} - \omega_4 I_{a4} + \omega_5 I_{a5}]$$

$$+ \omega_b\omega_1 I_{a1} + \beta_3\omega_3 + \alpha_3 V_3 + (\tilde{T}_{0c} + \tilde{T}_{4c} + \tilde{T}_{5c})$$

and

$$\hat{\Sigma}_{11} = I_{a0} + [\sum_{i\neq 1}^{5} m_i r_i^2] + I_{b3} + I_{c2} + (I_{b4} + I_{b5})\cos^2\delta + (I_{c4} + I_{c5})\sin^2\delta$$

$$\hat{\Sigma}_{13} = (I_{b4} + I_{b5} - I_{c4} - I_{c5})\sin\delta\cos\delta$$

$$\hat{\Sigma}_{22} = I_{b0} + [\sum_{i=1,3} m_i r_i^2] + I_{b1} + I_{c3}$$

$$\hat{\Sigma}_{33} = I_{c0} + [\sum_{i\neq 3}^{5} m_i r_i^2] + I_{b2} + I_{c1} + (I_{b4} + I_{b5})\sin^2\delta + (I_{c4} + I_{c5})\cos^2\delta$$

$$\Sigma_{11} = \frac{\hat{\Sigma}_{33}}{\hat{\Sigma}_{11}\hat{\Sigma}_{33} - \hat{\Sigma}_{13}^2}$$

$$\Sigma_{22} = \frac{1}{\hat{\Sigma}_{22}}$$

$$\Sigma_{33} = \frac{\hat{\Sigma}_{11}}{\hat{\Sigma}_{11}\hat{\Sigma}_{33} - \hat{\Sigma}_{13}^2}$$

$$\Sigma_{13} = -\frac{\hat{\Sigma}_{13}}{\hat{\Sigma}_{11}\hat{\Sigma}_{33} - \hat{\Sigma}_{13}^2}$$

It should be noted that the torques $\tilde{T}_{4j}$, $\tilde{T}_{5j}$ for j = a, b, c consist of external disturbance torques only, but the $\tilde{T}_{0j}$'s include both reaction jet torques T_{rj} and the disturbance torques. This will be denoted as

$$\tilde{T}_{0j} = T_{rj} + T_{0j}$$

and

$$\tilde{T}_{4j} = T_{4j}$$

$$\tilde{T}_{5j} = T_{5j}$$

for j = a, b, c

Note also that voltages V_4 and V_5 appear in the equations. These are the voltages which must be applied to the motors connected to the solar panels in order to keep the panels facing the Sun. They are not control variables, but are presumed known time functions.

Linearized Equations about Nominal Motion

In a well-designed control system, the state y is expected to be very close to the desired nominal motion represented by the state y_N, the control torques for which are derived by the application of the nominal controls V_N. Consequently, we can study the deviations from the nominal motion by means of linear "error equations".

Let us represent the angular velocities as

$$\omega_i(t) = \omega_{iN}(t) + \lambda_i(t)$$

for $i = a, b, c, 1, \ldots 5$ where ω_{iN} is the precalculated nominal motion and λ_i denotes the deviation from nominal behavior. Similarly we write

$$\theta_i(t) = \theta_{iN}(t) + \gamma_i(t) \qquad i = a, b, c$$

and

$$V_i(t) = V_{iN}(t) + u_i(t) \qquad i = 1, \ldots 5$$

where $\gamma_i(t)$ and $u_i(t)$ are again deviations and V_{iN} are the voltages required to produce the nominal behavior. We assume further that the reaction jets will not be used to control small deviations from nominal motion. Such deviations will be controlled using only the reaction wheel voltages. Furthermore, we will not be concerned with control of the solar panels. That is we well not attempt to generate u_4 and u_5. Since these controls will be generated by an independent control loop, wherever they appear they will be included (to first order) in error terms. Then, since the nominal motion is assumed known, we need only consider the deviations which are governed by linear differential equations obtained by inserting the above expressions for ω_i, θ_i and V_i into the complete state equations (30) and equating the $\dot{\lambda}_i$ and $\dot{\gamma}_i$ terms to the terms linear in λ_i, γ_i and u_i plus any disturbance torques. This gives

$$\begin{bmatrix}\dot{\lambda}_a\\ \dot{\lambda}_b\\ \dot{\lambda}_c\end{bmatrix} = -A \begin{bmatrix}\lambda_a\\ \lambda_b\\ \lambda_c\end{bmatrix} + B \begin{bmatrix}\lambda_1\\ \lambda_2\\ \lambda_3\end{bmatrix} + R \begin{bmatrix}u_1\\ u_2\\ u_3\end{bmatrix} + L \begin{bmatrix}\lambda_4\\ \lambda_5\end{bmatrix} + T_1$$

$$\begin{bmatrix}\dot{\lambda}_1\\ \dot{\lambda}_2\\ \dot{\lambda}_3\end{bmatrix} = -D \begin{bmatrix}\lambda_1\\ \lambda_2\\ \lambda_3\end{bmatrix} + C \begin{bmatrix}\lambda_a\\ \lambda_b\\ \lambda_c\end{bmatrix} - L \begin{bmatrix}\lambda_4\\ \lambda_5\end{bmatrix} - T \begin{bmatrix}u_1\\ u_2\\ u_3\end{bmatrix} - T_1 \qquad (31)$$

$$\begin{bmatrix}\dot{\gamma}_1\\ \dot{\gamma}_2\\ \dot{\gamma}_3\end{bmatrix} = P \begin{bmatrix}\lambda_a\\ \lambda_b\\ \lambda_c\end{bmatrix} + Q \begin{bmatrix}\gamma_1\\ \gamma_2\\ \gamma_3\end{bmatrix}$$

$$\begin{bmatrix}\dot{\lambda}_4\\ \dot{\lambda}_5\end{bmatrix} = Y \begin{bmatrix}\lambda_a\\ \lambda_b\\ \lambda_c\end{bmatrix} + X \begin{bmatrix}\lambda_1\\ \lambda_2\\ \lambda_3\end{bmatrix} + W \begin{bmatrix}\lambda_4\\ \lambda_5\end{bmatrix} + Z \begin{bmatrix}u_1\\ u_2\\ u_3\end{bmatrix} + T_2$$

where A is a 3x3 matrix with elements

$$A_{11} = [\Sigma_{11}\hat{\Sigma}_{13} + \Sigma_{13}f_1]\omega_{bN} + \Sigma_{13}[\omega_{2N}I_{a2} + \omega_{4N}I_{a4} - \omega_{5N}I_{a5}]$$

$$A_{21} = \Sigma_{22}[(I_{a0} - I_{c0} + I_{a1} - I_{c1} + I_{b3} - I_{a3} - m_1 r_1^2)\omega_{cN} - I_{a3}\omega_{3N}]$$

$$A_{31} = [\Sigma_{13}\hat{\Sigma}_{13} + \Sigma_{33}f_1]\omega_{bN} + \Sigma_{33}[\omega_{2N}I_{a2} + \omega_{4N}I_{a4} - \omega_{5N}I_{a5}]$$

$$A_{12} = [\Sigma_{11} f_2 - \Sigma_{13} \hat{\Sigma}_{13}]\, \omega_{cN} + [\Sigma_{11} \hat{\Sigma}_{13} + \Sigma_{13} f_1]\, \omega_{aN} + \Sigma_{11} \omega_{3N} I_{a3} - \Sigma_{13} \omega_{1N} I_{a1}$$

$$A_{22} = 0$$

$$A_{32} = [\Sigma_{13} f_2 - \Sigma_{33} \hat{\Sigma}_{13}]\, \omega_{cN} + [\Sigma_{13} \hat{\Sigma}_{13} + \Sigma_{33} f_1]\, \omega_{aN} + \Sigma_{13} \omega_{3N} I_{a3} - \Sigma_{33} \omega_{1N} I_{a1}$$

$$A_{13} = [\Sigma_{11} f_2 - \Sigma_{13} \hat{\Sigma}_{13}]\, \omega_{bN} + \Sigma_{11} [-\omega_{2N} I_{a2} - \omega_{4N} I_{a4} + \omega_{5N} I_{a5}]$$

$$A_{23} = \Sigma_{22} [(I_{a0} - I_{c0} + I_{a1} - I_{c1} + I_{b3} - I_{a3} - m_1 r_1^2)\, \omega_{aN} + I_{a1} \omega_{1N}]$$

$$A_{33} = [\Sigma_{13} f_2 - \Sigma_{33} \hat{\Sigma}_{13}]\, \omega_{bN} + \Sigma_{13} [-\omega_{2N} I_{a2} - \omega_{4N} I_{a4} + \omega_{5N} I_{a5}]$$

$$B = \begin{bmatrix} \Sigma_{11}\beta_1 + \Sigma_{13}\omega_{bN} I_{a1} & \Sigma_{11}\omega_{cN} I_{a2} - \Sigma_{13}\omega_{aN} I_{a2} & -\Sigma_{11}\omega_{bN} I_{a3} + \Sigma_{13}\beta_3 \\ -\Sigma_{22} I_{a1}\omega_{cN} & \Sigma_{22}\beta_2 & \Sigma_{22} I_{a3}\omega_{aN} \\ \Sigma_{13}\beta_1 + \Sigma_{33}\omega_{bN} I_{a1} & \Sigma_{13}\omega_{cN} I_{a2} - \Sigma_{33}\omega_{aN} I_{a2} & -\Sigma_{13}\omega_{bN} I_{a3} + \Sigma_{33}\beta_3 \end{bmatrix}$$

$$L = \begin{bmatrix} [\Sigma_{11}\omega_{cN} - \Sigma_{13}\omega_{aN}] & [-\Sigma_{11}\omega_{cN} + \Sigma_{13}\omega_{aN}]\, I_{a5} \\ \Sigma_{22}\beta_4 & -\Sigma_{22}\beta_5 \\ [\Sigma_{13}\omega_{cN} - \Sigma_{33}\omega_{aN}]\, I_{a4} & [-\Sigma_{13}\omega_{cN} + \Sigma_{33}\omega_{aN}]\, I_{a5} \end{bmatrix}$$

$$R = \begin{bmatrix} \Sigma_{11}\alpha_1 & 0 & \Sigma_{13}\alpha_3 \\ 0 & \Sigma_{22}\alpha_2 & 0 \\ \Sigma_{13}\alpha_1 & 0 & \Sigma_{33}\alpha_3 \end{bmatrix}$$

$$T_1 = \begin{bmatrix} \Sigma_{11}(T_{0a} + T_{4a} + T_{5a}) + \Sigma_{13}(T_{0c} + T_{4c} + T_{5c}) \\ \Sigma_{22}T_{0b} \\ \Sigma_{13}(T_{0a} + T_{4a} + T_{5a}) + \Sigma_{33}(T_{0c} + T_{4c} + T_{5c}) \end{bmatrix}$$

$$D = B + \begin{bmatrix} \frac{\beta_1}{I_{a1}} & 0 & 0 \\ 0 & \frac{\beta_2}{I_{a2}} & 0 \\ 0 & 0 & \frac{\beta_3}{I_{a3}} \end{bmatrix}$$

$$C = A - \begin{bmatrix} 0 & \omega_{cN}\frac{I_{c1} - I_{b1}}{I_{a1}} & \omega_{bN}\frac{I_{c1} - I_{b1}}{} \\ \omega_{cN}\frac{I_{c2} - I_{b2}}{I_{a2}} & 0 & \omega_{aN}\frac{I_{c2} - I_{b2}}{I_{a2}} \\ \omega_{bN}\frac{I_{c3} - I_{b3}}{I_{a3}} & \omega_{aN}\frac{I_{c3} - I_{b3}}{I_{a3}} & 0 \end{bmatrix}$$

$$T = R + \begin{bmatrix} \alpha_1/I_{a1} & 0 & 0 \\ 0 & \alpha_2/I_{a2} & 0 \\ 0 & 0 & \alpha_3/I_{a3} \end{bmatrix}$$

$$P = \begin{bmatrix} 0 & \dfrac{\cos\theta_{3N}}{\cos\theta_{2N}} & -\dfrac{\sin\theta_{3N}}{\cos\theta_{2N}} \\ 0 & \sin\theta_{3N} & \cos\theta_{3N} \\ 1 & -\tan\theta_{2N}\cos\theta_{3N} & \tan\theta_{2N}\sin\theta_{3N} \end{bmatrix}$$

$$Q = \begin{bmatrix} 0 & \dfrac{\sin\theta_{2N}}{\cos^2\theta_{2N}}(\omega_{bN}\cos\theta_{3N} - \omega_{cN}\sin\theta_{3N}) & -\dfrac{[\omega_{bN}\sin\theta_{3N} + \omega_{cN}\cos\theta_{3N}]}{\cos\theta_{2N}} \\ 0 & 0 & \omega_{bN}\cos\theta_{3N} - \omega_{cN}\sin\theta_{3N} \\ 0 & \dfrac{\omega_{cN}\sin\theta_{3N} - \omega_{bN}\cos\theta_{3N}}{\cos^2\theta_{2N}} & \tan\theta_{2N}(\omega_{bN}\sin\theta_{3N} - \omega_{cN}\cos\theta_{3N}) \end{bmatrix}$$

$$Y = \left[\begin{array}{c|c|c} A_{21} + [-\omega_{cN}(\cos^2\delta - \sin^2\delta) + 2\omega_{aN}\sin\delta\cos\delta]\dfrac{I_{b4} - I_{c4}}{I_{a4}} & 0 & A_{23} + [\omega_{aN}(\cos^2\delta - \sin^2\delta) - 2\omega_{cN}\sin\delta\cos\delta]\dfrac{I_{b4} - I_{c4}}{I_{a4}} \\ \hline -A_{21} + [\omega_{cN}(\cos^2\delta - \sin^2\delta) - 2\omega_{aN}\sin\delta\cos\delta]\dfrac{I_{b5} - I_{c5}}{I_{a5}} & 0 & -A_{23} + [\omega_{aN}(\cos^2\delta - \sin^2\delta) + 2\omega_{cN}\sin\delta\cos\delta]\dfrac{I_{b5} - I_{c5}}{I_{a5}} \end{array}\right]$$

$$X = \begin{bmatrix} -B_{21} & -B_{22} & -B_{23} \\ B_{21} & B_{22} & B_{23} \end{bmatrix}$$

$$W = \begin{bmatrix} -\Sigma_{22}\beta_4 - \beta_4 / I_{a4} & \Sigma_{22}\beta_5 \\ \Sigma_{22}\beta_4 & -\Sigma_{22}\beta_5 - \beta_5 / I_{a5} \end{bmatrix}$$

$$Z = \begin{bmatrix} 0 & -\Sigma_{22}\alpha_2 & 0 \\ 0 & \Sigma_{22}\alpha_2 & 0 \end{bmatrix}$$

$$T_2 = \begin{bmatrix} -\Sigma_{22}T_{0b} + T_{4b} / I_{a4} \\ \Sigma_{22}T_{0b} - T_{5b} / I_{a5} \end{bmatrix}$$

Thus the deviation from the nominal motion is governed by the linear differential equations (31) which are of the form

$$\dot{x} = Fx + Gu + w \tag{32}$$

where

$x = y - y_N = \{\lambda_a, \lambda_b, \lambda_c, \lambda_1, \lambda_2, \lambda_3, \gamma_1, \gamma_2, \gamma_3, \lambda_4, \lambda_5\}$

$u = v - v_N$

w is a vector due to disturbances to the nominal motion resulting from sources such as listed in section 4.

Since we assumed that deviations from the nominal will be corrected by applying correction voltages to the reaction wheels and not by activation of the reaction jets, u will be a 3-vector.

The matrices F and G are

$$F = \begin{array}{c} \begin{array}{cccc} \leftarrow 3 \rightarrow & \leftarrow 3 \rightarrow & \leftarrow 3 \rightarrow & \leftarrow 2 \rightarrow \end{array} \\ \left[\begin{array}{c|c|c|c} -A & B & 0 & L \\ \hline C & D & 0 & -L \\ \hline P & 0 & Q & 0 \\ \hline Y & X & 0 & W \end{array}\right] \end{array} \begin{array}{l} \updownarrow 3 \\ \updownarrow 3 \\ \updownarrow 3 \\ \updownarrow 2 \end{array}$$

$$G = \begin{array}{c} \leftarrow 3 \rightarrow \\ \left[\begin{array}{c} R \\ \hline -T \\ \hline 0 \\ \hline Z \end{array}\right] \end{array} \begin{array}{l} \updownarrow 3 \\ \updownarrow 3 \\ \updownarrow 3 \\ \updownarrow 2 \end{array} \qquad \text{and} \qquad w = \begin{array}{c} \leftarrow 1 \rightarrow \\ \left[\begin{array}{c} T_1 \\ \hline -T_1 \\ \hline 0 \\ \hline T_2 \end{array}\right] \end{array} \begin{array}{l} \updownarrow 3 \\ \updownarrow 3 \\ \updownarrow 3 \\ \updownarrow 2 \end{array}$$

Nominal Motion

To illustrate how the nominal motion may be determined, we will use the following simplifying assumptions.

1. The Earth and Mars are traveling in the solar ecliptic plane in known circular orbits about the Sun and the vehicle is in a known circular orbit about Mars.

2. The vehicle mechanical axis $\underline{\xi}_a$ is pointed to the center of the Earth.

3. The solar panel faces (i.e., $\underline{b}_4$ and $\underline{b}_5$) are pointing toward the center of the Sun.

Thus, in terms of the geometry of Figure (A.3) we can define nominal motion by

$$\theta_{1N}(t) = \mu_4(t) \quad , \qquad \theta_{2N}(t) = 0 \quad , \qquad \theta_{3N}(t) = 0$$

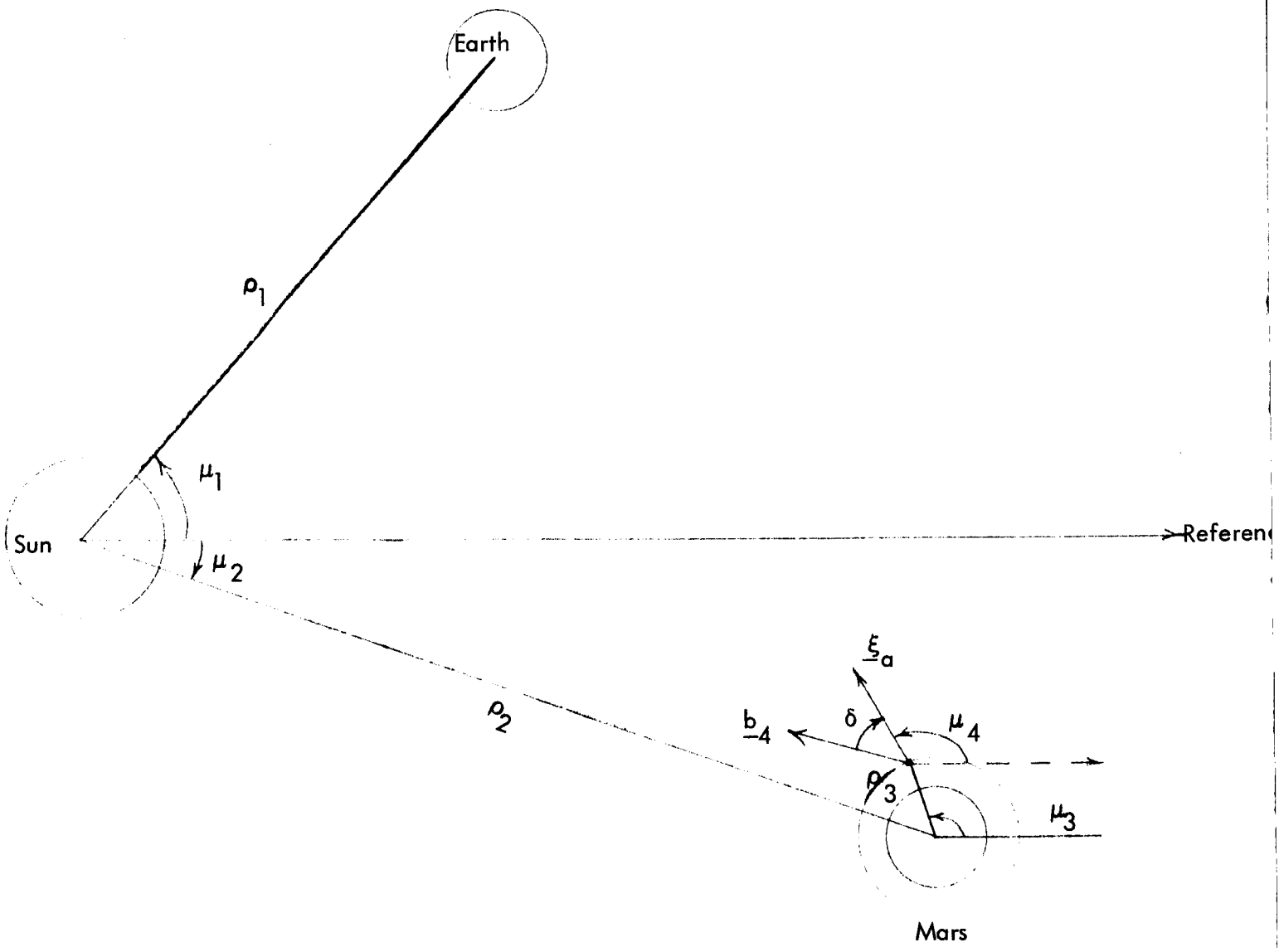

FIGURE A-3 ORIENTATION OF PLANETS

and from (17) we have $\omega_{aN} \equiv 0$, $\omega_{bN} = \dot{\mu}_4$, $\omega_{cN} \equiv 0$ which results in

$$P = \begin{bmatrix} 0 & 1 & 0 \\ 0 & 0 & 1 \\ 1 & 0 & 0 \end{bmatrix}$$

$$Q = \begin{bmatrix} 0 & 0 & 0 \\ 0 & 0 & 1 \\ 0 & -1 & 0 \end{bmatrix} \dot{\mu}_4$$

We have found that

$$\tan \mu_4(t) = \frac{\rho_1 \sin \mu_1 - \rho_2 \sin \mu_2 - \rho_3 \sin \mu_3}{\rho_1 \cos \mu_1 - \rho_2 \cos \mu_2 - \rho_3 \cos \mu_3}$$

and that to first-order

$$\dot{\mu}_4(t) = k_0 + k_1 \sin \left(\frac{2\pi}{T_3} \Delta t + \mu_0\right)$$

where the constants k_0, k_1, and μ_0 depend on the initial orientation of the three bodies and T_3 is the period of the vehicle's orbit (2.05 hours for an orbit 400 km above the surface),

$$k_0 = \frac{1}{1 + \tan^2 \mu_{40}} \; \frac{2\pi \left(\frac{\cos \mu_{10} + \tan \mu_{40} \sin \mu_{10}}{T_1}\right) - \frac{\rho_2}{\rho_1} \frac{\cos \mu_{20} + \tan \mu_{40} \sin \mu_{20}}{T_2}}{\cos \mu_{10} - \frac{\rho_2}{\rho_1} \cos \mu_{20} - \frac{\rho_3}{\rho_1} \cos \mu_{30}}$$

$$k_1 = \frac{\frac{\rho_3}{\rho_1} \frac{2\pi}{T_3} \left| \cos \mu_{40} \right|}{\cos \mu_{10} - \frac{\rho_2}{\rho_1} \cos \mu_{20} - \frac{\rho_3}{\rho_1} \cos \mu_{30}}$$

$$\mu_0 = \frac{\pi}{2} - \mu_{40}$$

where T_1 = 365.26 days is the period of the Earth orbit

T_2 = 686.98 days is the period of the Mars orbit

and μ_{i0} denote the initial orientation.

From the diagram we find that

$$\tan(\mu_4 - \delta) = \frac{\rho_2 \sin \mu_2 + \rho_3 \sin \mu_3}{\rho_2 \cos \mu_2 + \rho_3 \cos \mu_3}$$

but since $\rho_2 >>> \rho_3$ we get $\tan(\mu_4 - \delta) = \tan \mu_2$ and as shown in Figure (A.3) $(\mu_4 - \delta)$ and μ_2 differ by almost π so

$$\delta = \mu_4 - \mu_2 + \pi$$

To determine the nominal values ω_{2N}, V_{2N}, V_{4N}, V_{5N}, note that for the assumed nominal motion, in the absence of disturbances, we have

$$\omega_{1N} = \omega_{3N} \equiv 0, \qquad V_{1N} = V_{3N} \equiv 0$$

since the solar panels track the sun we have $\omega_{4N} = \dot{\delta}$ so that

$$\omega_{4N} = \dot{\mu}_4 - \dot{\mu}_2, \qquad \omega_{5N} = \dot{\mu}_2 - \dot{\mu}_4$$

We still must find ω_{2N}. Using the nominal values determined thus far in the state equations (28) and (29), for $\dot{\omega}_{bN}$, $\dot{\omega}_{4N}$ and $\dot{\omega}_{5N}$, we get

$$\dot{\omega}_{bN} = \ddot{\mu}_4 = \Sigma_{22}[\alpha_2 V_{2N} + \beta_2 \omega_{2N} + \alpha_4 V_{4N} + \beta_4 \omega_{4N} - \alpha_5 V_{5N} - \beta_5 \omega_{5N}]$$

$$\dot{\omega}_{4N} = \ddot{\mu}_4 - \ddot{\mu}_2 = -\dot{\omega}_{bN} - \frac{1}{I_{a4}}[\alpha_4 V_{4N} + \beta_4 \omega_{4N}]$$

$$\dot{\omega}_{5N} = \ddot{\mu}_2 - \ddot{\mu}_4 = \dot{\omega}_{bN} - \frac{1}{I_{a5}}[\alpha_5 V_{5N} + \beta_5 \omega_{5N}]$$

These are three equations in the four unknowns ω_{2N}, V_{2N}, V_{4N}, V_{5N}. An additional equation is obtained from the law of conservation of momentum. Let I_b be the total moment of inertia of the composite body about the ξ_b axis. Then

$$I_b \omega_{bN} + I_{a2} \omega_{2N} + I_{a4} \omega_{4N} - I_{a5} \omega_{5N} = \hat{K} = \text{const.}$$

From this and the known expressions for ω_{4N} and ω_{5N}

$$\omega_{2N} = \frac{\hat{K} - (I_b + I_{a4} + I_{a5})\dot{\mu}_4 + (I_{a4} + I_{a5})\dot{\mu}_2}{I_{a2}}$$

and

$$V_{4N} = \frac{1}{\alpha_4}[\beta_4(\dot{\mu}_2 - \dot{\mu}_4) + I_{a4}(\ddot{\mu}_2 - 2\ddot{\mu}_4)]$$

$$V_{5N} = \frac{1}{\alpha_5}[\beta_5(\dot{\mu}_4 - \dot{\mu}_2) + I_{a5}(2\ddot{\mu}_4 - \ddot{\mu}_2)]$$

$$V_{2N} = \frac{1}{\alpha_2}[-\beta_2 \omega_{2N} + (2\ddot{\mu}_4 - \ddot{\mu}_2)(I_{a4} + I_{a5})]$$

In order to obtain some numerical values for the nominal motion let us assume $\hat{K} = 0$ (i.e. no initial angular momentum) and the specific initial orientation of the planets

$$\mu_{10} = \mu_{20} = 0, \quad \mu_{30} = \pi, \quad \mu_{40} = \pi$$

This gives

$$\dot{\mu}_4 = -.484 \times 10^{-5} - .25 \times 10^{-5} \sin(.05\Delta t - \frac{\pi}{2}) \frac{\text{rad}}{\text{min}}$$

with Δt in minutes or

$$\dot{\mu}_4 = .806 \times 10^{-7} - .417 \times 10^{-7} \sin(8.5 \times 10^{-4} \Delta\tau - \frac{\pi}{2}) \frac{\text{rad}}{\text{sec}}$$

with $\Delta\tau$ in seconds. For $\Delta\tau = 0$ we get

$$\dot{\mu}_4(0) = -.3953 \times 10^{-7} \frac{\text{rad}}{\text{sec}}$$

$$\delta(0) = 0 \text{ rad.}$$

At $\Delta\tau$ = 1800 secs. (i.e. Δt = 30 min) we find

$$\dot{\mu}_4(\Delta\tau) = -.777 \times 10^{-5} \frac{\text{rad}}{\text{sec}}$$

$$\delta(\Delta\tau) = -28.576 \times 10^{-5} \text{ rad}$$

Since the linearized equations need the nominal values of δ_N, ω_{bN}, ω_{4N}, ω_{5N} which change only slightly over a thirty minute time interval we will use constant values chosen from the middle of the range of variation. Thus choose $\dot{\mu}_{4N} = \omega_{bN} = -.583 \times 10^{-7} \frac{\text{rad}}{\text{sec}}$

$$\delta_N = -15 \times 10^{-5} \text{ rad}$$

$$\omega_{4N} = -\omega_{5N} = -1.642 \times 10^{-7} \frac{\text{rad}}{\text{sec}}$$

$$\omega_{2N} = .112 \times 10^{-2} \frac{\text{rad}}{\text{sec}}$$

$$\sin \delta_N = \delta_N = -15 \times 10^{-5}$$

$$\cos \delta_N = 1 .$$

Typical Vehicle Parameters

A vehicle configuration was chosen to conform to the general specifications supplied by ERC that the vehicle have a total weight of about 3100 lbs. (~1550 kg.) with a 12 ft. (~4m.) telescope sunshield weighing 100 lbs (~50 kg.). Since the telescope diameter is about 30 in. the sunshield diameter was taken as 1 m. Cylindrical and rectangular components were assumed to facilitate the evaluation of moments of inertia.

TABLE A.1

MOMENTS OF INERTIA

For the body with sunshield as shown in Figure (4.1)

$$I_{a0} = .1125 \text{ kg-m}^2$$

$$I_{b0} = I_{c0} = 2062 \text{ kg-m}^2$$

For double wheels each of mass 5 kg., radius 10.61 cm and thickness 3 cm on a 30 cm. shaft centered at the body center of mass.

$$I_{ai} = .1125 \text{ kg-m}^2$$

$$I_{bi} = I_{ci} = .2539 \text{ kg-m}^2 \qquad i = 1, 2, 3$$

For solar panels as shown in Figure (4.1)

$$I_{a4} = I_{a5} = 33 \text{ kg-m}^2$$

$$I_{b4} = I_{b5} = 330 \text{ kg-m}^2$$

$$I_{c4} = I_{c5} = 330 \text{ kg-m}^2$$

For composite body about ξ_b

$$I_b = 2128 \text{ kg-m}^2$$

The power requirement is approximately 2000 watts. The information given in Report AFF DL-TR-64-168, Pt III of Wright-Patterson-Flight Dynamics Laboratory prepared by GE-Missiles and Space Division would indicate that 500 watts of power from a V-ridge concentrating array requires 56.8 ft.^{2} of active cell area, a paddle area of 133 ft.^{2}, and an array weight of 298 lbs/kw. Scaling up to 2 kw. indicates a paddle area of 533 ft.^{2} and weight 596 lbs. The values chosen were 440 lbs. and 253 ft.^{2} and are based on the expectation of improved efficiencies in conversion of solar energy and reduction of the paddle area to active cell area.

The reaction wheels were chosen to give a moment of inertia of approximately .1 kg-m^2. This number was obtained by scaling up from a value of .01 kg-m^2 given in [15] for a vehicle with moment 200 kg-m^2. Double wheels on a single shaft were chosen so that the center of mass of each wheel combination could be placed close to the center of mass of the body. This produces a better balanced vehicle.

Table A.1 contains the values of moments of inertia of the vehicle which were calculated using the dimensions indicated in Figure 4.1 .

The parameters α_i and β_i of the motors driving the reaction wheels were determined as follows: the motor time constant was assumed to be 30 sec. Thus, with $I = .1125$ kgm-m^2 we have

$$-\beta_i = \frac{I}{\tau} = \frac{.1125}{30} = 3.75 \times 10^{-3} \ \frac{\text{newton-meters}}{\text{rad/sec}} \quad , i = 1, 2, 3$$

The no load speed ω_{NL} was assumed to be 100 rad/sec (about 1000 rpm.). The stall torque T_s is found to be

$$T_s = -\beta \omega_{NL} = .375 \text{ newton-meters}$$

Now, assuming this torque is produced by a voltage of 25 volts we obtain

$$\alpha_i = 3.75 \times 10^{-1}/25 = 1.5 \times 10^{-2} \ \frac{\text{newton-meters}}{\text{volt}} \quad , \quad i = 1, 2, 3$$

The time constant of motors used to control the solar panels was assumed to be about 2 seconds, resulting in the following motor constants

$$\alpha_4 = \alpha_5 = 3 \times 10^{-4} \text{ newton-meters/volt}$$

$$\beta_4 = \beta_5 = -15 \frac{\text{newton-meters}}{\text{rad/sec}}$$

Using these numbers we find

$$\hat{\Sigma}_{11} = 4508 \text{ kg-m}^2$$

$$\hat{\Sigma}_{13} = \hat{\Sigma}_{31} = -.009 \text{ kg-m}^2$$

$$\hat{\Sigma}_{22} = 2062 \text{ kg-m}^2$$

$$\hat{\Sigma}_{33} = 5863 \text{ kg-m}^2$$

and since $\hat{\Sigma}_{13}$ is so small compared to $\hat{\Sigma}_{11}$ and $\hat{\Sigma}_{33}$ we get

$$\Sigma_{11} = 2.219 \times 10^{-4}$$

$$\Sigma_{22} = 4.8497 \times 10^{-4}$$

$$\Sigma_{33} = 1.706 \times 10^{-4}$$

$$\Sigma_{13} = \Sigma_{31} = 3.4 \times 10^{-10}$$

and

$$A = C = \begin{bmatrix} .2058 \times 10^{-12} & 0 & -.7586 \times 10^{-7} \\ 0 & 0 & 0 \\ .25 \times 10^{-8} & 0 & .1214 \times 10^{-12} \end{bmatrix}$$

$$B = \begin{bmatrix} .832 \times 10^{-6} & 0 & .273 \times 10^{-4} \\ 0 & .1818 \times 10^{-5} & 0 \\ .155 \times 10^{-12} & 0 & .64 \times 10^{-6} \end{bmatrix}$$

$$D = \begin{bmatrix} .033 & 0 & .273 \times 10^{-4} \\ 0 & .033 & 0 \\ .155 \times 10^{-12} & 0 & .033 \end{bmatrix}$$

$$L = \begin{bmatrix} 0 & 0 \\ .7275 \times 10^{-2} & -.7275 \times 10^{-2} \\ 0 & 0 \end{bmatrix} \qquad Y = \begin{bmatrix} 0 & 0 & 0 \\ 0 & 0 & 0 \end{bmatrix}$$

$$X = \begin{bmatrix} 0 & -.1818 \times 10^{-5} & 0 \\ 0 & .1818 \times 10^{-5} & 0 \end{bmatrix} \qquad W = \begin{bmatrix} -.4618 & .7275 \times 10^{-2} \\ .7275 \times 10^{-2} & -.4618 \end{bmatrix}$$

$$R = \begin{bmatrix} 3.328 \times 10^{-6} & 0 & 5.1 \times 10^{-12} \\ 0 & 7.274 \times 10^{-6} & 0 \\ 5.1 \times 10^{-12} & 0 & 2.558 \times 10^{-6} \end{bmatrix}$$

$$T = \begin{bmatrix} -.1333 & 0 & -5.1 \times 10^{-12} \\ 0 & -.1333 & 0 \\ -5.1 \times 10^{-12} & 0 & -.1333 \end{bmatrix}$$

$$Z = \begin{bmatrix} 0 & -7.274 \times 10^{-6} & 0 \\ 0 & 7.274 \times 10^{-6} & 0 \end{bmatrix} \qquad w = \begin{bmatrix} T_1 \\ -T_1 \\ 0 \\ T_2 \end{bmatrix}$$

so

$$w = \begin{bmatrix} 2.2185 \times 10^{-5}(T_{0a} + T_{4a} + T_{5a}) + (T_{0c} + T_{4c} + T_{5c}) \times 3.4 \times 10^{-10} \\ 4.8497 \times 10^{-4} T_{0b} \\ 3.4 \times 10^{-10}(T_{0a} + T_{4a} + T_{5a}) + 1.7056 \times 10^{-4}(T_{0c} + T_{4c} + T_{5c}) \\ -2.2185 \times 10^{-5}(T_{0a} + T_{4a} + T_{5a}) - 3.4 \times 10^{-10}(T_{0c} + T_{4c} + T_{5c}) \\ -4.8497 \times 10^{-4} T_{0b} \\ -3.4 \times 10^{-10}(T_{0a} + T_{4a} + T_{5a}) - 1.7056 \times 10^{-4}(T_{0c} + T_{4c} + T_{5c}) \\ 0 \\ 0 \\ 0 \\ -4.8497 \times 10^{-4} T_{0b} + .0303\, T_{4b} \\ 4.8497 \times 10^{-4} T_{0b} - .0303\, T_{5b} \end{bmatrix}$$

Note The independent noise quantities are T_{0b}, T_{4b}, T_{5b}, $(T_{0a} + T_{4a} + T_{5a})$, $(T_{0c} + T_{4c} + T_{5c})$.

Since it is more convenient to use minutes rather than seconds as the basic time unit, accelerations and velocities are converted to radians/min^2 and radians/min, respectively. If t denotes time in seconds and τ denotes time in minutes, then angular accelerations are converted by

$$\frac{d\hat{\omega}_i}{d\tau} = (60)^2 \frac{d\omega_i}{dt}$$

where $\hat{\omega}_i$ is an angular velocity in rad/min and ω_i is an angular velocity in rad/sec. In our equations each

$$\frac{d\lambda_i}{dt} = \sum_{\substack{j=a,\,b,\\ c,\,1}}^{5} F_{ij}\lambda_j + \sum_{j=1}^{3} G_{ij}u_j + w_i$$

thus

$$\frac{d\hat{\lambda}_i}{d\tau} = \sum_{\substack{j=a,\,b,\\ c,\,1}}^{5} \underbrace{(60\,F_{ij})}_{\hat{F}_{ij}}\underbrace{(60\lambda_j)}_{\hat{\lambda}_j} + \sum_{j=1}^{3} \underbrace{(3600\,G_{ij})}_{\hat{G}_{ij}} u_j + \underbrace{(3600\,w_i)}_{\hat{w}_i}$$

So we see that the matrices which multiply λ_j state variable in (31) must be multiplied by 60. The matrices multiplying the control voltage and disturbance torques must be multiplied by 3600.

Further each term

$$\frac{d\gamma_i}{dt} = \sum_{j=a}^{c} P_{ij}\lambda_j + \sum_{j=1}^{3} Q_{ij}\gamma_j$$

gives

$$\frac{d\gamma_i}{d\tau} = \sum_{j=a}^{c} \underbrace{P_{ij}}_{\hat{P}_{ij}}\underbrace{(60\lambda_j)}_{\hat{\lambda}_j} + \sum_{j=1}^{3} \underbrace{(60\,Q_{ij})}_{\hat{Q}_{ij}}\gamma_j$$

so we see that in (31) the P matrix remains the same but the Q matrix must be multiplied by 60.

This gives

$$\hat{G} = \begin{bmatrix} .012 & 0 & 1.8 \times 10^{-8} \\ 0 & .0262 & 0 \\ 1.8 \times 10^{-8} & 0 & .0092 \\ -597.96 & 0 & -1.8 \times 10^{-8} \\ 0 & -479.9 & 0 \\ -1.8 \times 10^{-8} & 0 & -479.9 \\ 0 & 0 & 0 \\ 0 & 0 & 0 \\ 0 & 0 & 0 \\ 0 & -.0262 & 0 \\ 0 & .0262 & 0 \end{bmatrix}$$

$$\hat{F} = \begin{bmatrix}
-.1235 \times 10^{-10} & 0 & 4.552 \times 10^{-6} & .4992 \times 10^{-4} & 0 & 1.639 \times 10^{-10} & 0 & 0 & 0 & 0 & 0 \\
0 & 0 & 0 & 0 & 1.091 \times 10^{-4} & 0 & 0 & 0 & 0 & .4365 & -.4365 \\
-1.502 \times 10^{-7} & 0 & -.073 \times 10^{-10} & .093 \times 10^{-10} & 0 & .3838 \times 10^{-4} & 0 & 0 & 0 & 0 & 0 \\
.1235 \times 10^{-10} & 0 & -4.552 \times 10^{-6} & -2 & 0 & -1.639 \times 10^{-10} & 0 & 0 & 0 & 0 & 0 \\
0 & 0 & 0 & 0 & -2 & 0 & 0 & 0 & 0 & -.4365 & .4365 \\
1.502 \times 10^{-7} & 0 & .073 \times 10^{-10} & -.093 \times 10^{-10} & & -2 & 0 & 0 & 0 & 0 & 0 \\
0 & 1 & 0 & 0 & 0 & 0 & 0 & 0 & 0 & 0 & 0 \\
0 & 0 & 1 & 0 & 0 & 0 & 0 & 0 & -.35 \times 10^{-5} & 0 & 0 \\
1 & 0 & 0 & 0 & 0 & 0 & 0 & .35 \times 10^{-5} & 0 & 0 & 0 \\
0 & 0 & 0 & 0 & -1.091 \times 10^{-4} & 0 & 0 & 0 & 0 & -27.709 & .4365 \\
0 & 0 & 0 & 0 & 1.091 \times 10^{-4} & 0 & 0 & 0 & 0 & .4365 & -27.709
\end{bmatrix}$$

$$\hat{w} = \begin{bmatrix} .0799\,T_a + .122 \times 10^{-5}\,T_c \\ 1.746\,T_{0b} \\ .122 \times 10^{-5}\,T_a + .614\,T_c \\ -.0799\,T_a - .122 \times 10^{-5}\,T_c \\ -1.746\,T_{0b} \\ -.122 \times 10^{-5}\,T_a - .614\,T_c \\ 0 \\ 0 \\ 0 \\ -1.746\,T_{0b} + 109\,T_{4b} \\ 1.746\,T_{0b} - 109\,T_{4b} \end{bmatrix}$$

where

$$T_a = T_{0a} + T_{4a} + T_{5a}$$

$$T_c = T_{0c} + T_{4c} + T_{5c}$$

REFERENCES

1. Friedland, B., et. al. "Stability of Attitude Control Systems Acted Upon by Random Perturbations" NASA Report CR-731, May 1967.

2. Athans, M. and Falb, P.F., "Optimal Control" McGraw-Hill Book Co., New York, 1966.

3. Wonham, W.M., "Stochastic Problems in Optimal Control," IEEE International Convention Record, Part 4, 1963, pp. 114 - 124.

4. Dynkin, E.B. "Markov Processes," 2 volumes, Academic Press, New York 1965.

5. Joseph, P.D. and Tou, J.T., "On Linear Control Theory," Trans. AIEE, Part II, September 1961, pp. 193 - 196.

6. Kalman, R.E. and Bucy, R.S., "New Results in Linear Filtering and Prediction Theory," ASME Trans. J. of Basic Engineering, March 1961, pp. 95 - 106.

7. Bryson, A.E. and Johanson, D.E., "Linear Filtering for Time-Varying Systems Using Measurements Containing Colored Noise," IEEE Trans. Automatic Control Vo. 10, January 1965, pp. 4 - 10.

8. Schwarz, R.J. and Friedland, B., Linear Systems, McGraw-Hill Book Co., New York, N.Y., 1965, pp. 215 - 216.

9. Gantmacher, F.R., The Theory of Matrices, Vol. I, Chelsea Publishing Company, New York, N.Y., 1959.

10. Report AFF DL-TR-64-168, Part III, Wright-Patterson-Flight Dynamics Laboratory, prepared by GE - Missiles and Space Division.

11. Bohn, J.L., "Zodiacal Dust: Measurements by Mariner IV," Science, Vol. 149, No. 3689, pp. 1240 - 1241, September 10, 1965.

12. Friedland, B. et. al., "Stability Problems in Randomly-Excited Dynamic Systems," 1966 Joint Automatic Control Conference preprint volume, pp. 848 - 861.

13. West, George S. and Roberts, S.T., "The Atmosphere of Mars: A Derivation of Engineering and Design Parameters," Proceedings of Southeastern Symposium on Missiles and Aerospace Vehicles Sciences of American Astronautical Society, December 1966, Paper No. 58.

14. Goldstein, H., Classical Mechanics, Addison Wesley, New York 1959.

15. Papsco, R.E., "The Stabilization and Control System for the Orbiting Astronomical Observatory," Navigation, Journal of the Institute of Navigation, Vol. 11, No. 1, Spring 1964.